BIOACTIVE GLASS-BASED COMPOSITE SCAFFOLDS FOR TISSUE ENGINEERING APPLICATIONS

Ana Gantar

Doctoral Dissertation
Jožef Stefan International Postgraduate School
Ljubljana, Slovenia

Supervisor: Prof. Dr. Saša Novak, Jožef Stefan Institute, Ljubljana, Slovenia

Evaluation Board:
Prof. Dr. Janez Štrancar, Jožef Stefan Institute, Ljubljana, Slovenia
Prof. Dr. Miomir Kneževič, Biotehnical Faculty, Ljubljana, Slovenia
Prof. Dr. Mauro Alini, AO Foundation, Davos, Switzerland

MEDNARODNA PODIPLOMSKA ŠOLA JOŽEFA STEFANA
JOŽEF STEFAN INTERNATIONAL POSTGRADUATE SCHOOL



Ana Gantar

BIOACTIVE GLASS-BASED COMPOSITE SCAFFOLDS FOR TISSUE ENGINEERING APPLICATIONS

Doctoral Dissertation

KOMPOZITNA OGRODJA Z BIOAKTIVNIM STEKLOM ZA UPORABO V TKIVNEM INŽENIRSTVU

Doktorska disertacija

Supervisor: Prof. Dr. Saša Novak Krmpotič

Ljubljana, Slovenia, April 2016

To my grandfather Tomislav. I know you are watching over me.

Acknowledgments

First, I would like to thank my Ph.D. supervisor, Prof. Dr. Saša Novak Krmpotič, for the encouragement, support, and guidance during my work and study at the Jožef Stefan Institute, as well as for all the advice, ideas, and long discussions.

Next, I would like to thank the Slovenian Research Agency for the financial support. Also, I would like to thank the COST Action MP1005 titled "From NAno to MAcro BIOmaterials (design, processing, characterization, modeling) and applications to stem cells regenerative orthopedic and dental medicine (NAMABIO)" for financial support of two short-term scientific missions, during which parts of this work were performed. Therefore, I would like to thank Prof. Dr. Rui L. Reis for giving me the opportunity to study and work at his group, 3B's (Research Group in Biomaterials, Biodegradables and Biomimetics) at the Department for Polymeric Engineering, University of Minho, Portugal. I would like to thank Dr. Vitor M. Correlo for all the help and in the laboratory and for helping me the with microCT analysis. I would especially like to thank Lucilia P. da Silva for help in the laboratory, mechanical characterization and cell testing.

Secondly, I would like to thank Dr. Iraida Loinaz for allowing me to perform laboratory work in the group of Materials (Division of Biomaterials) at the CIDETEC company in San Sebastian, Spain. Special thanks to Dr. Damien Dupin and Dr. Iraida Loinaz for being my hosts and supervisors. I would like to thank Dr. Pablo Casuso for helping me with the sample preparation and processing, rheology characterization, compression test analysis. I would also like to thank Dr. Adrián Pérez-San Vicente for helping me with cytotoxicity evaluation.

I would like to thank Dr. Nataša Drnovšek for introducing me to the bioactive glass and its synthesis, without it it would be impossible to prepare composite scaffolds.

I would like to thank Rok Kocen for helping me with the rheology measurements of gellan gum hydrogels and compression tests.

I would like to thank Dr. Slavko Kralj for helping me with the freeze-drying process and Prof. Dr. Darko Makovec for allowing me to use the lyophilization equipment at the Department for Materials Synthesis.

I would like to thank Maja Koblar at the Center for Electron Microscopy and Microanalysis (CEMM, IJS) for helping me with the SEM sample preparation and SEM analysis.

I would like to thank Prof. Dr. Janez Stepišnik from the Faculty of Mathematics and Physics, University of Ljubljana, for spectral characterization of diffusion.

Next, I would like to thank Prof. Dr. Odon Planinšek from the Faculty of Pharmacy, University of Ljubljana, for performing the differential scanning calorimetry analysis.

I would like to thank my colleagues at the Department for Nanostructured Materials. Thanks to Dr. Nataša Drnovšek, Dr. Martina Lorenzetti and Rok Kocen for their encouragements, help and brainstorming discussions.

I would like to thank Kaja Križman, Mateja Paščinski and Marko Lukek for all their technical assistance.

Finally, I would like to thank my mother for giving me the opportunity to study and for all her support and encouragement. Without her, this would be impossible. Very special thanks to Juš for being beside me on this journey, cheering me up during all those difficult moments.

Abstract

Tissue engineering is based on three components used for tissue formation or regeneration: scaffolds, stimulating molecules/materials and cells. With large tissue defects, scaffolds are crucial as they serve as (temporary) extracellular matrix, encapsulating cells and guiding them to form a new tissue. In bone regeneration, bone-stimulating scaffolds, with suitable properties, are preferred.

In this study, nano-sized bioactive glass particles (BAG), a highly bioactive material, was used with an aim to prepare a three-dimensional scaffold, with an ability to form bone mineral, even in vitro. The design of the scaffold should mimic the cancellous bone in it porosity, mechanical properties and degradation rate. Despite favorable bioactivity of the bioactive glass, it has a downside, as other inorganic bioactive materials, of being slightly alkaline, when degrading, and highly brittle, when in form of porous 3D scaffold. Therefore, we have combined BAG particles with two different polymers and prepared a) a porous 3D scaffold, available "off-the-shelf" and b) a hydrogel for injectable applications. For 3D scaffold gellan gum (GG), a natural polysaccharide obtained during fermentation of Sphingomonas paucimobilis and for the hydrogel thiolated polyethylene glycol ($(PEGSH)_4$), a synthetic polymer with self-healing abilities, were used. Both are degradable, however bioinert, but suitable to be designed into temporary 3D matrix.

Using freeze-drying technique anisotropic highly porous structures of GG-BAG were obtained. The structures were obtained from prepared cross-linked hydrogels, to which two chemically different bioactive glass powders were added – BAG-A (SiO_2-CaO) or BAG-B (SiO_2-CaO-Na_2O-P_2O_5), to study the effect of BAG chemistry to composite's properties. In the freeze-dried scaffolds, containing BAG-B increased pore size was observed, resulting in insufficient increase of Young's modulus and higher rate of degradation. Due to the unfavorable characteristics, it was conclude to use only BAG-A in further studies. GG-BAG-A exhibited favorable pore size, consequently favorable scaffold properties. The pore size depended also on the freezing temperature and percentage of added BAG. The most promising porosity and other scaffold characteristics were determined with GG-50A scaffold. With increasing percentage of BAG the porosity decreased to values not suitable for cell encapsulation. Despite the modification of the preparation process, decreased Young's modulus was exhibited.

Secondly, we prepared a composite scaffold in form of injectable hydrogel. The Au-$(PEGSH)_4$-BAG system is suitable for minimum invasive applications, as it gels *in situ* due the dynamic cross-linking via aurophilic attractions. The addition of BAG particles positively affected the viscoelasticity of the hydrogel and increased hydrogel's bioactivity.

Both presented composites were bioactive and the alkalinity of BAG was decreased with lower diffusion rate of Ca^{2+} ions through the polymer matrix, resulting in improved biocompatibility (lower cytotoxicity). The BAG addition to the polymer matrixes resulted in more favorable mechanical properties. The degradation rate of the Au-$(PEGSH)_4$-BAG system was unfortunately to fast, however with the GG-BAG composites the degradation rate was estimated to few months. Further, it was established

that the bioactivity of the BAG particles, substituted the lost weight during degradation by the formation of hydroxyapatite phase (the bone mineral).

With combination of materials, the characteristics of each components in the composite, the bioactive glass and the polymer, were improved.

Povzetek

Tkivno inženirstvo je veda, ki skuša s kombiniranjem treh osnovnih komponent, celično ogrodje – stimulativne substance – celice, regenerirati poškodovano tkivo. Zaradi omejene sposobnosti samoregeneriranja so za zdravljenje večjih defektov tri-dimenzionalna ogrodja ključnega pomena. Ta služijo kot začasni ekstracelularni matriks, ki zadržuje celice na mestu poškodbe in jih skuša stimulirati k tvorbi novega tkiva. Za uspešno regeneracijo kostnega tkiva imajo prednost ogrodja, ki spodbujajo tvorbo kosti podobnega minerala – hidroksiapatita.

Namen študije je bil pripraviti tridimenzionalno celično ogrodje z visoko stopnjo bioaktivnosti oz. sposobnostjo stimuliranja tvorbe kostnega tkiva. Prav tako smo pri oblikovanju celičnega ogrodja skušali v največji meri posnemati zdravo kostno tkivo, tj. strukturo, mehanske lastnosti, stopnjo razgradljivosti.

V predstavljeni študiji smo uporabili močno bioaktiven anorganski material – nanodelce bioaktivnega stekla (BS). Kljub prednostim pred drugimi bioaktivnimi anorganskimi materiali, je tudi bioaktivno steklo, oblikovano v 3D porozno celično ogrodje, krhko in med degradacijo alkalno. Zato smo delce bioaktivnega stekla združili z dvema vrstama polimera in pripravili a) porozno 3-dimenzionalno ogrodje, uporabno po potrebi (»off-the-shelf) in b) hidrogel, ki bi ga bilo mogoče v defekt vnesti z vbrizganjem. V prvem primeru smo uporabili naravni polimer – gelanski gumi (GG), ki je ekonomsko dostopen, enostaven za uporabo in biokompatibilen, v drugem pa sintetični polimer – modificirani polietilen glikolom ($(PEGSH)_4$). Oba polimera sta razgradljiva, zato primerna za pripravo začasnega celična ogrodja, vendar pa sta bioinertna.

S tehniko fazne separacije z zmrzovanjem in sublimacijo (»freeze-drying«) smo pripravili kompozitna celična ogrodja GG-BS z visoko poroznostjo. Porozne strukture smo pridobili iz ustrezno zamreženih hidrogelov gelanskega gumija, ki jim smo dodali različne dodatke dvokomponentnega (BS-A: SiO_2-CaO) ali štirikomponentnega (BS-B: SiO_2-CaO-Na_2O-P_2O_5) bioaktivnega stekla. V nadaljevanju smo preučevali vpliv kemijske sestave BS na lastnosti kompozitnih ogrodij. BS-B je negativno vlivalo na strukturo in poroznost sušenega kompozitnega ogrodja, kar se je kazalo tudi v slabših mehanskih lastnostih in hitrejši degradaciji v primerjavi s kompoziti, ki so vsebovali BS-A. Zaključili smo, da je v nadaljevanju študije smiselno izključiti uporabo BS-B. Želeno velikost por in njihovo porazdelitev smo dosegli v suhih kompozitnih ogrodjih, ki so vsebovala do 50 % BS-A. V kompozitih z visokim deležem BS se je poroznost močno zmanjšala. Kljub modificiranem postopku priprave ogrodja z visokim deležem BS nismo dosegli izboljšanja.

V nadaljevanju smo pripravili kompozitna ogrodja Au-$(PEGSH)_4$-BS v obliki hidrogela, ki ga je na mesto defekta mogoče vnesti z vbrizgavanjem, saj želira v trenutku *in situ* ob dodatku ustreznega zamreževalca. Dodatek BS delcev je ugodno vplival na viskoelastične lastnosti hidrogela, hkrati pa je prispeval k sposobnosti tvorbe hidroksiapatita.

Obe pripravljeni kompozitni ogrodji sta bili dokazano bioaktivni in sta zmanjšali problematično alkalnost BS delcev ob razgradnji z znižanjem hitrosti difuzije Ca^{2+} ionov

skozi polimerno matrico, kar je rezultiralo v izboljšani biokompatibilnosti (citotoksični testi). Prav tako sta obe kompozitni ogrodji izkazali zadovoljive mehanske lastnosti. Stopnja degradacije kompozitnih ogrodji je bila ocenjena na nekaj dni pri Au-$(PEGSH)_4$-BS do nekaj mesecev GG-BS . Med oceno degradacije smo ugotovili, da je del izgubljene mase nadomestila precipitacija hidroksiapatita zaradi prisotnosti bioaktivnih delcev v kompozitu.

Z ustrezno kombinacijo materialov smo torej dosegli izboljšanje lastnosti obeh komponent kompozita, polimera in bioaktivnega stekla

Contents

Acknowledgments **vii**

Abstract **ix**

Povzetek **xi**

Contents **xiii**

List of Figures **xvii**

List of Tables **xix**

Abbreviations **xxi**

Symbols **xxiii**

1 Introduction **1**
1.1 Tissue Engineering and Biomaterials 1
1.2 Definition and Classification of Biomaterials 3
1.3 Bone and Bone Tissue Engineering 6
1.4 Scaffolds for Bone Tissue Engineering 8
1.4.1 Ceramic and glass scaffolds 9
1.4.2 Natural polymeric scaffolds 10
1.4.3 Synthetic polymeric scaffolds 12
1.4.4 Inorganic-organic composite scaffolds 13
1.4.5 Cross-linking chemistry 13
1.4.6 Fabrication techniques 14

2 Aim and Hypothesis **17**

3 Material and Methods **19**
3.1 Gellan Gum - Bioactive Glass Scaffolds 19
3.1.1 Scaffold fabrication 19
3.1.1.1 Gellan gum hydrogel preparation 19
3.1.1.2 Gellan gum – bioactive glass hydrogel preparation 19
3.1.1.3 Preparation of porous gellan gum – bioactive glass scaffold with high bioactive glass percentage (foaming process) 20
3.1.1.4 Freeze-drying process 20
3.1.2 Characterization 20
3.1.2.1 Electron microscopy 20

3.1.2.2 X-ray microtomography 21
3.1.2.3 Compression test 21
3.1.2.4 Rheology measurements 21
3.1.2.5 Wettability measurements 21
3.1.2.6 Fourier transform infrared spectroscopy (FT-IR) 21
3.1.2.7 Differential scanning calorimetry (DSC) analysis 22
3.1.2.8 *In vitro* degradation, weight loss, swelling and pH change 22
3.1.2.9 Spectral characterization of diffusion 22
3.1.2.10 *In vitro* mineralization test 23
3.1.2.11 Cytotoxicity 23
3.2 Polyethylene Glycol – Bioactive Glass Nanocomposite Hydrogels 24
3.2.1 Materials 24
3.2.2 Sample preparation 24
3.2.2.1 Ellman's test 24
3.2.2.2 Fabrication of bioactive glass – polyethylene glycol nanocomposite hydrogels 24
3.2.3 Characterization 25
3.2.3.1 Electron microscopy 25
3.2.3.2 Rheology 25
3.2.3.3 Compression test 25
3.2.3.4 Self-healing experiment 26
3.2.3.5 *In vitro* BAG degradation (Franz cell, pH change, ICP-MS, *in vitro* mineralization) 26
3.2.3.6 *In vitro* evaluation by cell culture (MTS and Tripan blue assay) 26

4 Results **29**
4.1 Gellan Gum – Bioactive Glass Scaffolds 29
4.1.1 Samples preparation 29
4.1.2 Material characterization 32
4.1.2.1 Differential scanning calorimetry (DSC) analysis of water - GG and water - GG-BAG interactions 32
4.1.2.2 Fourier transform infrared spectroscopy (FT-IR) 33
4.1.3 Characterization of GG and GG-BAG composite materials in the form of hydrogels, dry scaffolds and rehydrated scaffolds 35
4.1.3.1 Microstructural observation of dry scaffolds by SEM 35
4.1.3.2 3D architecture and porosity 37
4.1.3.3 Mechanical properties 39
4.1.3.4 Wettability 41
4.1.3.5 Behaviour of the dry scaffolds immersed in aqueous media 42
4.1.3.6 *In vitro* formation of hydroxyapatite 46
4.1.3.7 Cytotoxicity 47
4.2 Polyethylene Glycol – Bioactive Glass Nanocomposite Hydrogels 49
4.2.1 Sample preparation 49
4.2.2 Characterization of polyethylene glycol – bioactive glass nanocomposites as possible injectable hydrogels 49
4.2.2.1 Observation of microstructure by SEM 49
4.2.2.2 Rheological behavior of nanocomposites with different BAG percentage at different pH values 50
4.2.2.3 Mechanical and deformation properties 53

4.2.2.4 Self-healing ability of nanocomposites and the effect of BAG presence on it....54
4.2.2.5 BAG degradation, pH change and *in vitro* formation of hydroxyapatite mineral....55
4.2.2.6 *In vitro* cell viability....56

5 Discussion **59**
5.1 Bioactive Glass - Reinforced Gellan Gum Scaffolds....60
5.2 Polyethylene Glycol – Bioactive Glass Nanocomposite Hydrogels....66
5.3 Potential Applications of the GG-BAG and Au-$(PEGSH)_4$-BAG Scaffolds....70

6 Conclusions **73**

References **75**

Bibliography **83**
Publications Related to the Thesis....83
Original Scientific Articles....83
Conference Paper....83
Published scientific conference contribution abstract....83
Final research reports....85

List of Figures

Figure 1.1: Representation of complexity of tissue engineering science. 1
Figure 1.2: Basic tissue engineering triad and its fundamental elements. 2
Figure 1.3: Bone structure. 6
Figure 1.4: Most applied tissue engineering constructs 9
Figure 1.5: Cross-linking possibilities to form hydrogel 14
Figure 1.6: Presentation of possible fabrication processes by steps applicable to different materials. 16
Figure 4.1: Schematic presentation of samples preparation. 30
Figure 4.2: Macro photographs of GG (A, B, C) and GG-BAG (D, E, F). Materials are in the form of hydrogels (A, D), dry scaffolds (B, E) and rehydrated scaffolds (C, F). ...30
Figure 4.3: Viscoelastic properties of GG hydrogel and GG-BAG composite hydrogel by storage (G') and loss modulus (G'') during cooling. 31
Figure 4.4: DSC analysis. Freezing temperatures (A) and entalpy values (B) for the preformed regime. 32
Figure 4.5: DSC curves (heating part) of GG, GG-33A, GG-50A and GG-70A hydrogels.33
Figure 4.6: FT-IR spectra of GG, GG-50A, and GG-70A samples. 34
Figure 4.7: FEG-SEM images of cross-section of freeze-dried GG (A, C) and GG-50A (B, D) scaffold prepared at different temperatures, -20 °C and -80 °C.....35
Figure 4.8: FEG-SEM images of the BAG-A particles (A) and cross-sections of the GG (B, C), and GG-BAG composites with 33 % or 50 % BAG-A (D, E) and 33 or 50 % BAG-B (G, H). Figures F and I present the cross-sections of the pore walls in samples GG-50 A and GG-50B, respectively. 36
Figure 4.9: FEG-SEM images of cross-sections of the (A) GG-70A, (B) GG-70A pore wall and (C, D) GG-90A. 37
Figure 4.10:Three-dimensional scan of dry scaffolds of GG (A) and GG-50A (B). 38
Figure 4.11:Porosity (A) and pore size distribution (B) for the composite GG-BAG dry scaffolds. 39
Figure 4.12:Young's modulus for hydrogels (A), dry scaffolds (B) and rehydrated scaffolds (C). 40
Figure 4.13:Compressive stress vs. strain curves for BAG and GG hydrogel (A), and their composites in the form of hydrogel (B), dry scaffold (C) and rehydrated scaffold (D) with various compositions. 41
Figure 4.14: Macro photographs of GG (A) and GG-50A (B) dry scaffolds and GG (C) and GG-50A (D) rehydrated scaffolds, all cross-sections. 43
Figure 4.15:MGSE measurements of GG (A) and GG-50A (B) rehydrated scaffolds.....43
Figure 4.16:Water uptake during 48 h rehydration of dry scaffolds in PBS (A) and weight loss of rehydrated scaffolds during 48 h immersion in PBS (B). 44
Figure 4.17:Degradation profile (weight change) of GG and GG-50A dry scaffolds in PBS over 30 days. 44
Figure 4.18:pH profile of BAG-A, GG-50A and GG during the PBS immersion over 3 days. 45

Figure 4.19:Change of diameters of GG (A) and GG-50A (B) dry scaffolds over time when immersed in PBS, representing swelling of the materials. 46
Figure 4.20:FEG-SEM images of the dried GG-50A after immersion in SBF for 30 days at two magnifications. 46
Figure 4.21:Representative confocal microscopy images of hASCs within GG (A, B), GG-50A (C, D) and GG-50B (E, F) rehydrated scaffolds after 72 hours of culture after Phalloidin-TRITC (red) (A, C, E) and Calcein AM (green)/Propidium Iodide (red) (B, D, F) staining. Cells nuclei were stained with DAPI (blue) (A, C, E). 48
Figure 4.22:FEG-SEM pictures showing the microstructure of freeze-dried Au-$(PEGSH)_4$-BAG hydrogel nanocomposites: Au-$(PEGSH)_4$-BAG_5 (A), Au-$(PEGSH)_4$-BAG_{10} (B) and Au-$(PEGSH)_4$-BAG_{20} (C); (D) Au-$(PEGSH)_4$-BAG_{10} at higher magnification..... 50
Figure 4.23:The variation of G' (■) and G'' (□) at 1 % deformation and 0.1 Hz in function of time for Au-$(PEGSH)_4$-BAG_{10} hydrogel nanocomposite directly injected on the rheometer plate. 51
Figure 4.24:Frequency sweep studies depicting shear storage (G') and loss modulus (G'') for a constant deformation (1 %) applied as a function of frequency for Au-$(PEGSH)_4$ hydrogel and hydrogel nanocomposites prepared with 5, 10 and 20 w/w % of BAG nanoparticles adjusted at pH~10 (A) and at pH~7(B); (C) and (D) represent the corresponding tan δ = G''/G' at pH 10 and pH 7. 52
Figure 4.25:Compression stress vs. deformation curves of Au-$(PEGSH)_4$-BAG_5, Au-$(PEGSH)_4$-BAG_{10} and Au-$(PEGSH)_4$-BAG_{20} hydrogel nanocomposites and Au-$(PEGSH)_4$ for comparison. 53
Figure 4.26:Digital pictures of Au-$(PEGSH)_4$-BAG_{10} hydrogel nanocomposite; as-prepared (A), cut into pieces with a scalpel (B) and self-healed overnight in a disc shaped mould (C); frequency sweep studies for Au-$(PEGSH)_4$-BAG hydrogel nanocomposites adjusted at pH 7 after being cut with a scalpel and self-healed in disc shape mould with light pressure overnight (D). 54
Figure 4.27: (A) Time-dependent concentration of silicon and calcium ions released during the degradation and detected by ICP-MS of BAG nanoparticles alone and Au-$(PEGSH)_4$-BAG_{10} hydrogel nanocomposite in ultrapure water using a Franz cell and (B) pH change. 55
Figure 4.28:The FEG-SEM image of Au-$(PEGSH)_4$-BAG_{10} after 30 days immersion in SBF. 56
Figure 4.29:Cytotoxicity evaluation of BAG, Au-(PEGSH)4 hydrogel and Au-$(PEGSH)_4$-BAG_{10} hydrogel nanocomposite by MTS (A) and Tripan blue assay (B). 57
Figure 4.30:Representative fluorescence microscopy images of HeLa cells respond to degradation products of Au-$(PEGSH)_4$ (PEG), Au-$(PEGSH)_4$-BAG_{10} (PEG-10BAHG) and BAG after 72 hours. 58
Figure 5.1: Double syringe experiment demonstrating a possible application. 71

List of Tables

Table 1.1: Classification of natural TE grafts.....3
Table 1.2: Young's modulus of bone building blocks and the bone itself.....7
Table 1.3: Mechanical properties of bone with a different direction of measurement.....7
Table 3.1: Final composition of prepared gellan gum hydrogels and gellan gum-bioactive glass composite hydrogels. 20
Table 3.3: Composition of polyethylene glycol-bioactive glass hydrogel nanocomposites.25
Table 4.1: Contact angle of water on hydrogel films of GG, GG-50A and GG-70A over time. 42
Table 4.2: Contact angle of water on dry scaffolds of GG, GG-50A and GG-70A. 42
Table 4.3: Ellman's test results. Measured absorbance of Au-$(PEGSH)_4$ and Au-$(PEGSH)_4$-BAG_{20} sample and calculated Eellman's number. 49

Abbreviations

$(PEGSH)_4$	... 4-arm thiolated polyethylene glycol
µ-CT	... Micro-computed tomography
3D	... Three-dimensional
ATR	... Attenuated total reflection
Au-$(PEGSH)_4$	... 4-arm thiolated polyethylene glycol cross-linked with gold
Au-$(PEGSH)_4$-BAG	... 4-arm thiolated polyethylene glycol-bioactive glass hydrogel nanocomposite cross-linked with gold
Au-S/SS	... Aurophilic interactions with thiolte groups
BAG	... Bioactive glass
BAG-A	... 2-component bioactive glass
BAG-B	... 4-component bioactive glass
Ca-AM	... Calcein-AM staining
CaP	... Calcium phosphates
CHAp	... Carbonated apatite
DAPI	... 4',6-diamidino-2-phenylindole
DSC	... Differential scanning calorimetry
DTNB	... 5,5'-Dithiobis(2-nitrobenzoic acid)
E	... Young's modulus
ECM	... Extracellular matrix
EDS	... In situ X-ray spectroscopy
EDXS	... Energy-dispersive X-ray spectrometer
FBS	... Fetal bovine serum
FD	... Freeze-drying
FEG	... Field emission gun
FT-IR	... Fourier transform infrared spectroscopy
GG	... Gellan gum
GG-BAG	... Gellan gum-bioactive glass composite
HA	... Hydroxyapatite
HAc	... Hyaluronic acid
hASC	... Human adipose stem cell
HeLa	... Cell line, derived from cervical cancer cells
ICP-MS	... Inductively coupled plasma-mass Spectrometry
MD	... Medical device
MTS	... Colorimetric sensitive quantification of viable cells in proliferation and cytotoxicity assay
n/n %	... Molar percentage
PBS	... Phosphate buffered saline
PCL	... Polycaprolactone
PEG	... Polyethylene glycol
PES	... Phenazine ethosulfate
PGA	... Polyglycolic acid

PI	... Propidium Iodide
PLA	... Polylactic acid
RM	... Regenerative medicine
rpm	... Revolutions per minute
SAOS	... Small amplitude oscillatory shear
SBF	... Simulated body fluid
SEM	... Scanning electron microscopy
SFF	... Solid free form
T	... Temperature
TCP	... Tricalcium phosphates
TE	... Tissue engineering
TIPS	... Thermally induced phase separation
TRIS	... tris(hydroxymethyl)aminomethane
UV-vis	... Ultraviolet-visible
VE	... Viscoelastic
w/v %	... Weight per volume percentage
w/w %	... Weight percentage

Symbols

G' ... Shear storage modulus
G'' ... Shear loss modulus
ωc ... Crossover frequency
$\tan \delta$ ... Loss factor
λt ... Relaxation time

Chapter 1

Introduction

1.1 Tissue Engineering and Biomaterials

In the past years, growing demands for high health and living standards of the population have aroused a development of new materials and, with that, medical devices (MD) to improve and make the everyday life easier. With all the growing research fields in medicine, tissue engineering (TE) has been developed. It is a multidisciplinary area that applies the principles of engineering, life sciences, cell and molecular biology toward the development of substitutes that restore, maintain, and improve tissue function. One of the main aims of TE is as well to lower the demand for donor tissues and organs.[1]

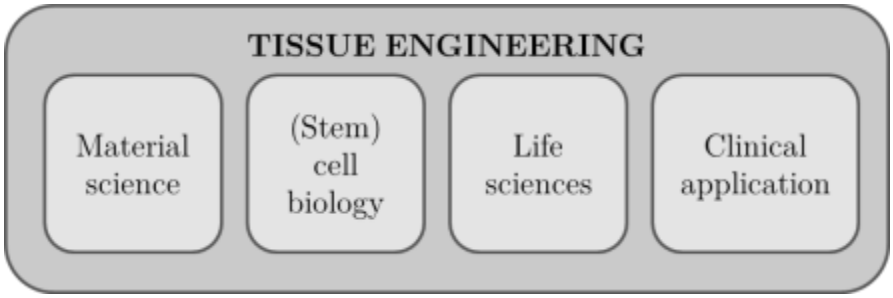


Figure 1.1: Representation of complexity of tissue engineering science.

The three basic elements usually combined by the TE are a scaffold of suitable properties to provide needed support and ready for transplantation; cells capable of forming a new functional extracellular matrix (EMC); and bioactive components supporting and guiding the cells to form new tissue. Elements to successfully regenerate tissues or organs can be used individually or in a combination of two or more. Hence, there are still some problems in the field of tissue engineering, like cells, engineering development, grafting, and safety, that need to be researched in greater detail.[2]

As mentioned above TE is a highly interdisciplinary field involving material science, which needs to be studied well to convert a bulk material to 3D scaffold, suitable for a TE successful construct. Parameters, which are highly significant to transform the bulk material to the scaffold, are material's nature and processing capacities. Once the material is shaped into a 3D scaffold, architecture (porosity, structure, size), biodegradability and scaffold – cell interactions (cell viability and cytotoxicity) are crucial characteristics for scaffold's success.[2]

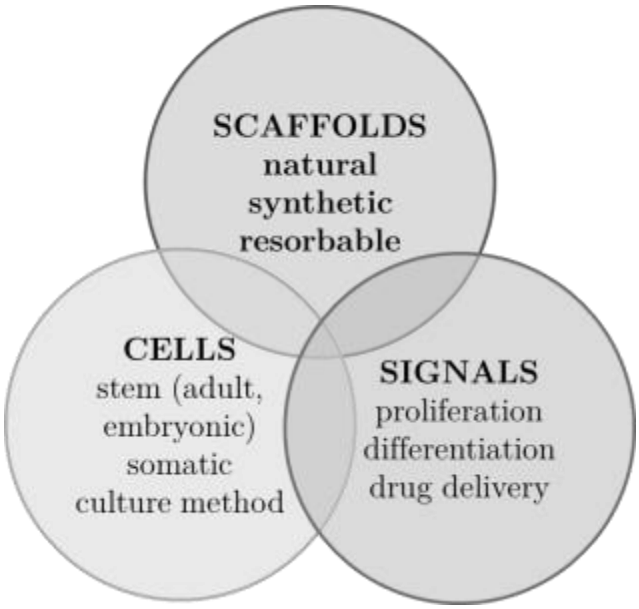


Figure 1.2: Basic tissue engineering triad and its fundamental elements.

Most TE applications are combining all of three basic TE building blocks: scaffolds, signaling molecules and cells mimicking the building structure of the biological tissues. The combination of all three may result in a complex system and can be a subject to failure due to many parameters that need to be regulated.

Why a 3D matrix is essential for TE constructs to succeed? With smaller defects, only cells and/or signaling molecules can ensure successful regeneration, however, with larger defects a 3D matrix – a scaffold – is crucial. As cells grow only in two dimensions, unable to refill a large void, the 3D scaffold provides a temporary guiding template. The scaffold should mimic extracellular matrix of the regenerating tissue, which is a meshwork-like substance with extracellular space that supports cell attachment and promotes cell proliferation. This 3D matrix should degrade at the same rate as the new tissue is forming.
Scaffolds that have been used in the clinical practice can be a graft from natural tissues or can be man engineered.[3]

Table 1.1: Classification of natural TE grafts[3].

Graft	Definition	Pros	Cons
Xenograft	tissue graft from another species	availability; a variety of shapes and sizes	the non-negligible risk of immunological reactions and infections
Allograft	human donor tissue graft; usually post-mortem	no morbidity sites	donor shortage; risk of infections
Autograft	tissue grafts from the patient, who receives the graft	gold standard; no transfection and rejection	donor site morbidity; chronic donor shortage; double surgical treatment

By using synthetic scaffolds, with or without cells/signalling molecules; one would overcome some of the limitations of the grafts discussed in Table 1.1 and possibly cover a large demand for new tissues. For scaffold to have the desired characteristic and to serve as just a temporary template, the material from which it is fabricated must be biocompatible and preferably biodegradable.[4]

1.2 Definition and Classification of Biomaterials

Biomaterials have been formally defined as "a systemically and pharmacologically inert substance designed for implantation within or incorporation with living systems" at the Clemson University Advisory Board [5]. Already in the early 1900's bone plates were successfully implemented to stabilize bone fractures and to accelerate their healing. In the 1950's and 60's, clinical trials of blood vessel replacements were performed, and the development of artificial heart valves and hip joints was in progress [6]. Unfortunately, at these beginnings of the TE and regenerative medicine (RM), material and design problems occurred, such as too early loss of mechanical support of the implant and corrosion of it, resulting in low biocompatibility of the implants or their component.

Nowadays, improved biomaterials and better-designed constructs are used in many different fields of medicine as artificial joints, bone plates and screws, cardiac pacemakers, intraocular and contact lenses and lately as biodegradable scaffolds. As the primary aim of biomaterials is to improve human health, key factors for biomaterials' success are its biocompatibility, functionality, biodegradability and availability.

The performance of materials in the body can be classified in many ways. Biomaterials, used as part of MD, must be safe, reliable, physiologically acceptable and preferably economically accessible. It can be any material of natural or synthetic origin or a composite. At the early stages of biomaterials area, these materials were suitable just to be in contact with the living tissue, but the latest research and development in this field strives to develop materials, which favorably interact with the host tissue, guide formation of new tissue and degrade in the desired period, leaving no residue behind.

Engineered materials, when placed in contact with a living organism, can provoke different reactions of the body, conditional with the type of the material. In general,

there are four terms to describe a biomaterial about its interaction with a living organism [5, 7, 8]:

- Biotoxic

This kind of material is usually not suitable to be implemented into a human body. They cause atrophy, pathological change or rejection of living tissue near the material because of chemical or another process. However, at the beginning of biomaterials area biotoxic materials, such as alloys containing Cadmium and other toxic elements, carbon, steels, and carbides, were implemented into living organisms.

- Bioinert

Materials with minimal interactions to the surrounding tissue are usually described as bioinert. These materials are stainless steel, aluminum, and titanium; also some distinct types of zirconia and polyethylene. Implementation of these materials may result in the formation of the fibrous capsule, causing the implant to fail as its functionality is based on the tissue integration with the implant.

- Bioactive

When material, after being placed into the human body, interacts with the surrounding tissue, it can be defined as a bioactive one. Interactions occur via time-dependent dynamic modification of the surface. Between the surrounding body fluids and bioactive implant, a reaction of exchanging ions a forms layer of biologically active carbonate apatite (CHAp) on the implant. The chemistry and crystal structure of the formed layer is identical to the bone mineral phase. Materials like synthetic hydroxyapatite [$Ca_{10}(PO_4)_6(OH)_2$], glass-ceramics and bioactive glasses form direct biochemical bonds on their surface with surrounding tissue and promote the growth of new tissues.

- Bioresorbable

The highly appropriate biomaterial for TE constructs is one, which is dissolved by the organism. It can be designed as a temporary matrix, which is gradually replaced by the newly formed tissue. To this group of materials belong some natural polymers as collagen, alginate, chitosan, etc., as well as some inorganic materials, tri-calcium phosphates, porous hydroxyapatite and bioactive glasses.

- Osteoconductive

The osteoconductive material serves as a scaffold for new bone growth that is perpetuated by the native bone.

Various materials can be used for scaffold design and can be classified regarding their chemical composition and structure to:

- Metals

Metals, such as Ti and Ti alloys, CoCr-alloys and stainless steel, are strong and durable materials, with sufficient strength to support even load-bearing application in bone regeneration. They are difficult to produce and do not regenerate the defect but replace the living tissue and their functions. They are often placed as a permanent implant in the human body. The biocompatibility of the metallic implant is of considerable concern because these implants can corrode in an *in vivo* environment. Corrosion may cause the implant to disintegrate, resulting in loss of the strength of the implant and damaging the surrounding tissue by the corrosion chip-offs.

- Ceramics and glass

Due to biocompatibility and high corrosion resistance, ceramic materials are widely used not only in dentistry but also in orthopaedics. Despite the brittleness, weakness in tension and non-resilience of ceramics, they have been successfully applied to load-bearing applications. Ceramics used in implants can be classified as non-resorbable (relatively inert), bioactive or surface reactive (semi-inert), and biodegradable or resorbable (non-inert). Alumina, zirconia and silicon nitrides are considered as inert bioceramics, however, they are not. Certain glass ceramics and dense hydroxyapatites are semi-inert. Calcium phosphates and calcium aluminates are classified as resorbable ceramics.

- Polymers

Polymers can originate from natural sources or can be synthetically developed. They are usually easy to fabricate and are resilient. Polymers are widely used in medicine for disposable supplies, dental materials, prosthetic materials, dressings, implants, extracorporeal devices, polymeric drug delivery systems, encapsulants, tissue engineered products, and orthodoxies. The main advantages of the polymeric biomaterials compared to metal or ceramic materials are how easy they can be fabricated into various shapes, like film, sheet, fibres, etc., their ability to be easily secondarily processed, their low cost, and their range of available mechanical and physical properties. Polymers have to be, as other biomaterials, biocompatible, sterilisable, of right mechanical and physical properties, and easy to manufacture. However, the lack of strength and acidic degradation products limit the use of polymers.

- Composites

Materials with two or more distinctive phases are composite materials. These phases rails can be determined on the scale larger than atomic. In addition, the mechanical properties such as elastic modulus are significantly changed in comparison with those of a monolithic material. Accordingly, reinforced plastics as well as natural materials such as bone are defined as composite materials. Natural composites in a human body are bone, dentin, cartilage, skin and others. They often exhibit hierarchical structures in which particulate, porous, and fibrous structural features, are seen on different micro-scales. In engineered biomaterials, it is important that each constituent of the composite is biocompatible. Some composites are used in TE and RM applications such as dental filling, reinforced bone cement and orthopedic implants with porous surfaces.

The bone cements and dental resins are strong and can be tailor-made. Recently, also a combination of ceramic particles and polymer matrixes has become the potential material for bone regeneration. The challenge with new biomaterials design is to achieve the complexity of the natural tissue by closely mimicking the extracellular matrix.

1.3 Bone and Bone Tissue Engineering

Bone is one of the main building blocks of the human skeletal tissue, which supports and protects various organs of the body, store minerals and produce red and white blood cells. It is a dense connective tissue, where the extracellular matrix is a composite inorganic-organic material. The inorganic materials make up to 70 % of bone, i.e. mostly hydroxyapatite mineral ($Ca_{10}(PO_4)_6(OH)_2$) and some other inorganic salts, the rest 30 % are organic, mostly collagen I fibrils, but there are also some proteins present. *In vivo,* bone contains between 10 % and 20 % water. The HA mineral gives bones their rigidity, which is nicely complemented by the elastic protein, collagen. The ratio between Ca:P in bone mineral is ranging from 1.37-1.87, whereas synthetic HA has a Ca:P ratio of (1.67). The hardening matrix encapsulates osteoblasts, osteoclasts and osteocytes and is constantly metabolically active, resulting in high regenerative potential. There are two types of mineralized tissue – cortical and cancellous. The harder outer layer of bone is the cortical or compact bone, which accounts for 80 % of the total bone mass in adult. The inner parts of the bones are filled with cancellous bone or the so-called spongy bone. It is an open porous network, with ten times more surface area than compact bone. Both, compact and cancellous bones are highly vascularized. [9]

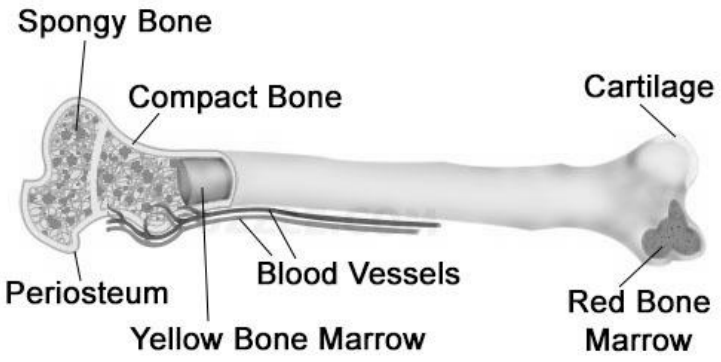


Figure 1.3: Bone structure.

In Table 1.2 the comparison of Young's modulus of bone, collagen and hydroxyapatite is given. The compressive and tensile strength of bone during loading of different directions are shown in Table 1.3.

Table 1.2: Young's modulus of bone building blocks and the bone itself [10].

Material	Young's Modulus, E (GPa)
Collagen (dry)	6
Bone mineral (Hydroxyapatite)	80
Cancellous bone	0.001-0.002
Cortical bone, longitudinal	11-21
Cortical bone, transverse	5-13

As previously mentioned, bones are subjected to bending moments during normal loading. These create both tensile and compressive stresses in different regions of the bone. There is a large difference in measured values of both tensile and compressive strength of the bone (Table 1.3). As forces, on our body, are differently supported by the bones, different bones may exhibit unlike strengths. In addition, the bone strength is decreased with increasing the age of a person.

Table 1.3: Mechanical properties of bone with a different direction of measurement [10].

	Longitudinal direction	Transverse direction
Tensile strength (MPa)	60-70	~50
Compressive strength (MPa)	70-280	~50

The bone mineral material exhibits normal Hookean elastic behavior, i.e. a linear stress-strain relationship, typical for ceramic materials. In contrast, polymeric collagen exhibits a J-shaped stress-strain curve [11]. Compact bone under tension or compression in wet conditions expresses more or less a straight line of stress-strain relation. As bone can be elongated for only 0.5 – 3 % it can be categorized as a brittle solid.

The skeleton provides mechanical support to soft tissues and provides levers for muscle action, and its ability to articulate in various opposing directions is fundamental to mobility and locomotion. It also has important roles in maintaining blood calcium levels, supporting blood formation and housing the brain and the spinal cord. Consequently, skeletal defects often incur considerable morbidity. In bone, certain tissue defects are caused by ageing, trauma, disease, tumours, and developmental abnormalities. Even though bone tissue has a high regeneration capacity; with large defects, its regeneration is limited and requires some assistance [10].

1.4 Scaffolds for Bone Tissue Engineering

Tissue engineering constructs or scaffolds are three-dimensional and highly porous structures with interconnected pore network, suitable for cell (in)growth and flow of nutrients and metabolic waste. Further, they should be biocompatible, bioresorbable with controllable degradation rate to match cell/tissue growth, and they should exhibit suitable mechanical properties to match the tissues at the site of the implementation. 3D constructs provide the necessary support for cells to proliferate and maintain their differentiated function, and their architecture defines the ultimate shape of the new tissue.

The TE construct for bone tissue regeneration should preferably possess high osteoconductive and angiogenic potentials, also biological safety, low patient morbidity, no size restrictions, and ready access to surgeons, long shelf life, and reasonable cost. For successful bone tissue, regeneration scaffold is crucial and should act as a temporary template, stimulating, guiding newly forming tissue. When fabricating this kind of scaffold mimicking structural, mechanical, degradation properties of the bone have shown the most promise. With this in mind, scaffold must be fabricated in a way to capture most favorable levels of all properties [12].

One of the major researched fields in tissue engineering is scaffold design, i.e. selection of suitable material, architecture, mechanical properties and degradation rate. The final scaffold design depends on the specific application; several general characteristics need to be considered for all scaffolds [1]:

- Biocompatibility: in terms of cell adhesion and normal cell functions, cells migration throughout the scaffold and cell proliferation, and negligible immune reaction.
- Biodegradability: to degrade at the suitable rate with which the body is forming its own new tissue. The by-products of scaffold's degradation should be non-toxic and able to exit the body without interference with other organs.
- Suitable mechanical properties: ideally, the scaffold should have mechanical properties consistent with the tissue that it is replacing and from a practical perspective, it must be strong enough to allow surgical handling during the implantation. Most probable key to success of any scaffold is the suitable relation between the mechanical properties and porous architecture that must be designed in a way to allow cell infiltration and vascularization.
- Scaffold architecture: interconnected pore structure and high porosity with mean pore size, depending on the target tissue.
- Scaffold application: overall, it must be practical, without complicated pre-implementation procedure in operating theater. Preferably scaffolds should be applicable with minimum invasive techniques, like injectable scaffolds, and should be available "off the shelf" without restricted environment preferences for storage.

The scaffold's potential to promote vascularization must not be left out from the important scaffold characteristics. As the bone is a highly vascularized tissue, the performance of the scaffold is dictated by its ability to induce new blood vessel formation. A blood vessel network supplies oxygen and nutrients, crucial for cell survival inside a scaffold. Some of osteoconductive or osteoinductive biomaterials/bone scaffolds

do not induce vascularization; therefore the choice of right material for bone regeneration construct is very important.

Scaffolds for bone tissue engineering can base on proteins and polysaccharides, isolated from natural sources, or can be fabricated from engineered biomaterials. In all cases, scaffolds can be a monophasic material or multi-material composite [13].

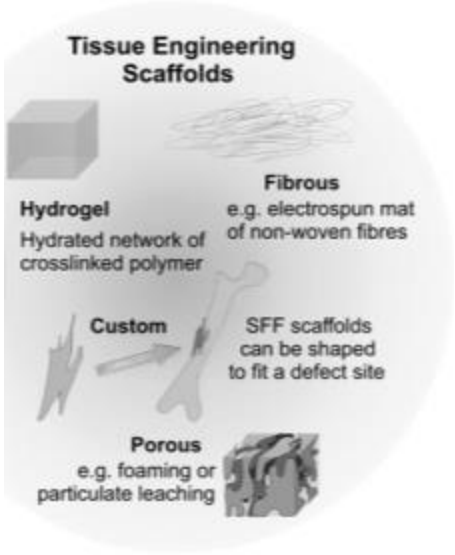


Figure 1.4: Most applied tissue engineering constructs [14].

1.4.1 Ceramic and glass scaffolds

Bioceramics are typically classified as bioinert or bioactive and have been applied to MD, which replaces the damaged tissue. Bioceramics have significant biocompatibility properties, particularly in bone as they share certain similarities. Hydroxyapatite- and beta-tricalcium phosphate-based scaffolds are already used in bone tissue engineering, however, due to some disadvantages like low solubility; there is still room for new biomaterials development and scaffold fabrication [15].

Calcium phosphates (CaP) are the most researched and applied bioceramics for bone regenerating scaffolds. As approximately 70 % of bone is made of calcium phosphates, i.e. hydroxyapatite, it is assumed for the CaP to have high biocompatibility. Calcium phosphates are osteoconductive, metabolized and degraded by the endogenous system for bone remodeling, although the speed of degradation varies depending on the crystallinity [16]. Thus, scaffolds for bone regeneration made of calcium phosphates are superior to autograft and allograft in terms of biosafety, quantity (unlimited), and invasiveness (low). Furthermore, they are made from limestone and mineral phosphates, being free from contamination by pathogens and free of donor site problems that occur with bone collection. However, the CaP scaffolds, used in clinical practice, are usually produced by a sintering process, which increases their mechanical properties, causes shrinkage in size and often decreases biodegradability, as well as shape adjustment during surgery. [17, 18]

Despite all the beneficial properties of CaP and HA, *in vivo* dissolution and degradation still represent a challenge. Due to limited solubility, the materials may not degrade completely, resulting in unwanted inflammatory reactions.

To resolve the low degradation issue, a novel amorphous material, bioactive glass (BAG), was suggested [19]. The advance over conventional bioceramics is in chemical

structure and the level of crystallinity. The BAG is an amorphous material with complete biodegradability leaving no solid or toxic degradation products when implanted. Chemical structure of the material is constructed of a network (Silicon oxides of Boron oxides), modified with different metal oxides (CaO, Na_2O, P_2O_5) or oxides of other metals. In the recent years BAG with different dopants have been much researched for different kinds of applications. The material's special characteristic is the ability to bond to soft and hard tissue. The BAG material, when immersed in simulated body fluid (SBF), precipitates HA crystals on its surface. This phenomenon is highly crucial for bone regeneration.

BAG can be produced by the quenching-milling or sol-gel process. In the recent years, by certain modifications of the existing sol-gel processes, the BAG particles obtained were nano-sized and mesoporous for easier processing as a scaffold (by itself or composite) or as a drug delivery system [20, 21].

Bioactive glass has attractive characteristics as a scaffold material for bone tissue engineering, but the application of glass scaffolds for the repair of load-bearing bone defects is often limited by their low mechanical strength and fracture toughness. Different techniques have been used to fabricate bioactive glass scaffolds, including sol–gel, thermally bonding of particles, fibers or spheres, polymer foam replication, freeze casting, and solid freeform fabrication. However, BAG scaffolds fabricated by these techniques usually do not have a favorable equilibrium between mechanical properties and 3D architecture. When one characteristic is designed to mimic bone, the other is fully sacrificed (high porosity equals low mechanical properties and vice versa).

1.4.2 Natural polymeric scaffolds

Natural polymeric scaffold usually exhibit appealing properties for tissue regeneration as biocompatibility and biodegradability. However, the lack of the bioactivity and mechanical stiffness limits their use in high load applications. These disadvantages can be resolved by different modifications or addition to the polymeric material (secondary phase, polymer blends etc.). The most commonly studied natural polymers for bone engineering are collagen/gelatin, chitosan, silk, alginate, hyaluronic acid, and peptides.

Collagen as a primary bone component was suggested as an ideal candidate for 3D scaffolds. It is composed of three polypeptides; each having a general amino acid sequence of $(\text{-Gly-X-Y-})_n$. The most abundant collagen in bone, collagen type I is composed of three left-handed helical polypeptide, which are tangled into a right-handed coil around a central molecular axis. Collagen expresses all the biocompatible properties required for the successful tissue regeneration. Despite its biocompatibility it is a highly pricey material and frequently replaced by lower quality gelatine (collagen derivate) [22, 23]. However, using collagen for cell substrate may cause some difficulties. Collagen, subject to its final form and process obtaining it, may potentially cause change in cell behaviour (e.g., changes in differentiation or proliferation), may have unsuitable mechanical properties, or undergo shrinkage [24].

Chitosan is a derivative of chitin, a structural element found in the exoskeleton of crustaceans such as shrimp, crab and lobster. Commercially available chitosan results from alkaline deacetylation of chitin. Chitosan possesses all the properties as the collagen does, but preferences as antibacterial, wound healing and bioadhesive properties make the material a great candidate for TE constructs. An important property of chitosan in the context of tissue engineering is the ease with which it can be functionalized. Reactive primary amines and primary and secondary hydroxyl groups present on chitosan allow

for the addition of side groups, peptides or amino acids, all of which can be important for optimizing chitosan for bone tissue engineering applications. In addition, chitosan is amenable to graft polymerization. Current difficulties with using chitosan as a polymer scaffold in tissue engineering, however, include low strength and inconsistent behaviour with seeded cells [25].

Silk fibroin, obtained from silkworms, is a natural polymer that has also been extensively used for tissue engineering applications [26-28]. This material has impressive mechanical properties, biocompatibility, controlled proteolytic biodegradability, and morphologic flexibility. Silk fibroin scaffolds typically degrade very slowly, they are stabilized without chemical cross-linking, and thus these systems retain their open porous features longer to promote the most consistent growth of cells and new tissue formation. The disadvantage of silk fibroin lies in high hydrophobicity causing low cell attachment, but low elasticity makes the material suitable for hard tissue engineering. Furthermore, its degradation products are acidic, which could cause a shift of physiological pH value.

Alginate is also an attractive polymer for 3D scaffolds for tissue regeneration. Alginic acid occurs as main cell wall constituent of brown macro alga in form of mix salts, making this material highly abundant and easily commercially available. Alginate is a linear unbranched polymer containing two different monomeric units, which easily processed into a 3D matrix by divalent metal ions cross-linking. Unfortunately, the two monomeric units degrade at different rates causing inflammations and construct failure. Further, alginate is one of the highly water-absorbent materials (hydrogel form) causing the 3D scaffolds swell to the point of possible failure. As the alginate is composed of two different building blocks, they degrade with various rates causing the scaffold to degrade unevenly and the problem of free-floating remains may occur. [29]

Hyaluronan is non-sulfated glycosaminoglycan distributed widely throughout connective, epithelial and nervous tissues. Hyaluronic acid (HAc) is a linear, negatively charged polysaccharide, constituted by a mixture of two sugars. It is soluble in water and is not resistant to enzymatic degradation [30]. The main advantage of hyaluronic acid is that it is an important component of the extracellular matrix. Moreover, it has the possibility of being administrated as an injectable system and is biocompatible. HA has also demonstrated potential as bone scaffold material [31]. It is naturally occurring, hydrophilic, not immunogenic, and has been found in the cytoplasm of osteoprogenitor cells. This natural polymer has been used in combination with other materials, factors, and drugs to enhance its osteogenic potential [32, 33].

A linear anionic polysaccharide, gellan gum (GG), is composed of tetrasaccharide repeating units of 1,3-ß-D-glucose, 1,4-ß-Dglucoronic acid, 1,4-ß-D-glucose, 1,4-α-rhamnose, containing one carboxyl side group[34]. There are two forms of gellan gum, acetylated, which is the initial product produced by Sphingomonas paucimobilis, and deacetylated, the processed and the most common form. As its production is uncomplicated, the low acyl gellan gum is economically accessible and does not transmit possible immunogenicity triggers. They form thermos-reversible gels with differences in mechanical properties from soft and elastic for acetylated form, to more firm for fully deacetylated polysaccharide [35]. Gellan gum can be easily processed into transparent gels that are resistant to heat and acid stress without the use of harsh reagents [36]. It is not cytotoxic and can be used as “off-the-shelf” [37] as well as an injectable system [38].

1.4.3 Synthetic polymeric scaffolds [39, 40]

Aliphatic polyesters such as polyglycolic acid, polylactic acid, and polycaprolactone are the most commonly used polyesters for tissue engineering applications. Their degradation products are present in the human body and can be removed by natural metabolic pathways. 3D scaffolds from these materials can be fabricated by various techniques, and by tuning the molar ratios of these polymers, mechanical properties and degradation rates can be favourably adjusted.

Polyglycolic acid (PGA) is the simplest linear, aliphatic polyester, which is crystalline. The degree of crystallinity results in high melting point and low solubility in organic solvents. Even though, the first synthetic and the absorbable suture was developed from it. PGA is relatively hydrophilic, so it degrades quite fast in aqueous media or *in vivo*, losing its mechanical integrity in two to four weeks.

Polylactic acid (PLA) is a chiral molecule. Comparing with PGA, the extra methyl group in the PLA repeating unit results in a more hydrophobic nature and lower molecular affinity to water, leading to a slower hydrolysis. Therefore, PLA scaffold of the implant is mechanically stable many months or even years *in vitro* or *in vivo*.

Polycaprolactone (PCL) is a commercially available semi-crystalline material. Its high solubility, low melting point (59-64 °C), and its exceptional ability to form blends have roused research to apply it as a biomaterial. Polycaprolactone degrades at a slower pace than PLA and can therefore be used in TE construct with a longer stability period. The material is nontoxic and tissue-compatible.

PGA, PLA, and PCL have been particularly prevalent as they already had a range of medical applications (e.g. in degradable sutures, stents, wound dressings) and had FDA approval for those devices [41]. However, these polymers are hydrophobic, which can be disadvantageous in tissue regeneration applications, due to poor wetting and lack of cellular attachment and interaction. Recently plasma treatment of the polymer surface has gone some way to overcoming this issue, although the effects may not be permanent [42].

Poly (ethylene glycol) (PEG) is a non-degradable polyether of the monomer ethylene glycol. Commonly, "PEG" is used to refer to the polymer with molecular weight less than 50,000 Da. High-molecular-weight form of PEG, however, is water-soluble and its solutions can be categorized as a hydrogel. PEG hydrogels for biomedical applications are typically composed of polymer chains that are cross-linked. These cross-linked networks frequently contain chemical bonds between the PEG chains and the cross-linkable moieties, which are prone to aqueous hydrolysis and are therefore characterized as biodegradable systems. The molecular weight of the PEG chains cross-linked in such hydrogels is below a threshold molecular weight to allow for complete resorption by the renal elimination of the individual chains.

Favorable characteristics of PEG are its high hydrophilicity, bioinertness, and outstanding biocompatibility. PEG is frequently used as a hydrophilic polymeric building block in copolymers with more hydrophobic degradable or non-degradable polymers for drug delivery, gene delivery, and tissue engineering scaffolds, medical devices, and implants. PEG has also been immobilized on polymeric biomaterial surfaces to make them resistant to protein adsorption and cell adhesion. These effects are attributed to highly hydrated PEG chains on the polymer surfaces that exhibit steric repulsion based

on an osmotic or entropic mechanism. A variety of PEG-containing block copolymers for injectable drug delivery have been developed over the last decades.

Copolymers, in general, are attractive for tissue engineering applications because their physicochemical properties are highly controllable. Gel formation dynamics, crosslinking density, and material mechanical and degradation properties can be controlled by regulating molecular weights, block structures, degradable linkages, and crosslinking modes.

As mentioned before, biopolymeric materials can be classified regarding their origin to – natural or synthetic. Further, regarding their structural composition they are classified as homopolymeric, copolymeric and multipolymer material. Homopolymers are referred to polymer network derived from a single species of monomer, where copolymeric and multipolymer polymeric networks are composed of at least two different monomeric units. Depending on the structural characteristics of the polymer, the degradation rate may differ. In co- and multi-polymers, monomeric units may degrade at different speeds, causing scaffold to degrade unevenly, resulting in a possible unwanted immunogenic reaction. Like ceramics, polymers can also be amorphous, semi-crystalline or crystalline. The degree of crystallinity also affects the degradation and other characteristics of the scaffold.

1.4.4 Inorganic-organic composite scaffolds

From a biological perspective, the inorganic-organic nanocomposite scaffolds replicate the structure of the bone tissue, where the polymer component mimics the collagen-rich ECM and the inorganic component, the carbonated HA. The composite scaffolds have a significant advantage over single material scaffold as the bioactivity, biodegradability, mechanical properties and biological, physical and structural characteristics can be designed to best fit the requirements for a successfully regenerating defect. It is expected that most favourable scaffolds could be obtained by composite materials of two or more building blocks (inorganic-organic system).

As mentioned above, bioceramics are mechanically stronger than polymers and play a crucial role in providing mechanical stability to construct before the formation of a new bone. However, most bioceramics are very brittle, which can cause a catastrophic failure of the material. Choosing nanocomposite materials for scaffolds fabrication may result in a scaffold with favourable properties of both phases (organic and inorganic). By introducing nanoparticles or nanofibers into organic polymer matrices, nanocomposite materials are fabricated. The size of the filler particles is an important parameter. As the nano-sized particles have a larger surface area, they can form a stronger interface with polymer matrix in composites, and hence, improved mechanical properties are expected. Still, problems associated with particle agglomeration may be more pronounced when using nanoparticles.

1.4.5 Cross-linking chemistry

Polymeric networks that absorb and hold massive amounts of liquid (aqueous media) are termed hydrogels. In the polymeric networks, hydrophilic groups or domains are present, which are hydrated in an aqueous environment thereby creating the hydrogel structure. As the term ‘network’ implies, crosslinks have to be present to avoid dissolution of the hydrophilic polymer chains/segments into the aqueous phase. Either chemical or physical methods have been used to create hydrogels. In chemically crosslinked gels, covalent bonds are present between different polymer chains. In physically crosslinked gels, instant

dissolution is prevented by physical interactions, which exist between different polymer chains. [43, 44]

Chemically crosslinked gels (Figure 1.5) can be obtained by radical polymerization of low molecular weight monomers in the presence of crosslinking agents. On the other hand, physically crosslinked hydrogels are synthesized by ionic interaction, crystallization, protein interaction and hydrogen bond. When ionic interactions form a hydrogel, they can be obtained under mild conditions, at room temperature and physiological pH. This process of cross-linking does not require the presence of ionic groups in the polymer. The use of metallic ions results in stronger hydrogel [45]. During the degradation of the polymeric hydrogel or scaffold the bonds between the polymers chains can be broken in physiological conditions either enzymatically or chemically, in most of the cases by hydrolysis [46].

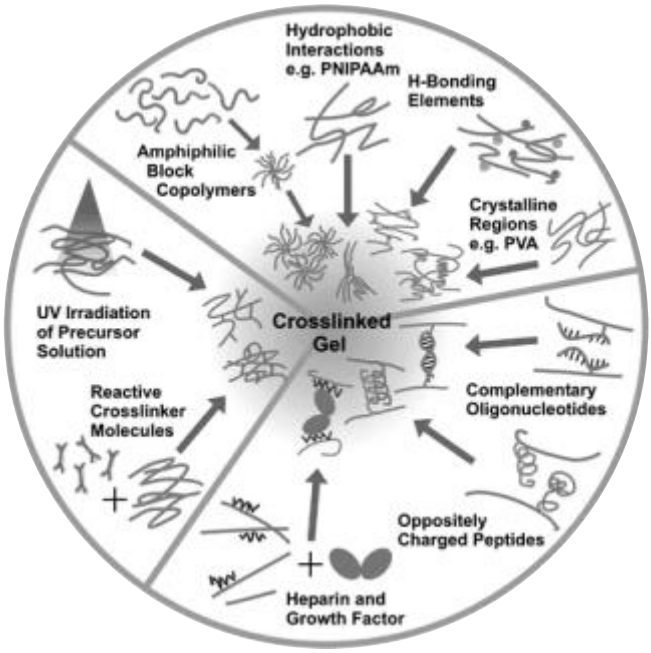


Figure 1.5: Cross-linking possibilities to form hydrogel [14].

An ideal hydrogel injectable system would be delivered as a viscous solution that would precisely fill irregularly shaped defects before gelling, *in situ*, under mild conditions. This may be achieved by the simultaneous delivery of reactive precursors from separate syringe barrels. Unfortunately, the kinetics of chemical crosslinking can be inappropriate, either too fast to allow the mixture to flow or slower than would be convenient. Conversely, by their very nature physical hydrogels do not have such aggressive reactivity. Furthermore, they are formed in equilibrium reactions, which can be controlled, by the solvent, salt concentration, pH or temperature. Therefore, the careful design of crosslinking groups can yield materials, which gel when introduced to a physiological environment [47, 48].

1.4.6 Fabrication techniques

Common techniques to fabricate 3D composite scaffold are thermally induced phase separation (TIPS), solvent casting/particle leaching, and electrospinning. With these fabrication processes an anisotropic scaffold architecture and porosity, which is more similar to the structure of the natural tissues, is obtained. [49, 50]

One of the scaffold fabricating techniques that base on thermally induced phase separation (TIPS) is freeze drying (FD), also called lyophilization. It is a dehydration technique, which enables liquid that has been previously frozen to be removed under a vacuum (sublimation). With freeze-drying storage life of the product is prolonged. The initial freezing process is carried out in a manner to obtain a desired crystalline structure of the product, where it is important that the product is frozen below its eutectic temperature. In the freezing step phase separation occurs – polymer rich and low polymer phases are obtained. Next the primary (sublimation) phase takes place, where the partial pressure of the vapor surrounding the sample/material must be lower than the pressure of the vapor from the ice, at the same T. In this phase it is highly significant for the energy supplied in form of heat to remain lower than the product's eutectic T. In the second drying phase, it is aimed to eliminate the final traces of water absorbed from the product. In freeze-drying, it is essential to avoid the liquid phase. Therefore, it is unconditionally crucial to lower the partial pressure of water, below the triple point pressure. Freeze-drying is a complex operation where the following aspects play a significant role: freezing, drying, vacuum influence, the shelf, on which the product is placed, and essential control aspects during freeze-drying. Upon completed freezing of the product, the product will have attained a frozen structure which cannot be reformed during freeze drying. The qualities of the finished product and sublimation depend greatly on this crystal structure. In fact, it is considered the most crucial stage of the freeze-drying.

Scaffolds obtained are highly porous with anisotropic morphology and extensive pore interconnectivity. By changing the polymer concentration in the solution, the volume fraction of the secondary phase and freezing temperature of FD process, microporosity, pore morphology, mechanical properties, bioactivity and degradation rates of produced scaffolds can be carefully designed. The disadvantages of this technique are shrinkage issue and long-time solvent sublimation. [51]

To produce a biocomposite scaffold by solvent casting, the polymer must be dissolved in an organic solvent, to which inorganic particles are added and then the mixture is cast into the predefined 3D mold and left for the solvent to evaporate. The simplicity of fabrication without the need for specialized equipment is the primary advantage of this process. Despite the simple steps of this fabrication technique, there are still some disadvantages like the limitation of scaffolds shape that could be produced, possible retention of toxic solvent and the denaturation of the proteins and other molecules incorporated into the polymer by the use of organic solvents. In addition, the use of organic solvents may decrease the activity of bioinductive molecules (e.g. protein). [52]

As with the solvent casting, inorganic-organic scaffolds can also be obtained by the solvent aggregation method. First, polymeric microspheres are formed from water – oil/water emulsion. Then, by addition of salt or sugar particles, ceramic granules, and pre-hardened microspheres, solvent-aggregated polymer-ceramic scaffolds are formed. To obtain a 3D structure of controlled porosity, the solvent casting must be combined with particle leaching and microsphere packing process. The solvent casting method shares similar advantages and disadvantages with the solvent casting technique. [53]

Electrospinning of polymeric scaffold shows high potential. Here, the polymer solution is injected through a needle under an electric field where a spinning surface gives shape to the scaffold out of forming fibers. Although it was primarily designed for polymeric scaffolds, ceramic-polymer composites were also successfully fabricated using this approach. [54]

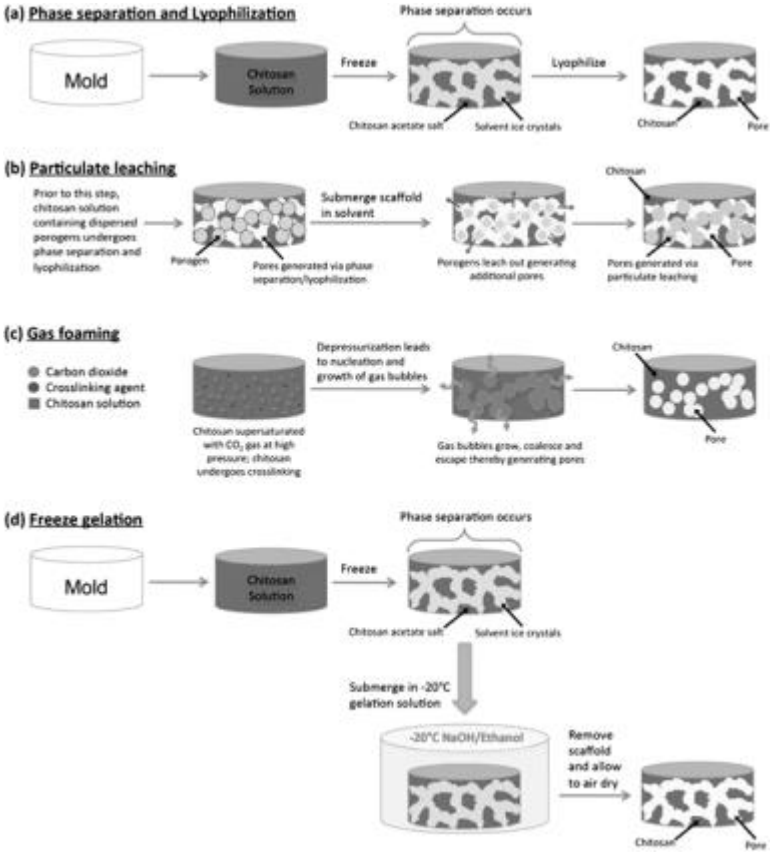


Figure 1.6: Presentation of possible fabrication processes by steps applicable to different materials. Phase separation, lyophilization, particle leaching, gas foaming, freeze gelation [55].

More isotropic scaffold architecture can be obtained by solid free form (SFF) techniques, like fused deposition modeling, stereolithography, selective laser sintering, 3D printing and wax printing. All SFF systems use a structure of scaffold architecture designs, usually generated by hierarchical image-based or computer-aided techniques, and build the 3D structure on a platform that moves to allow layering. The problem with these processes is an insufficient resolution at the micro scale. [56]

Chapter 2

Aim and Hypothesis

Inorganic-organic composite scaffolds have been extensively investigated in recent years for potential applications in hard tissues regeneration. The trend is introducing 3D TE constructs made out of materials, which are not only biodegradable at the appropriate rate but also osteoconductive. Despite the rising number of scientific publications, there is still no general agreement on the optimal material composition and design of scaffolds. Lately, gellan gum was introduced into biomedical field. Already several publications can be found, studying gellan gum for different tissue engineering applications, like bone [57], cartilage [58] and skin regeneration [59]. They report that it can be easily processed into a hydrogel or highly porous matrix (dry scaffold) with relatively favourable, but not optimal properties. Additionally, new family of injectable supramolecular hydrogels based on interactions between thiols and metal ions has been developed. The advantages of these supramolecular hydrogels are self-healing capacity and shear-thickening behavior. Mechanical properties of hydrogels could be adjusted by varying the amount of supramolecular cross-linker. 4-arm thiolated PEG, which is one of the synthetic polymers already used in medicine, has been proposed for bone tissue engineering applications [60]. However, similarly as the GG, Au-(PEGSH)4 lacks the ability to form bone-like mineral phase.

Regardless of all the promising characteristics of the both gellan gum and polyethylene glycol, they hardly present cell adhesion properties, similar to other hydrogels; as they all lack cell anchorage points and/or are highly hydrophilic promoting water molecules bonding to the polymer backbone, inhibiting cell adhesion. In addition, the polymer hydrogels and dry scaffolds have low ability to carry mechanical loading due to their extremely low modulus of elasticity. To overcome the above-mentioned limitations of the gellan gum and 4-arm thiolated PEG, the approach used in this study was incorporating biodegradable, osteoconductive inorganic particles – nanoparticulate bioactive glass. It was proposed that in addition to the formation of hydroxyapatite during biodegradation, mechanical properties and osteoconductivity of tissue engineered constructs (GG and Au-(PEGSH)4) will be enhanced by BAG particles incorporation.

Thus, the main objective of this study was to prepare and characterize two types of composite scaffolds, one in the form of “off-the-shelf” dry scaffold, and the other as injectable hydrogel, both with the ability to form bone mineral and carry higher loads than the polymers alone. The effect of nanoparticulate bioactive glass powders with two different compositions (a 4-component and a 2-component BAG) on the properties of both types of scaffolds was studied. To fabricate scaffolds with favorable properties, like suitable architecture, i.e. high porosity with sufficiently large and interconnected pores,

degradability and bioactivity, bioactive glass was added in different percentages. Freeze-drying was used as a technique for fabrication of dry scaffolds.

Chapter 3

Material and Methods

3.1 Gellan Gum - Bioactive Glass Scaffolds

3.1.1 Scaffold fabrication

3.1.1.1 Gellan gum hydrogel preparation

Gellan gum powder (Sigma, USA) was dissolved in ultrapure water in concentration of 2.0 w/v %, constantly stirring at 90 °C to linearize the GG chains. To ensure complete linearization of the GG chains, the solution was stirred for at least 30 minutes, at first at 400 rpm for 25 minutes, then at 100-150 rpm to eliminate air bubbles from the solution, which could disturb the microstructure/porosity of the scaffold in making. Afterwards, the 0.18 w/v % warm (50 °C) $CaCl_2$ (Sigma, USA) solution was added to the GG solution. Quickly, the solution was cast into the Petri dish, where it was let to cool. Due to the temperature drop and the presence of certain ions, the solution spontaneously cross-linked and jellified. Discs of Ø 10 ± 0.47 mm and 5 ± 0.32 mm height were cut out and stored in a phosphate buffered saline (PBS) solution (Sigma, USA) for further stabilization for a maximum of 48 hours. For cell culture studies, all materials were sterilized by ethylene oxide.

3.1.1.2 Gellan gum – bioactive glass hydrogel preparation

Bioactive glass powders were synthesized by modified sol-gel precipitation under alkaline conditions described elsewhere [21] and thermally treated at 600 °C to remove any organic residues. BAG with two compositions were used: (A) a 2-component BAG-A with 70 n/n % SiO_2 and 30 n/n % CaO, and (B) a 4-component BAG-B containing 66 n/n % SiO_2, 22 n/n % CaO, 10 n/n % Na_2O and 2 n/n % P_2O_5.

Next, gellan gum powder was dissolved in ultrapure water. The solution was stirred at 90 °C to linearize the GG chains. Meanwhile, the desired amount of BAG powder was dispersed in ultrapure water using an ultrasonic finger for 3 minutes with a power of 400 W at 50 % amplitude and a 0.5 s pulse (Hielscher Ultrasonics, Germany). The aqueous dispersion of BAG particles was then mixed into the GG solution, left stirring, then the 0.18 w/v % $CaCl_2$ solution was added to the mixture (the final concentrations of $CaCl_2$ are in Table 3.1), which was afterward poured into the Petri dish to jellify and cross-link. Discs of Ø 10 ± 0.47 mm and 5 ± 0.32 mm height were cut out and stored in phosphate buffered saline (PBS) solution (Sigma, USA) for further stabilization for a maximum of 48 hours. For cell culture studies, all materials were sterilized by ethylene oxide.

3.1.1.3 Preparation of porous gellan gum – bioactive glass scaffold with high bioactive glass percentage (foaming process)

With high percentage of BAG powder in the composite (GG-70BAG and GG-90BAG), the above mentioned process of GG-BAG hydrogel preparation had to be modified to obtain porous structures. During the highly BAG reinforced sample preparation, liquid hydrogen peroxide (H_2O_2, Sigma, USA) was added to the GG-70BAG and GG-90BAG mixture. Again 2 w/v % gellan gum solution was prepared. Meanwhile, BAG powder was dispersed in ultrapure water by ultra-sonification. The solution and the dispersion were combined, then the warm solution of $CaCl_2$ was added and mixed well (see Table 3.1 for detailed composition). In the last step, H_2O_2 was added, obtaining a final concentration of 10 w/w % of pure H_2O_2. Again, the mixture was mixed well and placed into the oven at 45 °C for 2 h for the degradation reaction of the H_2O_2 to occur and for the mixture to spontaneously jellify. The degradation of the H_2O_2 formed bubbles into the structures during the drying/jellifying step, forming additional interconnected pores. In the end, the samples were frozen (at -20 °C) and freeze-dried.

Table 3.1: Final composition of prepared gellan gum hydrogels and gellan gum-bioactive glass composite hydrogels.

Sample name	water [w/w %]	gellan gum [w/w %]	BAG-A* [w/w %]	BAG-B* [w/w %]	$CaCl_2$ [w/w %]
GG	98.01	1.96	0		0.030
GG-33A	97.06	1.94	0.97		0.029
GG-50A	96.13	1.92	1.92		0.029
GG-70A	93.72	1.88	4.38		0.028
GG-90A	83.31	1.67	15		0.025
GG-33B	97.06	1.94		0.97	0.029
GG-50B	96.13	1.92		1.92	0.029

*BAG-A: 2-component bioactive glass particles (70 % SiO_2 and 30 % CaO (n/n %))

*BAG-B: 4-component bioactive glass particles (66 % SiO_2, 22 % CaO, 10 % Na_2O and 2 % P_2O_5 (n/n %))

3.1.1.4 Freeze-drying process

To obtain a highly porous, three-dimensional structure (dry scaffold), freeze-drying was applied. The method exploits thermally-induced phase separation. After 48 h stabilization in PBS, samples are frozen at -20 °C or -80 °C overnight prior the freeze-drying. Then frozen samples are placed into the freeze-dryer, where the vacuum of 0.1 mbar is generated. The material is freeze-dried for 72 hours in Telstar Cryodos-80 freeze-dryer (Telstar, Spain) or Lio-5 (Kambič, Slovenia).

3.1.2 Characterization

3.1.2.1 Electron microscopy

The microstructure of the GG-BAG composites in the form of dry scaffolds was observed in cross-section using a field-emission-gun scanning electron microscope (FEG-SEM)

(JEOL JSM 7600F, USA) equipped with an energy-dispersive X-ray spectrometer (EDXS) system from INCA Oxford Instruments.

3.1.2.2 X-ray microtomography

The three-dimensional structure and porosity of the dry scaffolds were further analyzed (one representative sample per composition) by micro-computed tomography (µ-CT) using a high-resolution µ-CT scanner (Skyscan, Konitch, Belgium) with a pixel size resolution of 11.3 µm and an integration time of 1.6 ms. The X-ray source was set to 32 keV and 191 µA. The data sets were reconstructed using standard cone-beam reconstruction software (NRecon v1.4.3, Skyscan, Belgium).

3.1.2.3 Compression test

The mechanical properties of the samples in all three forms (hydrogels, dry scaffolds and rehydrated scaffolds) were analyzed using compression tests (Instron 5542, Instron, USA). Discs with the dimensions described above were loaded at a rate of 0.2 mm/min until failure. The apparent Young's modulus was estimated from the slope of the linear region of the stress-strain curves in the 0-1% strain range. Five replicates per sample were tested.

3.1.2.4 Rheology measurements

Small amplitude oscillatory shear (SAOS) measurements were done on a rheometer (AntonPaar MCR 301, Austria) using 50 mm cone and plate fixture, with a cone angle of 1 °. The sample holder was preheated to 90 °C, the exact amount of the sample in a form of a solution was pipetted and dropped onto the fixture. This assures a good contact between the sample and the fixture. To prevent evaporation of water from the sample, paraffin oil was poured around the perimeter of the sample. Due to its low viscosity, the results were not affected.

In the end, the samples were visually checked that there was no mixing of the sample with the paraffin oil. The specimens were cooled down to 25 °C at the rate of 0.5 K/min, and during cooling viscoelastic properties were measured. To determine the linear viscoelastic (VE) region of hydrogels, separate strain sweep tests were made. Based on these results, a common strain value was chosen and later used to record VE properties during cooling, and frequency sweeps. Each sample was used for a strain sweep test in a strain-controlled mode at the end, to ensure that all the measurements done in the linear region.

3.1.2.5 Wettability measurements

The wetting angles of GG and GG-BAG composite hydrogels and dry scaffolds were measured using a tensiometer (Attension, KSV Instruments).

3.1.2.6 Fourier transform infrared spectroscopy (FT-IR)

Fourier transform infrared (FT-IR) measurements of GG and GG-BAG hydrogels, dry scaffolds and rehydrated scaffolds were monitored with an FT-IR spectrophotometer (PerkinElmer Spectrum 100 FT-IR) equipped with an ATR (Attenuated Total Reflection) in the mid-IR range 400-1400 or 2000 cm^{-1}.

3.1.2.7 Differential scanning calorimetry (DSC) analysis

The DSC thermograms of GG hydrogel and GG-BAG composite hydrogels were analysed using DSC 1, Mettler Toledo instrument (Columbus, OH, USA) with a dry nitrogen purge (flux gas of 50 cm^3/min). Both temperature and heat flux were calibrated with indium at a scanning rate of 10 °C/min. All the experiments were performed with a regime of starting from 25 °C, cooling the hydrogel to -80 °C and then heating back to 25 °C, and again repeating the cooling. Samples used for the DSC analysis had the final composition shown in Table 3.1 and were in the form of a hydrogel.

3.1.2.8 *In vitro* degradation, weight loss, swelling and pH change

The dissolution of the GG and GG-BAG rehydrated scaffolds was evaluated by measuring the weight loss during immersion in the PBS solution for 48 hours (after 48 h rehydration step). The rehydrated scaffolds were immersed into 20 mL of PBS solution each and placed on a shaker at an ambient temperature of 37 °C. After 48 hours the samples were removed from the solution. Before weighing, the excess water was removed by placing the disc between sheets of filter paper. Prior to degradation, the water uptake of the dry scaffolds was assessed by measuring the weight gain after 48 h immersion.

A more detailed degradation process (weight loss profile) was determined for GG and GG-50A dry scaffolds over time of 30 days. Six samples per material were immersed in 5 mL PBS and placed into shaker at ambient temperature 37 °C. Their weight was measured after 1, 2, 4, and 8 h and 1, 7, 14, 21 and 30 days of immersion. Prior to weighting excess water was removed by placing samples in between sheets of filter paper.

During the degradation of GG and GG-50A dry scaffolds also pH was measured (pH meter Metrohm, Switzerland), evaluating the pH profile over time of 3 days in PBS. The concentration of the material was 1 mg/mL. Results were compared to the pH profile of BAG compressed powder, measured by the same procedure described above.

The degree of swelling in GG and GG-50A dry scaffolds was evaluated by measuring the diameter of the samples. Three samples per material were immersed in 10 mL of PBS and placed at the temperature of 37 °C. The samples were fabricated in the shape of a ring with an inner diameter of 8.28 ± 0.16 mm and an outer diameter of 17.33 ± 0.18 mm for GG after 1 h PBS immersion. The inner and outer diameters of GG-50A were 8.72 ± 0.29 mm and 17.26 ± 0.11 mm, respectively. The diameters were measured at time points of 1, 2, 4 and 8 h and 1, 2, 3 and 7 days.

3.1.2.9 Spectral characterization of diffusion

Measurements were done on a TecMag NMR spectrometer with a 2.35 T horizontal bore superconductive magnet equipped with micro-imaging accessories and reversed Helmholtz gradient coils with 5.9 T/m peak magnetic field gradient. The sample bed was a 30 mm long cylindrical cell with the diameter $d = 5$ mm and oriented with cylinder axis perpendicular to the static magnetic field and to the gradient direction. The CPMG pulse train of π-RF pulses, of the length $\delta = 2.8$ μs and applied to spins in the static magnetic field gradient, were used to measure the molecular DPS in a water-saturated rehydrated scaffolds of GG and GG-50A. We optimized the first echo spacing to $T/2 - \delta / \pi$. The parameters of measurement correspond to the range of offset frequencies $\Delta \omega / \omega_1 = \gamma G d \delta / \pi = \pm 0.14$, which is narrow enough that the observe peak of spin echo contains only the direct coherence pathway. In order to exclude the effect of spin relaxation, the acquisition time was kept constant at $\tau = NT = 40$ ms.

3.1.2.10 *In vitro* mineralization test

The ability of the GG and GG-BAG composites to induce apatite formation was estimated by immersing the hydrogel discs in simulated body fluid (SBF) for up to 30 days at 36.5 °C, according to a procedure described elsewhere [61]. After 14 and 30 days, the samples were dried, and their surfaces and cross-sections were observed with the FEG-SEM.

3.1.2.11 Cytotoxicity

The *in vitro* biological characterization was performed using human adipose stem cells (hASC) obtained from the protocol of the 3B's Research Group and Hospital da Prelada (Porto, Portugal). All the subjects enrolled in this research responded to an Informed Consent form, which was approved by the ethical committees of both these institutions (2007) and this protocol was found to be acceptable to all the subjects. The hASCs were isolated as described elsewhere [62] and cultured in an alpha-MEM medium (Invitrogen, USA) supplemented with 10 % fetal bovine serum (FBS) (Invitrogen, USA) and 1 % Antibiotic/Antimycotic (Invitrogen, USA). The cells in a concentration of 5×10^5 cells/scaffold were seeded onto the dry scaffolds, placed in 24-well plates and incubated for 1 hour for full hydration of the structure to form a rehydrated scaffold. A total of 1 ml of the complete culture medium was then added and the constructs were further incubated for 72 hours in a 5 % CO_2 atmosphere at 37 °C. The culture constructs were then stained with Calcein-AM (Ca-AM, Invitrogen, USA) and Propidium Iodide (PI, Invitrogen, USA) for the cell-viability evaluation. After the fixation with formalin cytoskeleton F-actin the fibres were stained with Phalloidin-TRITC (Sigma, USA) and the nuclei were counterstained with 4',6-diamidino-2-phenylindole (DAPI, Sigma, USA). The samples were observed with an AxioImager Z1m microscope (Zeiss, Germany) or Olympus Fluoview FV1000 laser confocal microscope (Olympus, Japan).

3.2 Polyethylene Glycol – Bioactive Glass Nanocomposite Hydrogels

3.2.1 Materials

All chemicals were purchased from Sigma-Aldrich, USA, if not stated otherwise.

3.2.2 Sample preparation

3.2.2.1 Ellman's test

Before preparing a Au-$(PEGSH)_4$-BAG nanocomposites, the concentration of the thiolated groups on the PEG was determined by Ellman's test (quantitative determination of sulfhydryl (-SH) groups). 4-armed thiolated polyethylene glycol was dissolved in the tris(hydroxymethyl)aminomethane (TRIS) buffer solution, to which the pH was adjusted to the value ~8.0. The Ellman's reagent, 5,5'-Dithiobis(2-nitrobenzoic acid) (DTNB), was separately dissolved in distilled water. The sample and the DTNB solution were mixed in a specific ratio, obtaining a transparent yellow solution, as the Ellman's reagent reacts with free thiole groups. The ultraviolet-visible (UV-vis) spectroscopy experiments were performed on a Jasco V-750 spectrophotometer. The high of an absorbance band at ~412 nm was determined, from which the concentration of free thiolated groups was calculated using the equation below [1]. The y in the equation is absorbance and x is concentration of the free thiolated groups present in the sample. Four samples per material were measured right after mixing them with the reactive components and after 5 minutes to ensure correctness of the results.

$$y=0.1664x-0.0286 \quad [1]$$

3.2.2.2 Fabrication of bioactive glass – polyethylene glycol nanocomposite hydrogels

4-arms thiol terminated poly(ethylene glycol) ($(PEGSH)_4$, Mn~10000 g mol^{-1}), gold (III) chloride hydrate ($HAuCl_4 \times 2H_2O$) and phenol red ($C_{19}H_{14}O_5S$) were purchased from Sigma-Aldrich (USA). To prepare composite hydrogels (10 w/v %), 100 mg of the $(PEGSH)_4$ was dissolved in 0.691 mL of deionized water. 5 µL of phenol red (0.07 M) was added as a visual pH indicator. Different amounts of bioactive glass (BAG; 50 mg, 100 mg and 200 mg) were added to the aqueous solution of $(PEGSH)_4$ and redispersed by ultra-sonication, resulting in a ratio $(PEGSH)_4$:BAG of 2:1, 1:1 and 1:2. 8.1 µL of 1.0 M aqueous solution of $HAuCl_4$ dissolved in 0.3 mL of deionized water, was added to the $(PEGSH)_4$-BAG mixture to form a 3D network. The pH of the hydrogels was adjusted to pH 7 by addition of HCl (1.0 M) (pH meter Metrohm, Switzerland). The compositions of the starting solutions and suspensions are given in Table 3.3.

Table 3.2: Composition of polyethylene glycol-bioactive glass hydrogel nanocomposites.

Sample name	Composition	Description
BAG	70 n/n % SiO_2 + 30 n/n % CaO	Powder, particles size ~100 nm, agglomerate size ~10 μm
Au-(PEGSH)$_4$	10 w/w % aqueous solution	4-armes thiol terminated poly(ethylene glycol) cross-linked with gold
Au-(PEGSH)$_4$-BAG$_5$	10 w/w % (PEGSH)4 solution with 5 w/w % BAG	hydrogel nanocomposite cross-linked with gold
Au-(PEGSH)$_4$-BAG$_{10}$	10 w/w % (PEGSH)$_4$ solution with 10 w/w % BAG	hydrogel nanocomposite cross-linked with gold
Au-(PEGSH)$_4$-BAG$_{20}$	10 w/w % (PEGSH)$_4$ solution with 20 w/w % BAG	hydrogel nanocomposite cross-linked with gold

3.2.3 Characterization

3.2.3.1 Electron microscopy

The distribution of BAG nanoparticles within freeze-dried Au-(PEGSH)$_4$-BAG hydrogel nanocomposites was observed using SEM (JEOL JSM5610-LV, USA). Freeze-dried samples of Au-(PEGSH)$_4$-BAG hydrogel nanocomposites deposited on carbon tape were sputter-coated with a thin layer of gold before the inspection to prevent sample-charging effects. SEM images of the samples were taken at an accelerating voltage of 20 kV. *In situ* X-ray spectroscopy (EDS) (INCA 300, Oxford) was used to estimate the elemental composition (Ca and Si) of BAG nanoparticles.

3.2.3.2 Rheology

Rheological measurements were carried by AR2000Ex (TA Instruments) rheometer using a parallel plates geometry (20 mm diameter acrylic plate). The pH of Au-(PEGSH)$_4$-BAG hydrogel nanocomposites and Au-(PEGSH)$_4$ hydrogel was previously adjusted at pH 7 and 10 with a Crison GLP22 pH meter. The experiments were conducted at constant temperature, i.e. 20 °C. Shear storage and loss moduli (G' and G", respectively) were obtained at a constant deformation (1 %) with increasing frequency (from 0.01 to 50 Hz). Gelation point of Au-(PEGSH)$_4$-BAG hydrogel nanocomposite with a ratio 1:1 ((PEGSH)$_4$:BAG) was monitored by studying the evolution of G' and G'' at 0.1 Hz for 600 min after mixing the two precursor solutions directly on the rheometer.

3.2.3.3 Compression test

Mechanical properties of the nanocomposite hydrogels in compression mode were estimated by INSTRON (3365 model) tensometer controlled by Bluehill Lite software. The samples prepared were formed in a disc shape 8.88 ± 0.32 mm in diameter and 8.77 ± 1.62 mm in height. One sample for each composition was tested.

3.2.3.4 Self-healing experiment

The self-healing ability of the Au-$(PEGSH)_4$-BAG hydrogel nanocomposites was examined by cutting the hydrogel samples into pieces and after that placing them again into the same mold. After 24 hours, the Au-$(PEGSH)_4$-BAG hydrogel nanocomposites were removed from the cylinder to observe its consistency.

The self-healing ability of Au-$(PEGSH)_4$-BAG hydrogel nanocomposite was examined by comparing the dynamic rheological properties of the material before and after the self-healing process of the same hydrogel cut into pieces and placed in the same mold with slight pressure during 24 hours.

3.2.3.5 *In vitro* BAG degradation (Franz cell, pH change, ICP-MS, *in vitro* mineralization)

The degradation of BAG nanoparticles and Au-$(PEGSH)_4$-BAG hydrogel nanocomposite was studied using a Franz cell placed into a water bath at 37 °C to simulate body temperature. The samples, with already adjusted pH (pH~7), were placed in the upper chamber of the cell, which is separated from the lower chamber by a cellulose membrane (cut-off 10,000 g mol^{-1}). Both chambers were then filled with ultrapure water. Over a period of 7 days, 100 µL aliquots were taken from the lower chamber. These were then diluted with an aqueous solution of 0.2 % HNO_3 and the concentration of Ca and Si (released during degradation) determined using Inductively Coupled Plasma-Mass Spectrometry (ICP-MS, ICPE-9000, Shimadzu). pH values of BAG, Au-$(PEGSH)_4$and Au-$(PEGSH)_4$-BAG_{10} specimens were measured during an 80-hour degradation.

The enhanced ability of Au-$(PEGSH)_4$-BAG_{10} hydrogel nanocomposite to induce apatite formation was estimated by immersing the hydrogels in simulated body fluid (SBF) for 7 and 30 days at 37 °C, according to the procedure described elsewhere [61], and compared to Au-$(PEGSH)_4$ hydrogel placed in the same conditions. Apatite crystals were observed by FEG-SEM of the dried hydrogel nanocomposite.

3.2.3.6 *In vitro* evaluation by cell culture (MTS and Tripan blue assay)

The effect of the degraded species from BAGS nanoparticles, Au-$(PEGSH)_4$ dynamic hydrogels and Au-$(PEGSH)_4$-BAG_{10} hydrogel nanocomposite on HeLa cell growth was evaluated using Cell Titer 96® Aqueous One Solution Cell Proliferation Assay (Promega) at day 1, 2 and 3. HeLa cells were seeded at a density of 3000 cells cm^{-2} in 24 well plates. 200 mg of each material was placed into an insert, which was set in each well of HeLa cultures. As a proliferation control for HeLa cells, cell culture media and Triton X-100 were used. Cells were cultured at 37 °C in a humidified incubator for 2 hours with 20 µl of Cell Titer 96® Aqueous One Solution Reagent containing tetrazolium compound [3-(4,5-dimethylthiazol-2-yl)-5-(3-carboxymethoxyphenyl)-2-(4-sulfophenyl)-2H-tetrazolium)] and an electron coupling reagent, phenazine ethosulfate (PES) per 100 µl of cultured media. The absorbance per well was measured at 490 nm using a micro-plate reader (Multiscan Sscent, Thermo). Cell doublings were calculated as follows: a number of cell doublings = log 2 (no. of cells at day 7/no. of cell-seeded).

Cell viability after BAG nanoparticles and hydrogels co-culture was assessed with Live-Dead assay (Invitrogen). HeLa cells were seeded at a density of 3000 cells cm^{-2} in 22-mm diameter coverslips (Menzel-Glaser). Samples were processed according to the manufacturer´s recommendation. On day 3, the inserts with the BAG nanoparticles or the hydrogels were removed from the 24 well culture plates, and cells attached to the coverslip were rinsed with PBS1X (Gibco) and processed for Live-Dead assay. Cells were

incubated with the ethidium-calcein mixture and incubated for 30 minutes at room temperature. After this treatment, the slides were prepared for microscopy on glass slides by mounting with Vectashield (Vector). A fluorescence microscope (Leica, DM 2000) and associated software were used to visualize the viability of cells.

Chapter 4

Results

4.1 Gellan Gum – Bioactive Glass Scaffolds

4.1.1 Samples preparation

Gellan gum (GG) and gellan gum-bioactive glass (GG-BAG) composites were prepared in three forms: A) hydrogel, B) dry scaffold and C) rehydrated scaffold. The processing steps are schematically presented in Figure 4.1 and the macro photographs of the products are in Figure 4.2. The hydrogel was obtained by addition of cross-linker $CaCl_2$ (the concentration of which was 0.025-0.03 w/w %) and temperature drop, prior which all GG solutions had to be heated to 90 °C to linearize the GG chains. The prepared hydrogels were highly dense and contained 83 to 98 % of water, depending on the composition (see Table 3.1). The hydrogel samples were immersed in PBS for 48 h stabilization, to complete hydration and achieve the equilibrium state by total solute/ion exchange. With freeze-drying highly porous structures (dry scaffolds) were obtained. In this form, the material would be available "off-the-shelf" suitable for storing for a longer period (months) without significant changes. Prior to application, dry scaffold must be rehydrated. Therefore, they were immersed in the PBS solution or other media for a certain period, to adopt their final shape (rehydrated scaffolds). Optionally, the cells can be introduced at this stage. The rehydrated scaffolds are visually similar to the initial hydrogel.

The GG concentration of 2 w/w % was selected to prepare all hydrogel samples as the solution was easily processed. With 3 w/w % GG solution the processing time was much prolonged and viscosity highly increased, in particular with BAG powder addition. With higher percentage, 4 w/w % and more, the gelzan powder did not completely dissolve in water.

Two different BAG compositions were used to prepare the composites; 2-component BAG-A with composition of 70 % SiO_2 and 30 % CaO (n/n %) and 4-component BAG-B, containing 66 % SiO_2, 22 % CaO, 10 % Na_2O and 2 % P_2O_5 (n/n %). Optionally, during the preparation of the samples, the BAG particles were dispersed in water by an ultrasonic finger before adding into the GG solution.

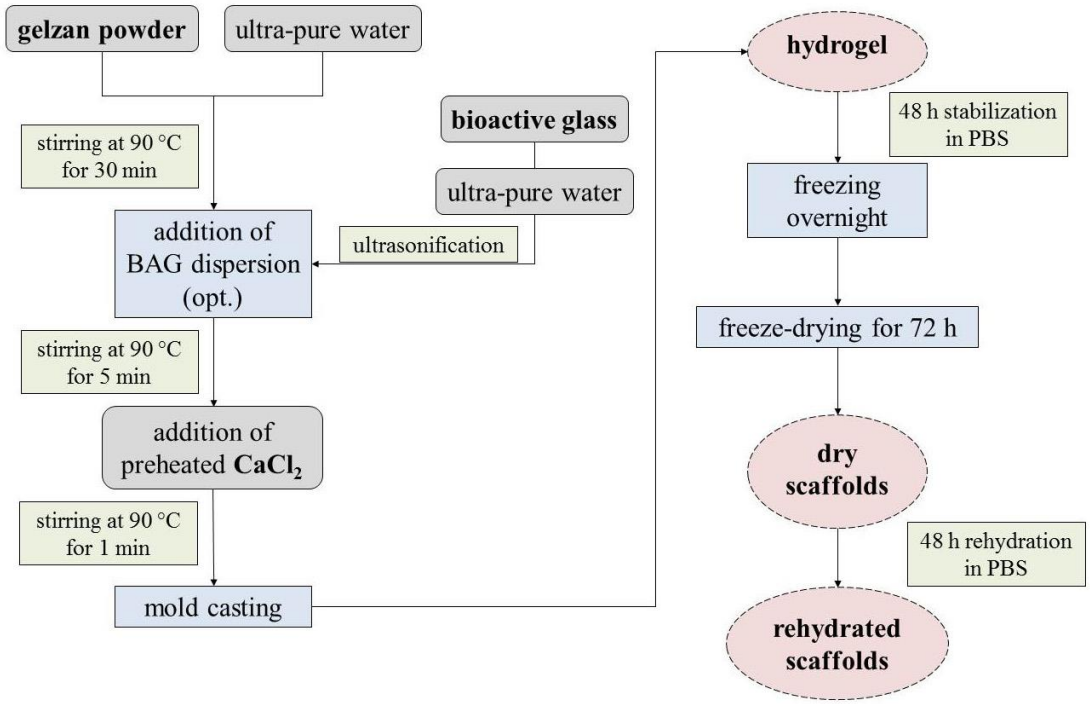


Figure 4.1: Schematic presentation of samples preparation.

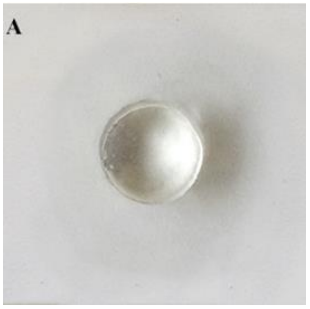
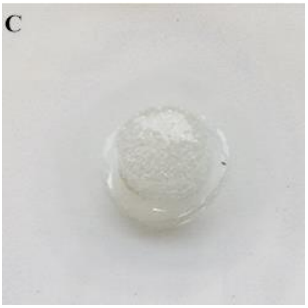
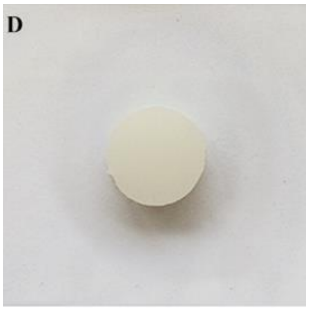
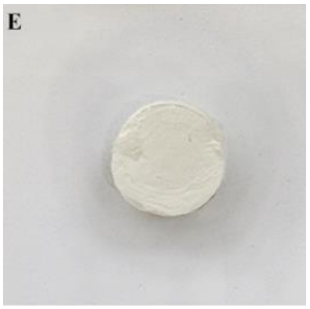
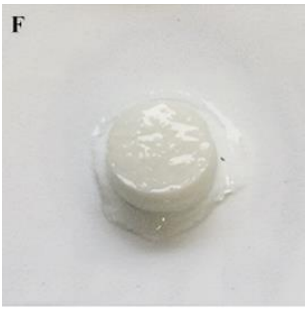
	hydrogel	dry scaffold	rehydrated scaffold
GG			
GG-BAG			

Figure 4.2: Macro photographs of GG (A, B, C) and GG-BAG (D, E, F). Materials are in the form of hydrogels (A, D), dry scaffolds (B, E) and rehydrated scaffolds (C, F).

The effect of BAG particles addition on gelation T of GG was examined by studying viscoelastic properties of the samples in the linear viscoelastic region. First, strain sweeps were performed within a wide range of shear strain, at which frequency of oscillation was set to 1.59 Hz (10 rad/s). The results suggested the used shear strain during cooling should be below 0.1 % in order to stay in linear viscoelastic region and not to destroy the network. The samples, GG solution or GG-50A dispersion, were then poured onto preheated (T = 90 °C) rheometer fixture. The cooling step took 2 hours and 10 min, after which the sample's viscoelastic properties were measured and even further for another hour at constant temperature.

In Figure 4.3 viscoelastic properties of the tested samples during gelation are presented. At the beginning of the measurement, all the samples showed low shear moduli, i.e. storage (G') and loss modulus (G''), as they have not yet formed a solid hydrogel network. As evident, for the sample with BAG addition both moduli increased during cooling.

Figure 4.3 also reveals the effect of the samples composition on the temperature of gelation. GG solution started to gel at approximately 40 °C and formed a firm gel at 36 °C. For the composite GG-50A, the gelation appeared at higher temperatures, starting at approximately 58 °C and ending at approx. 42 °C.

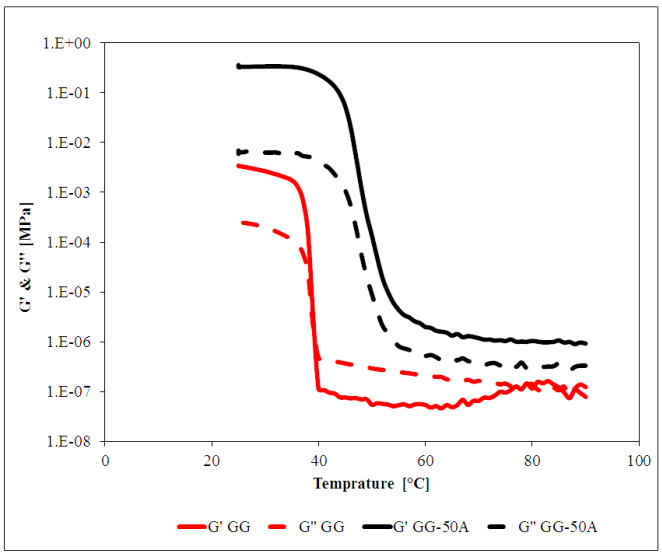


Figure 4.3: Viscoelastic properties of GG hydrogel and GG-BAG composite hydrogel by storage (G') and loss modulus (G'') during cooling.

4.1.2 Material characterization

4.1.2.1 Differential scanning calorimetry (DSC) analysis of water - GG and water - GG-BAG interactions

In order to understand the physical properties of the gellan gum hydrogel, it is important to investigate the state of water and its interactions with the gels. The samples of GG and GG-BAG composite hydrogels (GG-33A, GG-50A and GG-70A) were studied regarding water behaviour when cooled and when heated by one specific regime described in Section 3.1.2.7. The samples were in the form of hydrogels, compositions are specified in Table 3.1.

In the first cooling cycle the freezing T was determined (Figure 4.4A), ranging from -16 to -17.5 °C for all samples. During the second cooling cycle, freezing temperatures obtained were comparable with the temperatures from the first cycle. In both cooling cycles, the enthalpies measured were in range of 143 to 165 Jg^{-1} (Figure 4.4B), and did not differ between the cycles. During the heating cycle (Figure 4.5) with GG and GG-33A, two endothermic peaks were observed, while for the GG-50A and GG-70A one peak was determined. The position of the main endothermic peak shifted to higher temperature with increased BAG concentration.

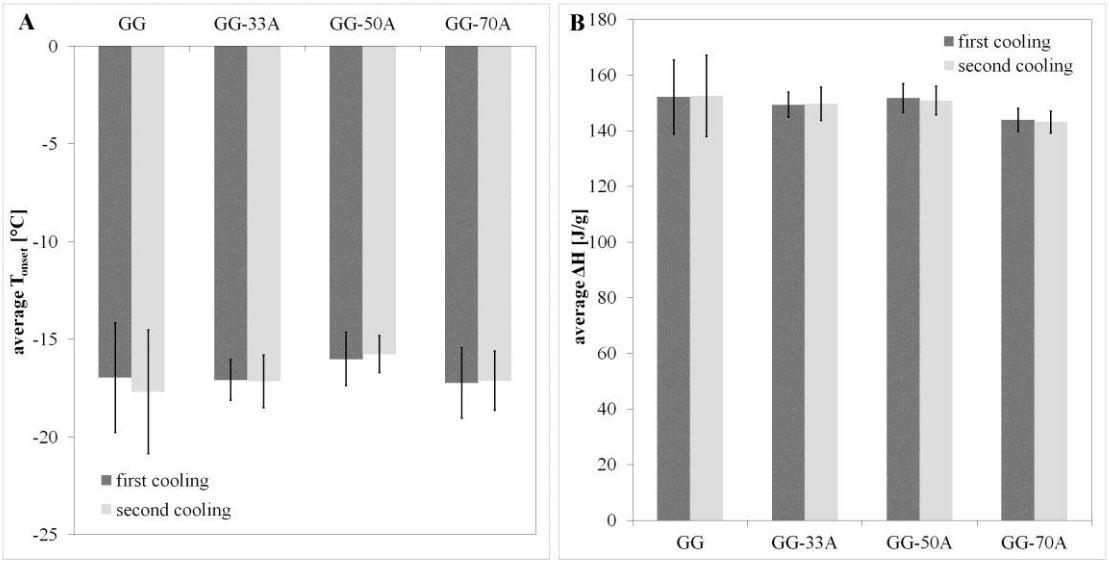


Figure 4.4: DSC analysis. Freezing temperatures (A) and entalpy values (B) for the preformed regime.

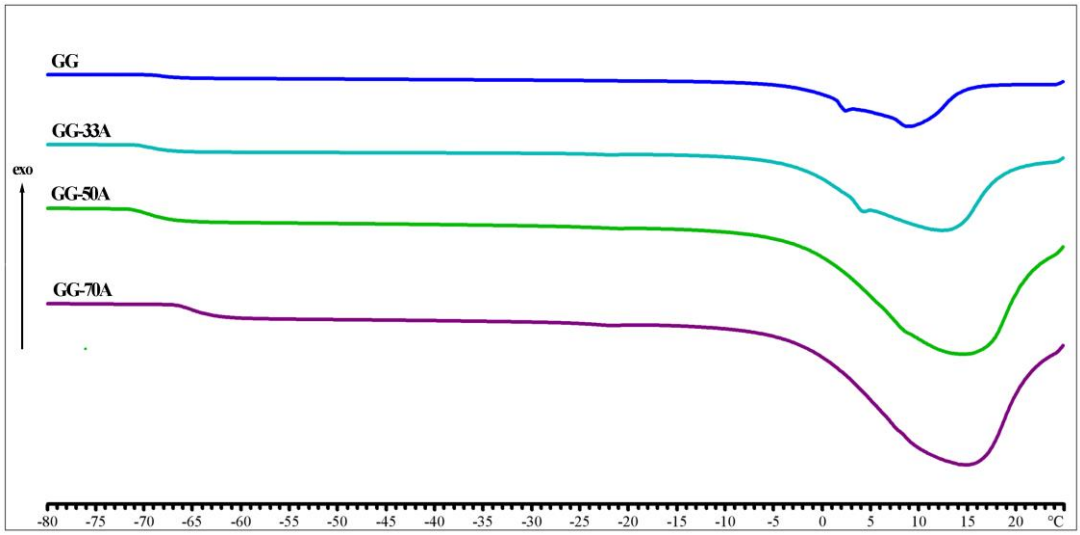


Figure 4.5: DSC curves (heating part) of GG, GG-33A, GG-50A and GG-70A hydrogels.

4.1.2.2 Fourier transform infrared spectroscopy (FT-IR)

The nature of bonds between GG and BAG and water interactions with the material in the samples of various states (hydrogels, dry scaffolds and rehydrate scaffold) were studied by FT-IR. Figure 4.6A-C shows FT-IR spectra in the range of 400-2000 cm^{-1} for GG and GG-50A and GG-70A composites, all cross-linked with $CaCl_2$.

The bands positioned at 463 (Si-O-Si symmetrical bending) and 1070 cm^{-1} (symmetrical stretching of Si-O-Si bonds) correspond to silica network in the bioactive glass. The bands at around 1037, 1412, 1645, 3350 cm^{-1} relate to gellan gum. Band at 1037 cm^{-1} corresponds to polysaccharidic ring of gellan gum (C-O stretching), 1412 cm^{-1} relates to symmetrical stretching of COO-. The band at 1618 cm^{-1} corresponds to asymmetrical stretching of COO- group, where the band at 1645 cm^{-1} corresponds to C=C stretching. The wide broadening band around 3350 cm-1 represents a merge of two peaks, one at 3420 cm^{-1} presenting O-H stretching and one at 2920 cm^{-1} presenting C-H stretch, both present in the glucopyranose ring.

The spectres of all hydrogels and rehydrated scaffolds are similar, only the intensity of certain peaks differs depending on the material's form. All tested samples exhibited strong bands at around 3350 and 1645 cm^{-1}, when in contact with aqueous media. The bands were not present in the spectres of dried composite scaffolds. The band at 1070 cm^{-1} was observed only for the composites (GG-50A and GG-70A) in the form of hydrogel and GG-70A rehydrated scaffold. There is a possible overlapping of 1037 and 1070 cm^{-1} peaks present as the peaks are in some tested samples viable, in others not. When materials were in the form of the dry scaffold, the spectres differ with the composition of the scaffold. GG dry scaffold exhibited the band at around 3350 and 1618 cm^{-1}, but the intensity of the peaks were lower with composites GG-50A and GG-70A. The low-intensity bands at 1412 cm^{-1} and 1037 cm^{-1} was common to all dry scaffolds tested. The composite material expressed the additional band at around 463 cm^{-1}.

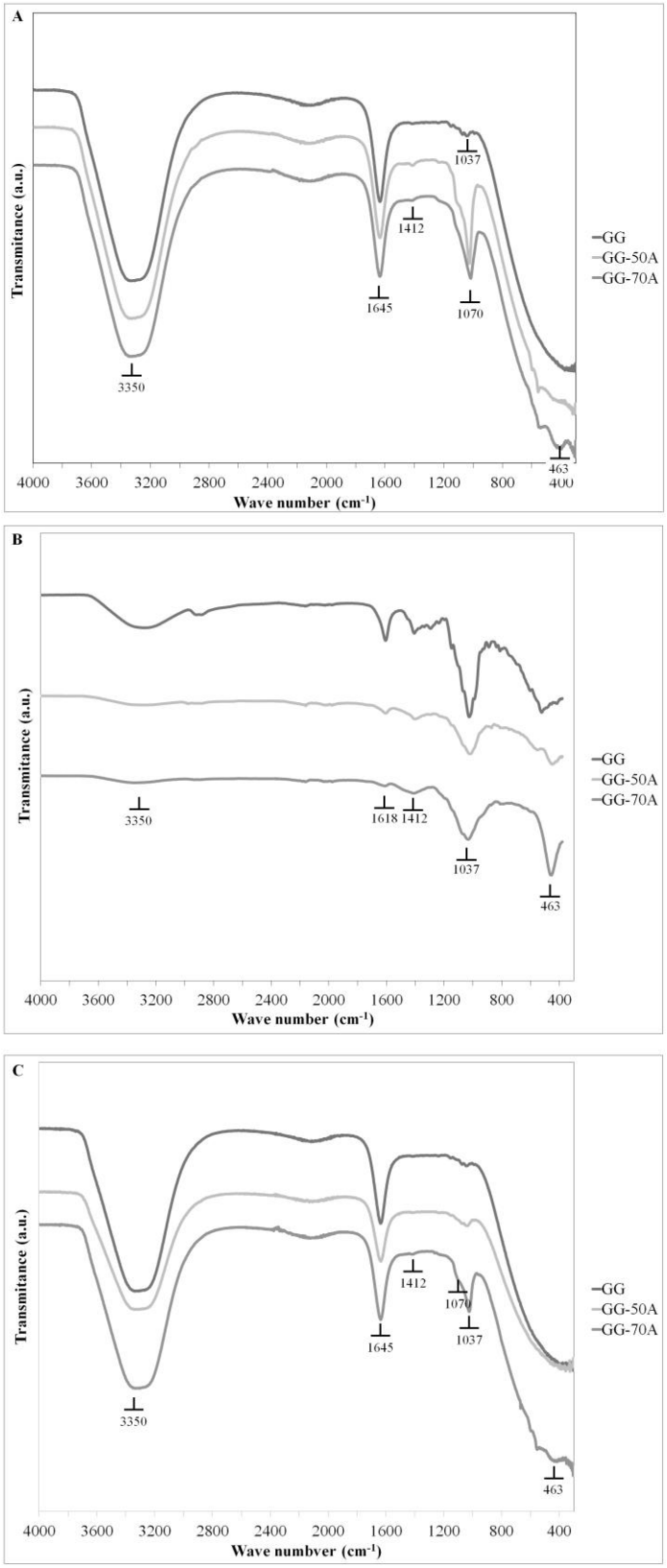


Figure 4.6: FT-IR spectra of GG, GG-50A, and GG-70A samples. The samples were in the form of hydrogels (A), dry scaffolds (B) and rehydrated scaffolds (C).

4.1.3 Characterization of GG and GG-BAG composite materials in the form of hydrogels, dry scaffolds and rehydrated scaffolds

4.1.3.1 Microstructural observation of dry scaffolds by SEM

Scanning Electron Microscopy (SEM) was employed to observe the architecture and microstructure of dry scaffolds, with special emphasis on pore size, their connectivity, homogeneity and BAG particles distribution.

Cross-sections of the GG and GG-50A dry scaffolds, prepared by freezing at -20 °C or -80 °C are presented in Figs 4.7. The microstructure of all presented samples appears homogenous, with uniform pore size and good pore interconnectivity. When frozen at -20 °C (Figs. 4.7A, B), the pore size was estimated to ~400 µm for GG and 350 µm for GG-50A, while after freezing at -80 °C (Fig. 4.7C, D), the average pore size was ~200 and 150 µm, respectively.

Due to the most promising microstructure, the dry scaffold prepared by freezing at -80 °C were selected for further studies of the effect of BAG content and chemical composition on the properties of scaffolds.

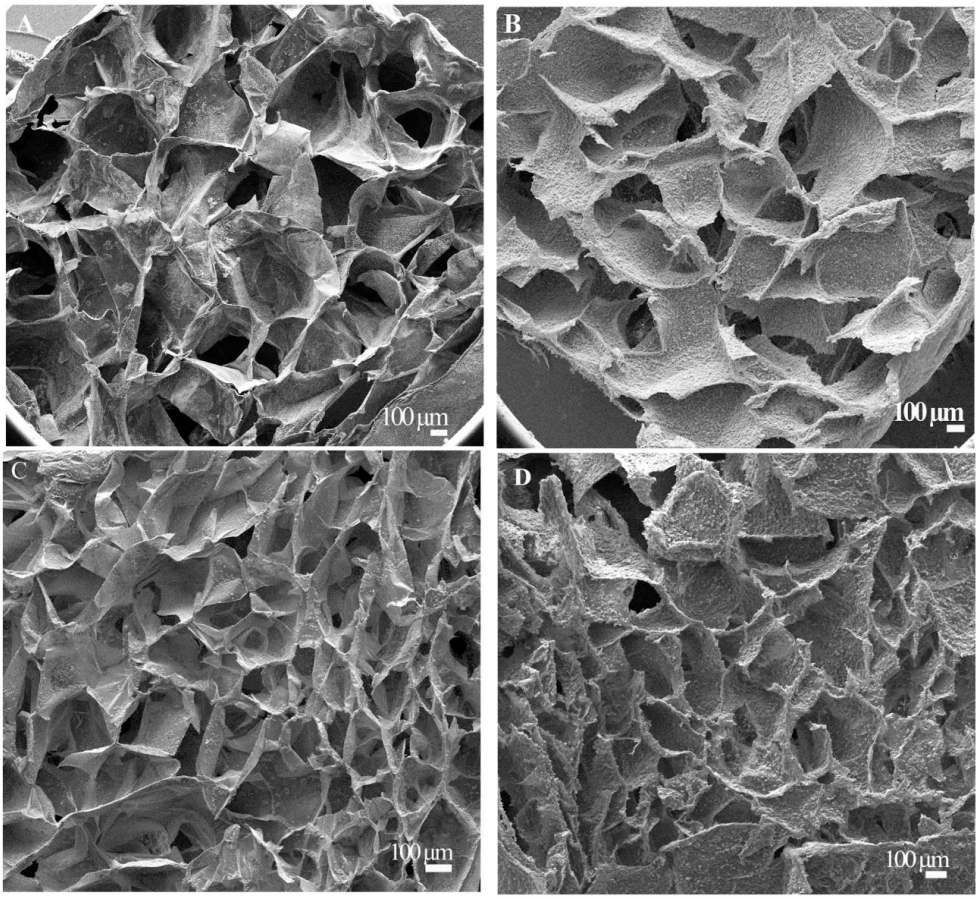


Figure 4.7: FEG-SEM images of cross-section of freeze-dried GG (A, C) and GG-50A (B, D) scaffold prepared at different temperatures, -20 °C and -80 °C.

Bioactive glass particles BAG-A and BAG-B used in this study as a bioactive reinforcement of gellan gum have similar globular shape and size of ~200 nm; micrograph of the BAG-A particles is shown in Fig. 4.8A. The adjacent images (Fig. 4.8B and C)

illustrate the microstructure of freeze-dried gellan gum and cross-section of its pore wall, respectively. Further, microstructure of dry GG-BAG composites with two different additions and compositions of BAG are illustrated in Fig. 4.8D, E, G and H. It is evident that the BAG addition strongly affected the microstructure: in comparison to the GG (Figure 4.8B), 33 w/w % of BAG-A or BAG-B resulted in a drastic reduction of the pore size (Figures 4.8D, G), which further decreased with 50 w/w % BAG (Figure 4.8E, H). There is no clear effect of the BAG composition on the microstructure. In both samples the BAG particles appeared to be homogeneously distributed in the GG matrix. Observations of the cross-sections at higher magnification (Figures 4.8F, I) revealed that, independently on the BAG composition, the BAG particles were embedded into the GG structures in the form of up-to-10-µm-large agglomerates. Moreover, in comparison with the ~10-µm-thick and apparently dense GG pore walls with a smooth surface (Figure 4.8C), the pore walls of the GG-BAG composites appeared thicker and their surface was rougher due to the embedded BAG agglomerates.

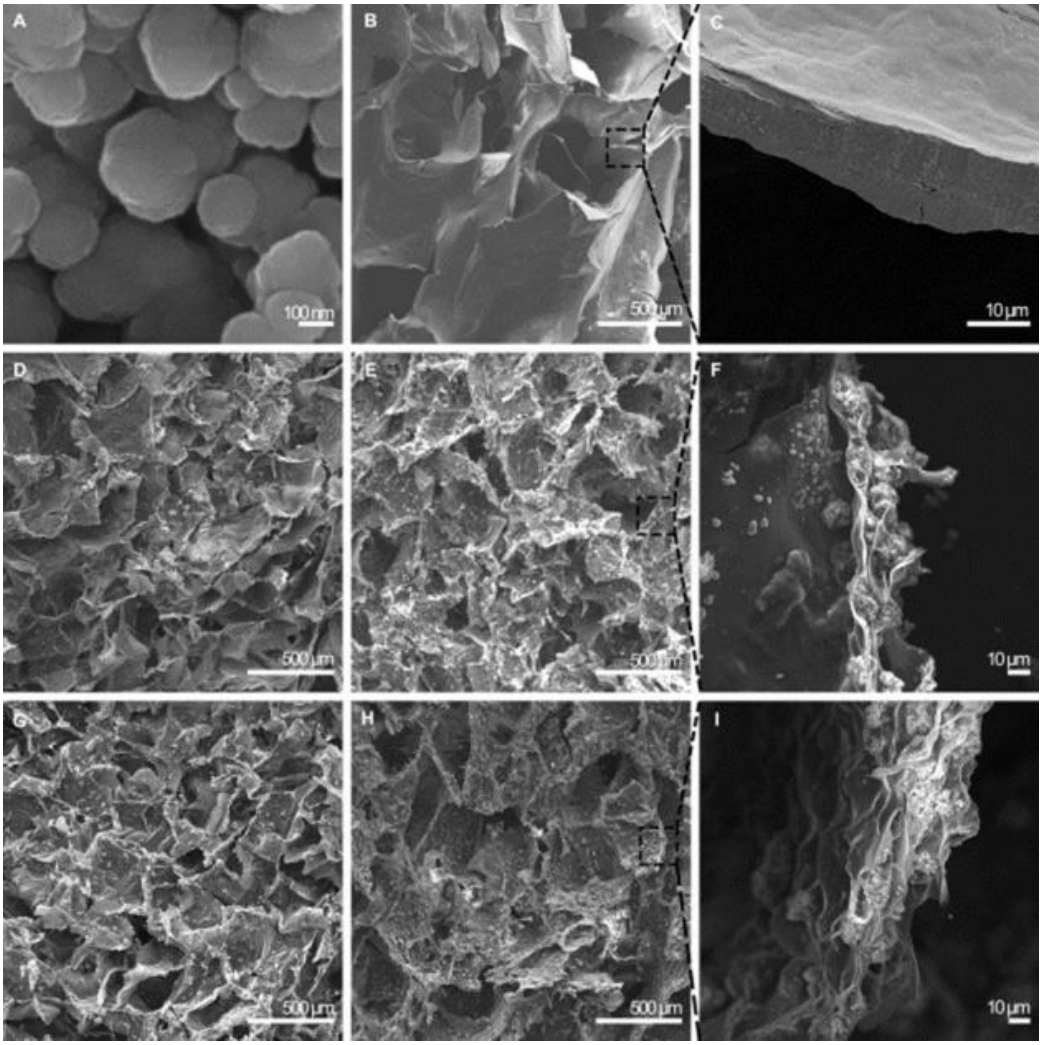


Figure 4.8: FEG-SEM images of the BAG-A particles (A) and cross-sections of the GG (B, C), and GG-BAG composites with 33 % or 50 % BAG-A (D, E) and 33 or 50 % BAG-B (G, H). Figures F and I present the cross-sections of the pore walls in samples GG-50 A and GG-50B, respectively.

Figure 4.9A-D shows the microstructure of composites, where 70 w/w % and 90 w/w % of BAG-A powder was introduced into GG matrix. In both composites, the particles were homogenously distributed throughout the polymer matrix. Due to the high percentage of the BAG particles in the mixture, the water amount was minimal; resulting in low porosity of the dry scaffolds. With the increasing percentage of water, but still keeping the ratio of starting components the same, the formation of gel was limited.

The inner scaffold struts of GG-70A were ~60 µm thick (Fig. 4.9B), up to 6-times more than in the GG-50A samples, while the GG-90A composite was nearly dense.

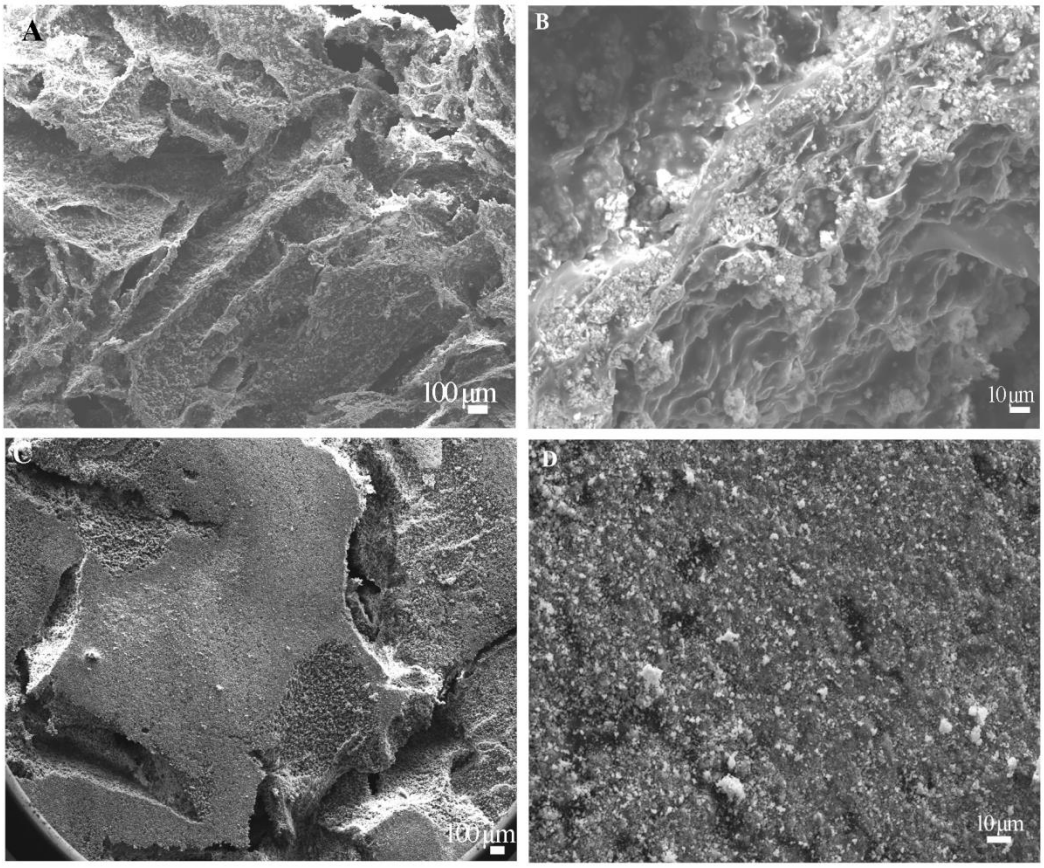


Figure 4.9: FEG-SEM images of cross-sections of the (A) GG-70A, (B) GG-70A pore wall and (C, D) GG-90A.

4.1.3.2 3D architecture and porosity

The microstructures of dry scaffolds were further analyzed by µ-CT. In comparison with the GG structures presented in Figure 4.8A, the composite scaffold GG-50A (Figure 4.10B) revealed a more homogeneous porosity and smaller pores. Moreover, the results of the analysis confirmed that an increased addition of BAG from 33 to 50 w/w % resulted in a porosity decrease from 85 % to 75 % (Figure 4.11A). The analysis also confirmed that the amount of BAG reinforcement greatly affected the pore size (Figure 4.11B). While the pores in the GG were estimated to be larger than 1 mm, the addition of BAG resulted in an average pore size of 500-600 µm, and 180-230 µm for 33 and 50 w/w % of BAG. It is also evident from Figure 4.11B that the increased amount of BAG from 33 to 50 w/w % results in a significantly narrower pore size distribution.

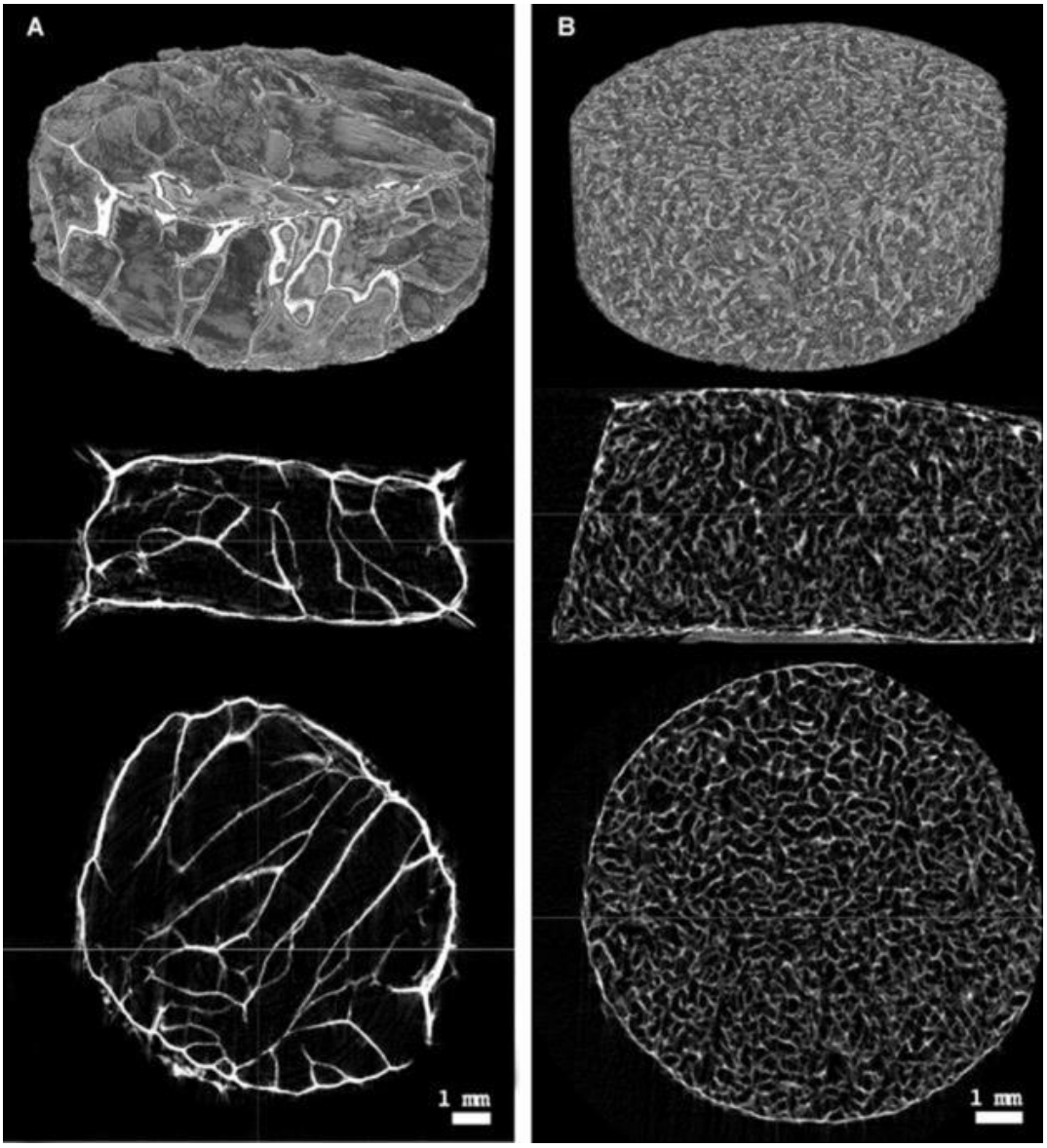


Figure 4.10: Three-dimensional scan of dry scaffolds of GG (A) and GG-50A (B).

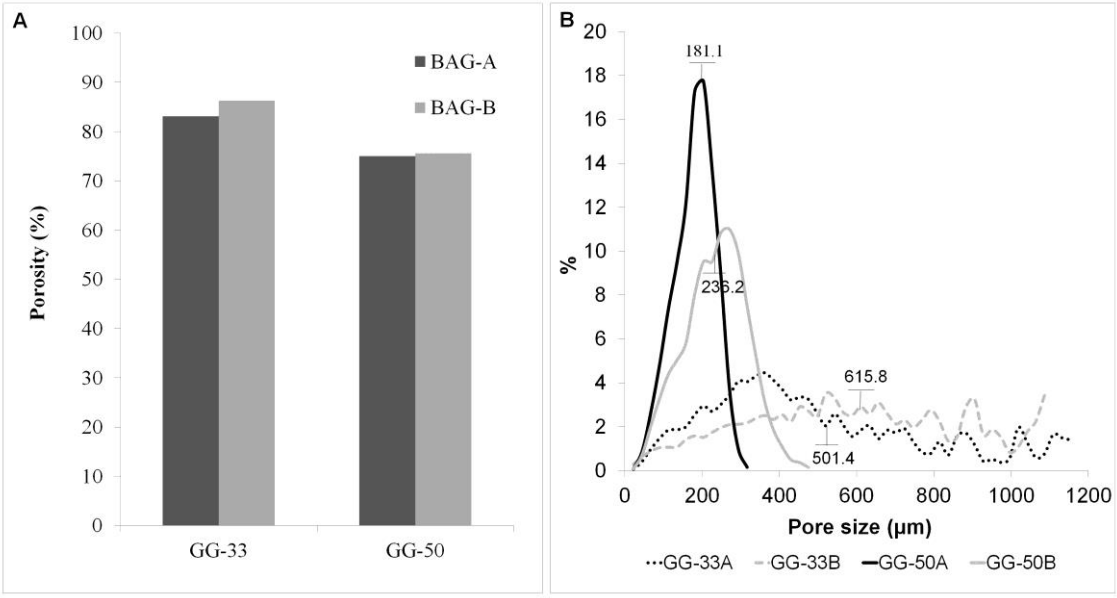


Figure 4.11: Porosity (A) and pore size distribution (B) for the composite GG-BAG dry scaffolds.

4.1.3.3 Mechanical properties

Figures 4.12A-C illustrate the effect of the incorporation of the BAG particles on Young's modulus of the GG-based hydrogels, dry scaffolds and rehydrated scaffolds. The Young's modulus of the GG hydrogel increased after the addition of 33 % BAG-A, while no significant difference was observed with further addition of BAG-A (Figure 4.12A). In contrast, the addition of 33 % BAG-B decreased the Young's modulus, while with 50 % the modulus remained unchanged.

After freeze-drying, independently on the composition and amount of BAG, the Young's modulus of the composite dry scaffolds was twice as high as that for the GG (Figure 4.12B); for the GG the modulus was 0.7 MPa, while the value increased up to ~1.5 MPa for the GG-33A and up to ~1.8 MPa for the GG-50A. Upon rehydration (rehydrated scaffolds), this effect was reverted to the values similar to those observed for the as-prepared hydrogels (Figure 4.12C).

As an illustration, the stress-strain curves for the average examined materials of each group are presented in Figures 4.13A-D. Figure 4.13A demonstrates a significant difference in the behaviour of the GG and sintered BAG (BAG-A): under loading, the BAG exhibited no plastic deformation due to the high Young's modulus (225 MPa), and much higher achieved values of the compressive stress than for the GG. More detailed behaviours for both materials and their composites in various forms are presented in Figures 4.13B for the hydrogels, 4.13C for the dry scaffolds and 4.13D for the rehydrated scaffolds (note the lower y-axis scale than in Figure 4.13A). In contrast to BAG, which exhibits a brittle-fracture mode leading to a catastrophic failure by loading, the GG and GG-BAG hydrogels exhibited large elastic and plastic deformations, both of which are dependent on the amount and, in particular, on the composition of the BAG. For the hydrogels (Figure 4.13B), as well as for the rehydrated scaffolds (Figure 4.13D), it is evident that the 33 or 50 % BAG-A resulted in a much higher mechanical strength than

with the BAG-B, while the effect of the amount of BAG is less pronounced. As shown in Figure 4.13C, for the dry scaffolds the failure did not occur up to at least 20 % of strain. In this case, the influence of the amount of BAG prevailed over its composition.

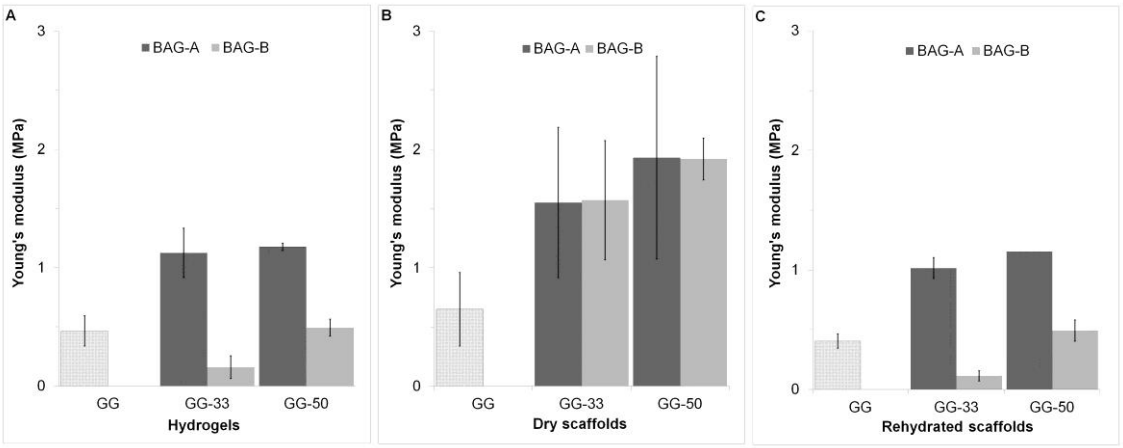


Figure 4.12: Young's modulus for hydrogels (A), dry scaffolds (B) and rehydrated scaffolds (C).

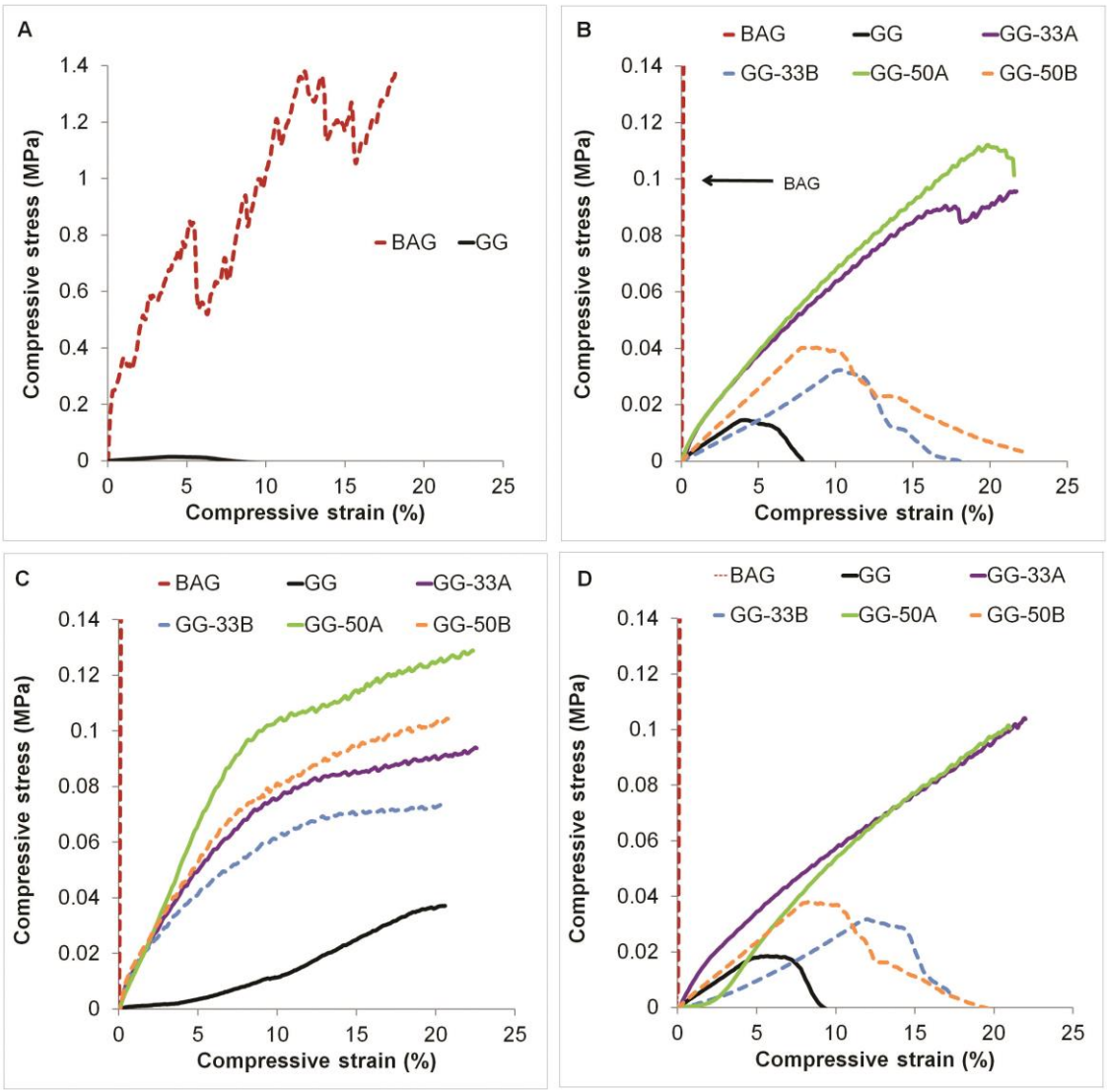


Figure 4.13: Compressive stress vs. strain curves for BAG and GG hydrogel (A), and their composites in the form of hydrogel (B), dry scaffold (C) and rehydrated scaffold (D) with various compositions.

4.1.3.4 Wettability

Wettability is an important parameter affecting several properties of the biomaterial (hydrogel or scaffold), such as the water absorption, *in vitro* and *in vivo* degradation and cell interaction. To determine the surface wettability, contact angle of aqueous media was measured.

First, contact angle of ultrapure water droplet was measured over 112 ms on surfaces of GG, GG-50A and GG-70A hydrogel films. The contact angle values of all tested materials have decreased over time and became stable. The wetting of GG and GG-50A hydrogels were similar and revealed hydrophilic behaviour with contact angle in the range from 12 to 16 °.

Table 4.1: Contact angle of water on hydrogel films of GG, GG-50A and GG-70A over time.

Contact angle [°]			
Time [ms]	GG	GG-50A	GG-70A
0	15	27	24
16	13	20	17
32	12	17	18
48	11	16	18
64	11	15	17
80	13	14	16
96	12	13	16
112	13	13	16

Next, an attempt to measure the contact angle on dry scaffolds of GG, GG-50A and GG-70A was made (Table 4.2). The contact angle for dry GG scaffold was 25 °, water droplet remained on its porous surface. Oppositely, immediate water absorption was observed for dry composite scaffolds.

Table 4.2: Contact angle of water on dry scaffolds of GG, GG-50A and GG-70A.

Sample	Contact angle [°]
GG	25
GG-50A	total absorption of media
GG-70A	total absorption of media

4.1.3.5 Behaviour of the dry scaffolds immersed in aqueous media

With the aim to verify the behavior of the dry scaffolds when immersed in aqueous media, the degradation rate, pH profile and swelling were examined.

When the dry scaffolds were immersed in PBS for 48 h rehydration, rapid weight gain was observed due to water uptake. As it is evident from Figure 4.17A, the highest weight gain of 900 % was observed for GG, ~750 % for the composites with 33 % BAG and ~600 % for the composite with 50 % BAG. No significant effect of the BAG composition was observed.

As a result of scaffolds rehydration, the pores shrunk significantly and the resulting rehydrated scaffolds revealed only a small amount of residual porosity (Fig. 4.14). In parallel with this study, a study of the diffusion coefficient of water within GG and GG-50A rehydrated scaffold was performed by Stepišnik [63], using TecMag NMR spectrometrometry. The pore diameter in GG rehydrated scaffold was 2.57 μm and the diffusion coefficient $1.06\times10\text{-}9$ m^2s^{-1} (Figure 4.15A). In the GG-50A rehydrated scaffold the pore diameter was 2.42 μm and the diffusion coefficient was $2.38\times10\text{-}9$ m^2s^{-1}(Figure 4.15B).

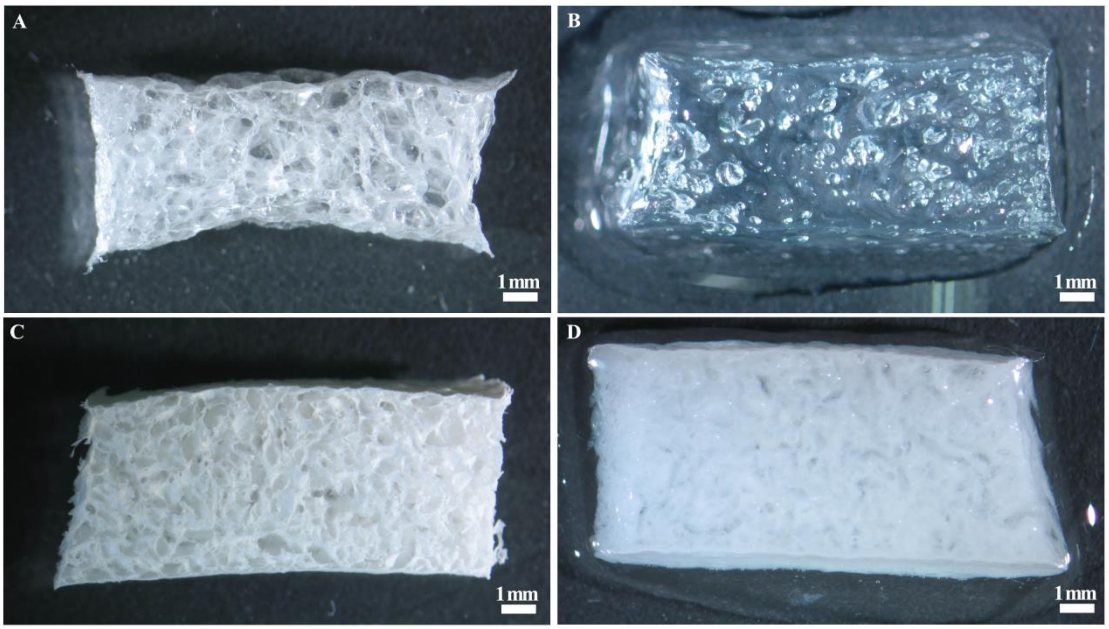


Figure 4.14: Macro photographs of GG (A) and GG-50A (B) dry scaffolds and GG (C) and GG-50A (D) rehydrated scaffolds, all cross-sections.

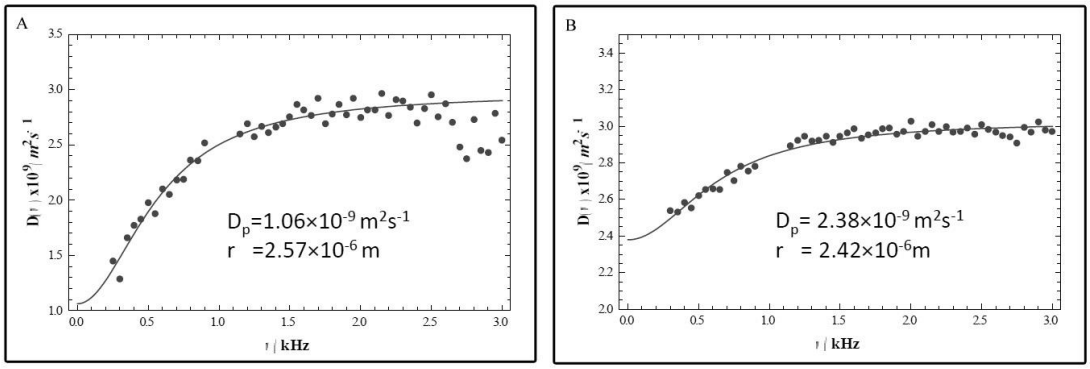


Figure 4.15: MGSE measurements of GG (A) and GG-50A (B) rehydrated scaffolds.

During a 48 h immersion in PBS at 37 °C, the weight of the GG and GG-BAG composite rehydrated scaffolds was reduced due to partial dissolution, Figure 4.16B. In 48 h, for the GG rehydrated scaffolds the weight loss was 9.5 %. A similar result was also observed for the composite GG-33A, while much larger weight loss (17 %) was observed for GG-33B and GG-50B. The lowest weight loss (~5 %) was observed for the sample GG-50A.

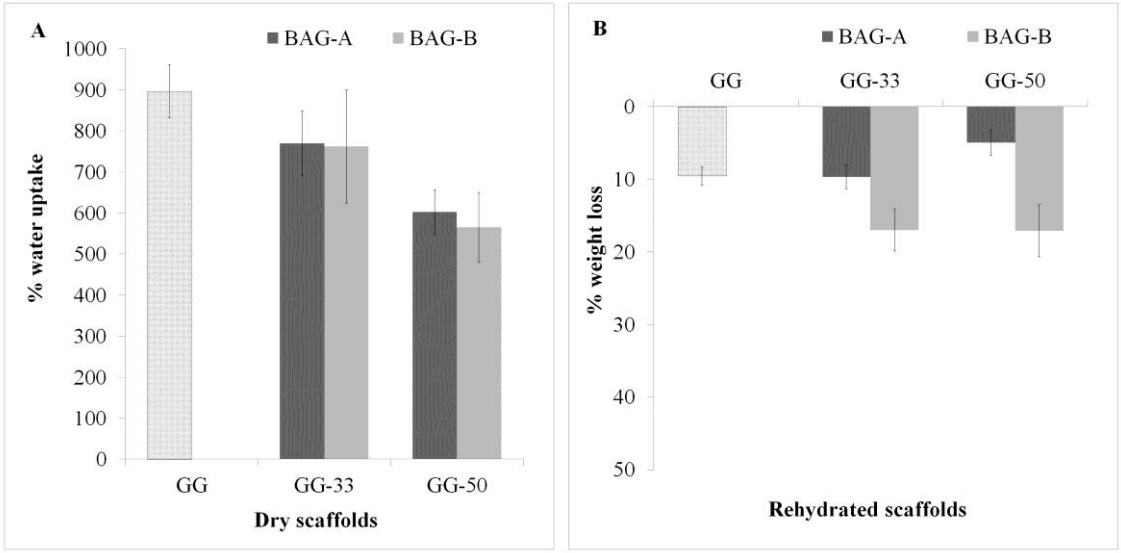


Figure 4.16: Water uptake during 48 h rehydration of dry scaffolds in PBS (A) and weight loss of rehydrated scaffolds during 48 h immersion in PBS (B).

Figure 4.17 presents the weight change of GG and GG-50A dry scaffolds over 30-days of immersion in PBS. As shown in Fig. 4.16A, within the first two days, massive weight gain due to rehydration of dry scaffolds was observed. After reaching the maximum, the weight remained constant approximately three weeks. The minor weight loss that was observed in 3-day degradation test (Fig. 4.16B) was negligible in this long term experiment (Fig 4.17). In the final part of the degradation profile, small weight loss is observed for the GG, while for the GG-50A it remained constant.

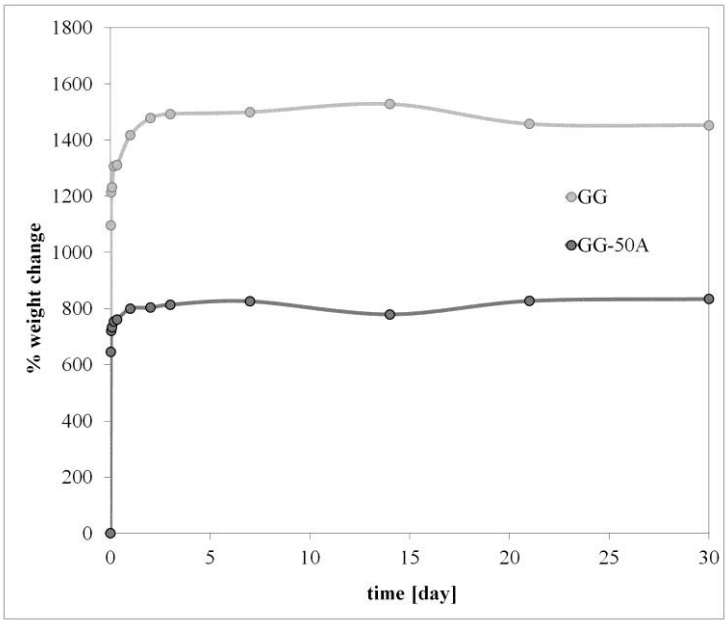


Figure 4.17: Degradation profile (weight change) of GG and GG-50A dry scaffolds in PBS over 30 days.

Degradation of the rehydration scaffolds resulted also in pH change, which was monitored during the PBS immersion for GG and GG-50A and was compared with pH profile of compacted BAG powder (Fig. 4.18). The starting pH values for the examined materials were 7.5, 7.6 and 9.3 for GG, GG-50A and BAG, respectively. With increasing time of immersion the pH values stabilized between 7.4-7.6 for GG and GG-BAG, while the pH value for BAG was much higer, over 9.5.

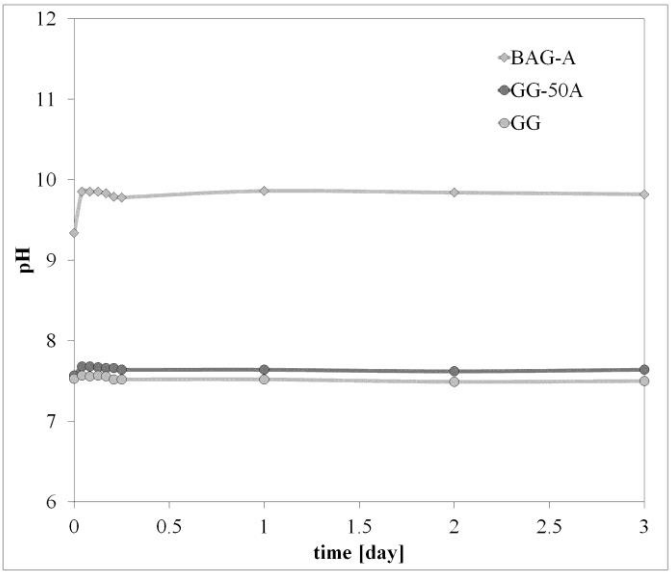


Figure 4.18: pH profile of BAG-A, GG-50A and GG during the PBS immersion over 3 days.

The dimensional change due to swelling was examined on ring-shaped samples, where inner and outer diameter was measured during the immersion in PBS for 176 hours. Figure 4.19A and B presents change of inner and outer diameter of GG and GG-50A. The samples underwent a massive water uptake, but after one day and until the end of the experiment the inner and outer diameters of both tested materials remain constant. The differences between starting diameters and diameters at the end were 10.9 % for outer diameter of GG and 6.9 % for GG-50A (decrease in diameter). The inner diameter decreased for 14.5 % for GG and 6.3 % in GG-50A samples.

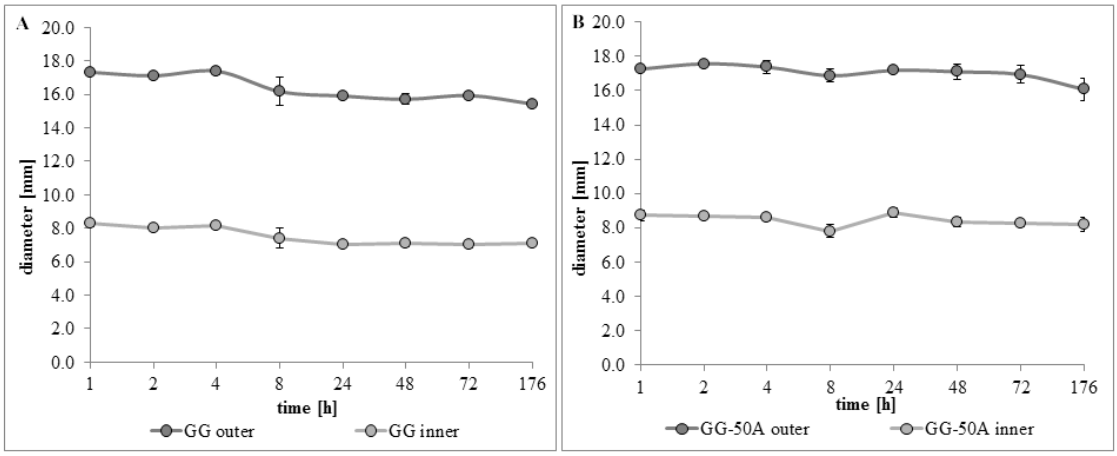


Figure 4.19: Change of diameters of GG (A) and GG-50A (B) dry scaffolds over time when immersed in PBS, representing swelling of the materials.

4.1.3.6 *In vitro* formation of hydroxyapatite

Important characteristic of biomaterial for bone TE applications is the ability of the material to form hydroxyapatite (HA) when immersed in (simulated) body fluid. This ability was tested by immersing GG and GG-50A hydrogels in the specific volume of SBF. After the immersion of the GG and GG-50A composite hydrogels in the SBF for 30 days, a change in morphology was observed.

As expected, no specific morphology change was observed for the samples of GG after 30 days, while cauliflower-like crystals were formed on the GG-BAG hydrogel composites already after 14 days. Moreover, HA was found not only on the surface, but also in the central parts of the samples indicating high diffusivity. After 30 days, the surface of the composite materials was fully covered with HA crystals (Figure 4.20), for which a Ca/P ratio of 1.67 was confirmed by EDS analysis.

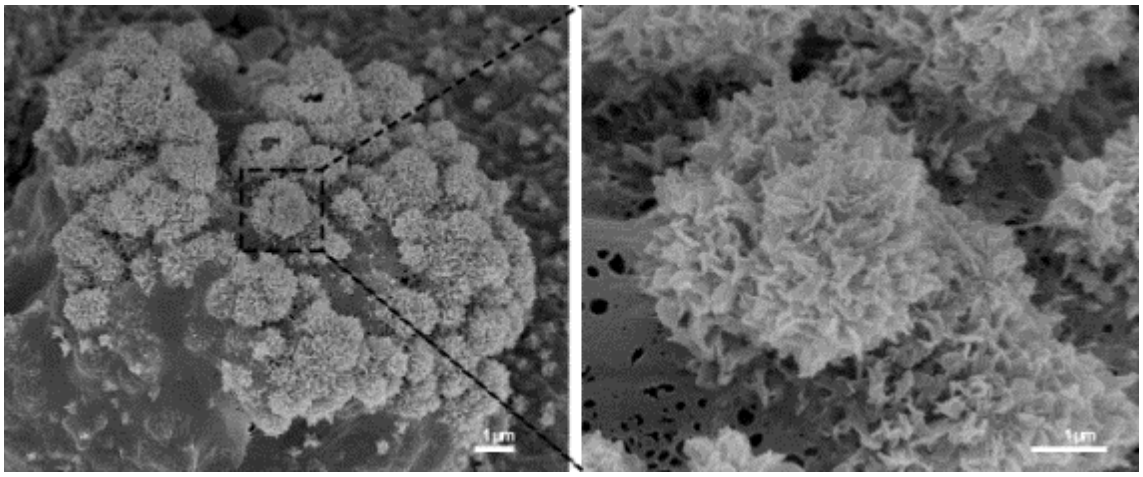


Figure 4.20: FEG-SEM images of the dried GG-50A after immersion in SBF for 30 days at two magnifications.

4.1.3.7 Cytotoxicity

The effect of the composition and the amount of BAG in GG on the human adipose stem cells' (hASC) adhesion and viability was assessed to provide information about the biological performance of the GG and GG-BAG rehydrated scaffolds. The confocal (left column) and fluorescent images (right column) of the hASC after 72 hours of culture on the gellan-gum rehydrated scaffolds (A, B), GG-50A rehydrated scaffolds (C, D) and GG-50B (E, F) are presented in Figure 4.21. After 72 hours of culture, the hASCs were able to attach to all the rehydrated scaffolds and spread within the structures, as was observed by the organized actin filaments and the typical fibroblastic morphology (Fig. 4.21A, C, E). Equally important, the majority of cells within the rehydrated scaffolds were viable after 72 hours of culture, as demonstrated by the Calcein/PI staining (Fig. 4.21B, D, F). The rehydrated scaffolds containing BAG particles showed a strong, red, auto-fluorescence characteristic for the BAG particles.

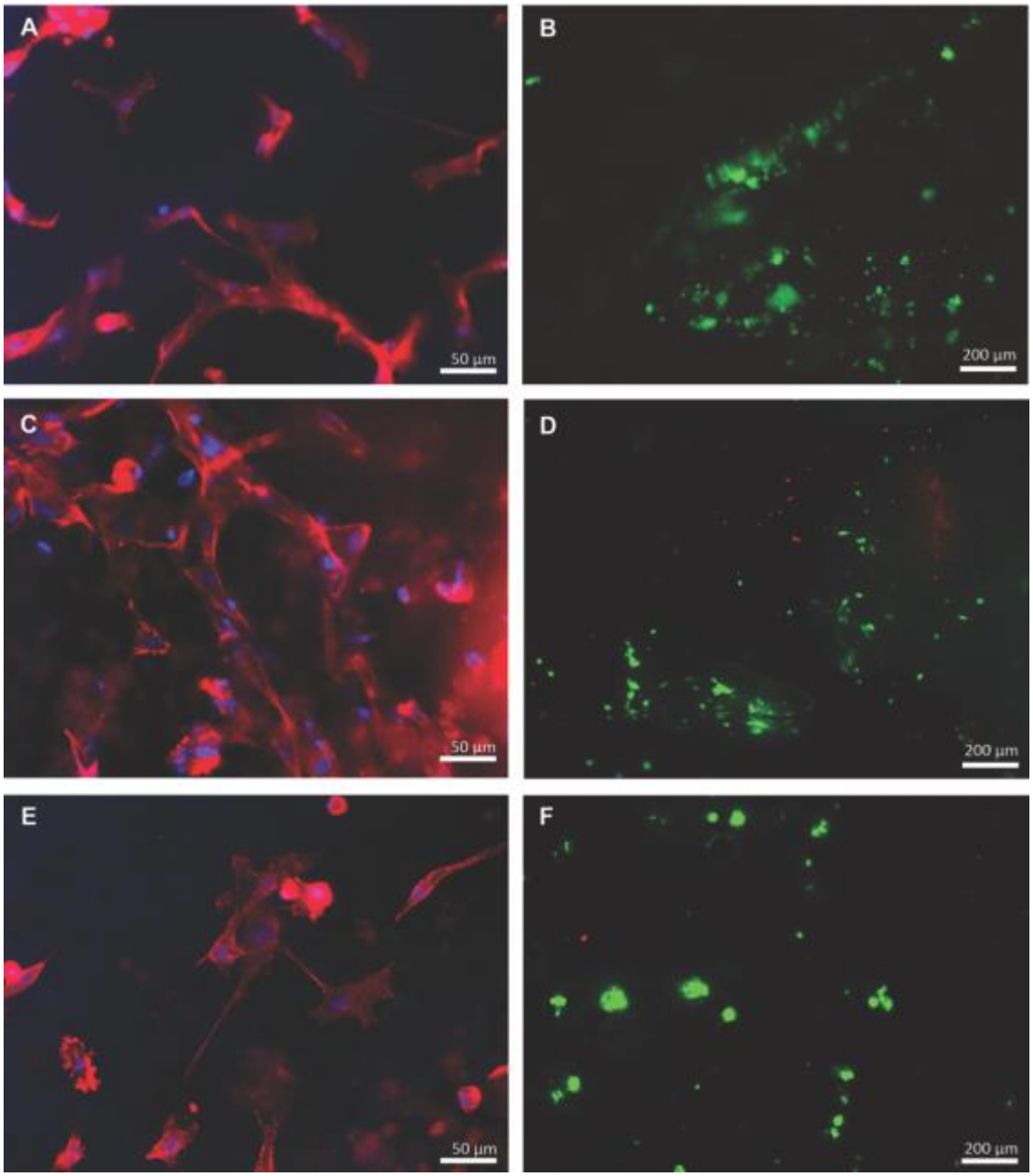


Figure 4.21: Representative confocal microscopy images of hASCs within GG (A, B), GG-50A (C, D) and GG-50B (E, F) rehydrated scaffolds after 72 hours of culture after Phalloidin-TRITC (red) (A, C, E) and Calcein AM (green)/Propidium Iodide (red) (B, D, F) staining. Cells nuclei were stained with DAPI (blue) (A, C, E).

4.2 Polyethylene Glycol – Bioactive Glass Nanocomposite Hydrogels

4.2.1 Sample preparation

Prior to the sample preparation, the concentration of the thiolated groups in Au-$(PEGSH)_4$ and Au-$(PEGSH)_4$-BAG processing solution was determined by Ellman's test. By the evaluation of thiol concentration, the corresponding amount of cross-linker was used to achieve the preferred cross-linking degree. In Table 4.3 the measured absorbance and calculated concentration of thiol groups are given.

Table 4.3: Ellman's test results. Measured absorbance of Au-$(PEGSH)_4$ and Au-$(PEGSH)_4$-BAG_{20} sample and calculated Eellman's number.

Sample	Absorbance	Concentration (mmol/L)	Molarity SH (µmol)	Ellman number (µmol/mg)
Au-$(PEGSH)_4$	0.19	1.35	1.35	0.25
Au-$(PEGSH)_4$-BAG_{20}	0.57	3.58	1.79	0.34

The absorbance was measured with Au-$(PEGSH)_4$, from which the Ellman number of 0.25 µmol/mg was calculated. The molarity of thiol group present in the investigated material was 1.35 µmol. In the Au-$(PEGSH)_4$-BAG_{20} specimen the measured absorbance was 0.57, from which the measured Ellman's number was 0.34 µmol/mg.

The increased absorbance in the Au-$(PEGSH)_4$-BAG_{20} specimen is presumed due to the presence of BAG particles in the sample, as the same material of Au-$(PEGSH)_4$ in both measurements of the Ellman's number. It is not believed that there are any interactions between the materials occurred.

To obtain Au-$(PEGSH)_4$ or Au-$(PEGSH)_4$-BAG hydrogel, first 4-arm thiolate polyethylene glycol was dissolved in the ultrapure water. In the separate vial BAG particles were dispersed using ultrasonication, and then mixed into the $(PEGSH)_4$ solution. In the end, the required amount of Au crosslinker was added, well-mixed in and let to set overnight to obtain a fully formed hydrogel. pH of the fabricated hydrogel was adjusted by adding HCl or NaOH solutions, to reach the values close to the physiological ones. Three different hydrogel nanocomposites were prepared with 5, 10 and 20 w/w % of BAG nanoparticles, designated as Au-$(PEGSH)_4$-BAG_5, Au-$(PEGSH)_4$-BAG_{10} and Au-$(PEGSH)_4$-BAG_{20}, respectively.

4.2.2 Characterization of polyethylene glycol – bioactive glass nanocomposites as possible injectable hydrogels

4.2.2.1 Observation of microstructure by SEM

The microstructures of freeze-dried Au-$(PEGSH)_4$-BAG hydrogel nanocomposites with an increasing amount of BAG nanoparticles are presented in Figure 4.22. It can be clearly observed that for all three compositions, agglomerated BAG nanoparticles are

homogeneously dispersed in Au-$(PEGSH)_4$ matrix (Figure 4.22). It is worth mentioning that the agglomerates, size corresponds to that observed for the pristine BAG nanoparticles observed in Figure 4.8A.

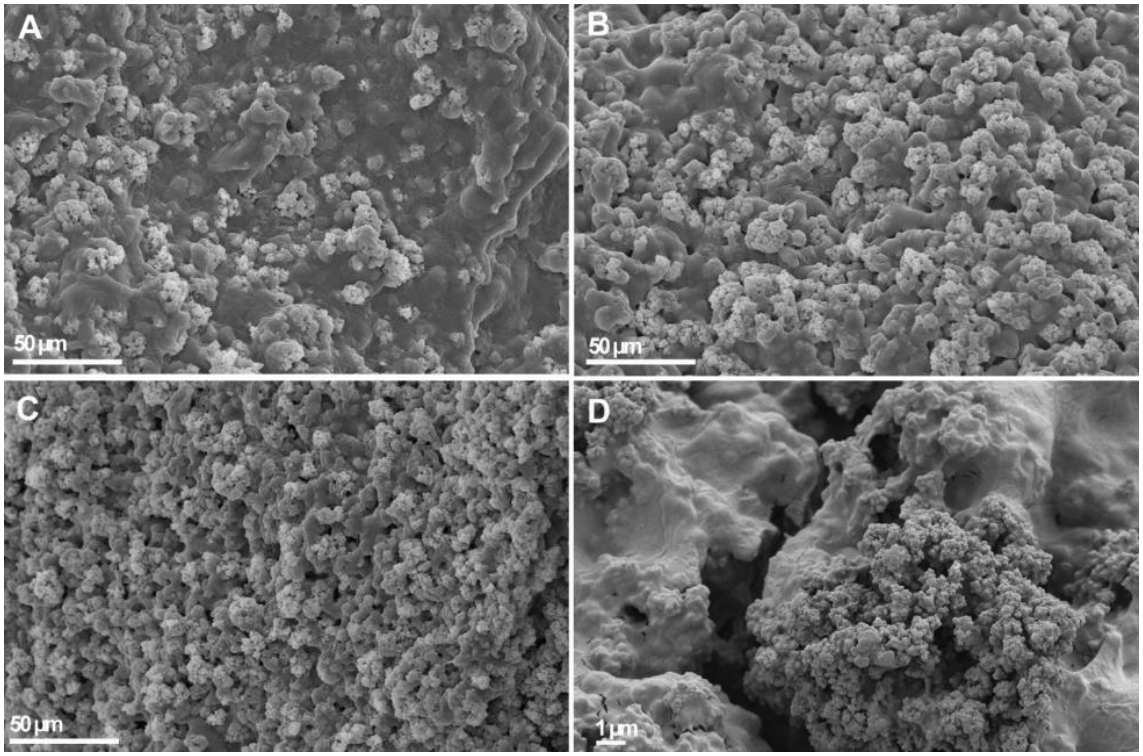


Figure 4.22: FEG-SEM pictures showing the microstructure of freeze-dried Au-$(PEGSH)_4$-BAG hydrogel nanocomposites: Au-$(PEGSH)_4$-BAG_5 (A), Au-$(PEGSH)_4$-BAG_{10} (B) and Au-$(PEGSH)_4$-BAG_{20} (C); (D) Au-$(PEGSH)_4$-BAG_{10} at higher magnification.

4.2.2.2 Rheological behavior of nanocomposites with different BAG percentage at different pH values

Attempts to estimate the gelation time of Au-$(PEGSH)_4$-BAG_{10} hydrogel nanocomposites were carried out by monitoring the variation of the shear storage modulus (G') and the shear loss modulus (G'') at 1 % deformation and a constant frequency of 0.1 Hz. After injection of $(PEGSH)_4$-BAG_{10} solution/suspension and cross-linker solution directly on the rheometer plates G' was already greater than G'', which is characteristic of the hydrogel state (Figure 4.23). Thus, the hydrogel is formed quasi instantaneously after mixing the two solutions with no delay time observed.

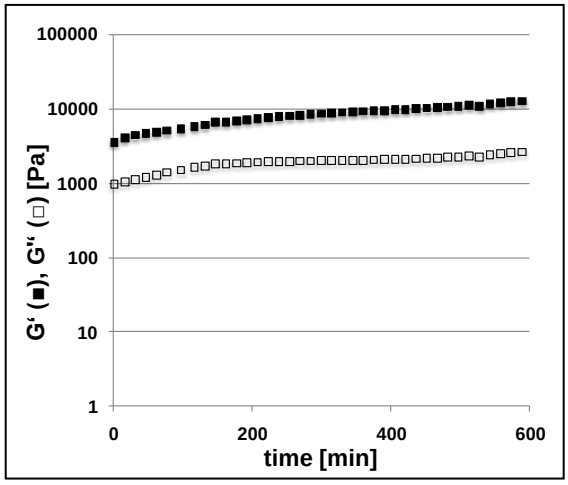


Figure 4.23: The variation of G' (■) and G'' (□) at 1 % deformation and 0.1 Hz in function of time for Au-$(PEGSH)_4$-BAG_{10} hydrogel nanocomposite directly injected on the rheometer plate.

The viscoelastic behavior of Au-$(PEGSH)_4$ and Au-$(PEGSH)_4$-BAG hydrogel nanocomposites, all at pH 10, was determined by dynamic rheology studies as shown in Figure 4.24A as a function of frequency within the extended range associated with most daily activities, i.e. from 0.1 to 10 Hz [64]. At the beginning, the shear storage modulus (G') is greater than the loss modulus (G'') at all frequencies for all hydrogels, which is characteristic of freestanding hydrogels. At low frequency, sufficient disulfide bridges between $(PEGSH)_4$ polymers offer the formation of a 3D network with G' > G''. At increasing frequencies, the deformation applied to the material is too fast for the polymer chains to rearrange, resulting in increasing G' and decreasing G'' due to additional entanglements. As the Au-based dynamic hydrogel contains more reactive thiolate at pH 10 than the same hydrogel at pH 7 due to the pKa of $(PEGSH)_4$ located at pH 8.3. Hence, as the pH is reduced from 10 to 7, a number of nucleophilic thiolates decreases, resulting in a less dynamic hydrogel and a more stable 3D structure as Au-S/disulfide exchange occurs at a slower rate.

For Au-$(PEGSH)_4$ dynamic hydrogel at pH 10, crossover frequency (ω_c) could be estimated at around 10 Hz. As estimated by the frequency sweep studies in Figure 4.24A, the addition of BAG nanoparticles appeared to affect the rheological properties of Au-$(PEGSH)_4$. At the beginning, both G' and G'' increased with the amount of BAG nanoparticles added which indicates that stiffer hydrogels were obtained with the addition of BAG nanoparticles. With only 5 and 10 w/w % BAG nanoparticles, ω_c shifted to around 8 Hz for both hydrogel nanocomposites. For Au-$(PEGSH)_4$-BAG_{20}, ω_c was estimated to be at around 5 Hz.

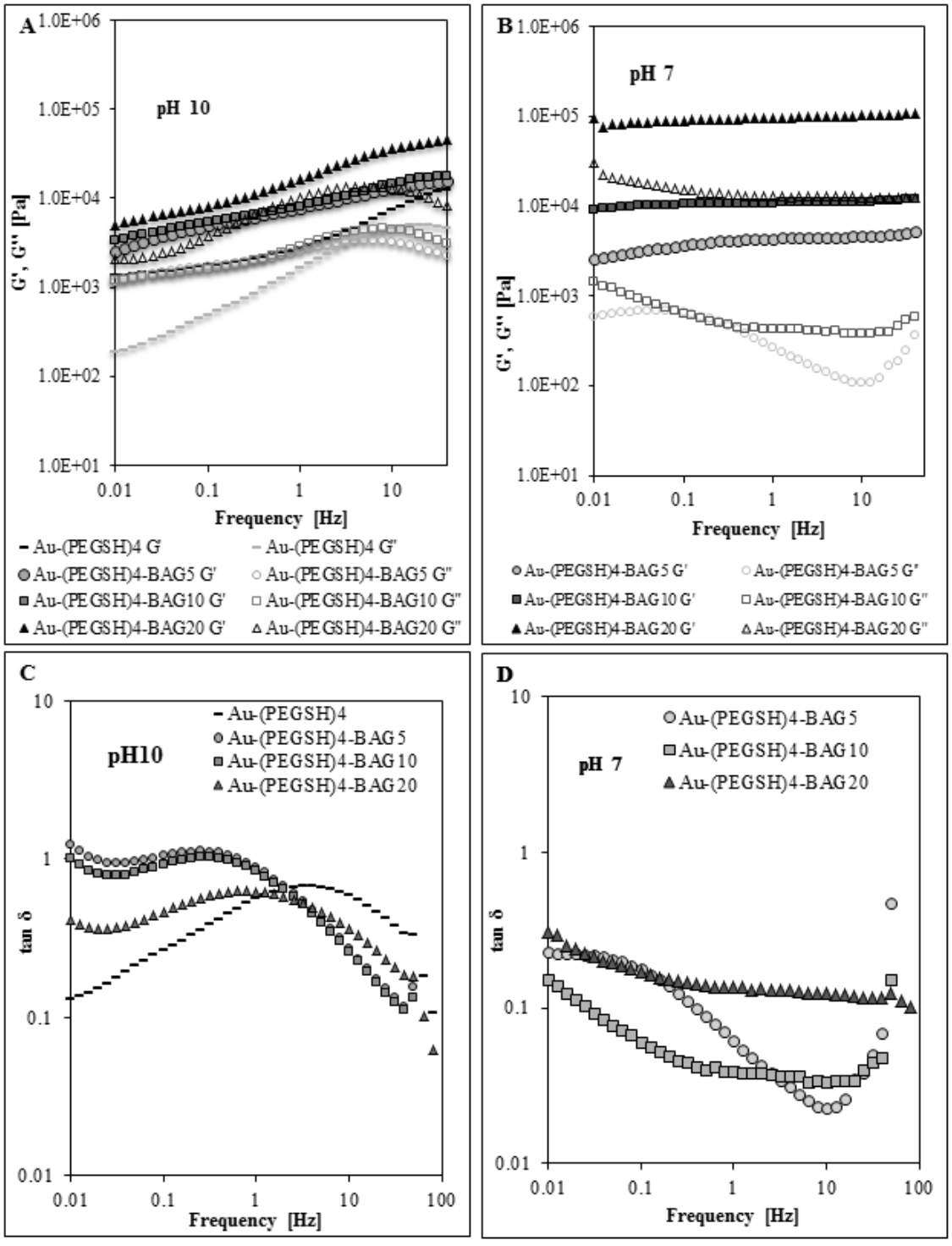


Figure 4.24: Frequency sweep studies depicting shear storage (G') and loss modulus (G'') for a constant deformation (1 %) applied as a function of frequency for Au-$(PEGSH)_4$ hydrogel and hydrogel nanocomposites prepared with 5, 10 and 20 w/w % of BAG nanoparticles adjusted at pH~10 (A) and at pH~7(B); (C) and (D) represent the corresponding tan δ = G''/G' at pH 10 and pH 7.

An important characteristic for a scaffold prepared for bioapplications is the pH of the final material, which should match the physiological environment as much as possible.

Therefore, the pH of all hydrogels was adjusted from 10 to 7 by addition of HCl solution (1 M), and the rheological behaviour of the resulting hydrogels was studied. As expected, different rheological properties were obtained when the pH for the hydrogel nanocomposites was adjusted at pH 7. From Figure 4.24B it is evident that, at pH~7, G' for the hydrogel nanocomposites exhibit a higher value compared to the same hydrogel nanocomposites prepared at pH~10. Increasing G' was markedly observed as the amount of BAG nanoparticles added to the hydrogel was increased, with a maximum observed for Au-$(PEGSH)_4$-BAG_{20}. In addition, G' appears to be constant over the range of frequencies for all hydrogel nanocomposites. In contrast, G' was decreasing at increasing frequency, resulting in a more rigid material. The loss factor for Au-$(PEGSH)_4$ hydrogel nanocomposites is higher, at around 0.04 for Au-$(PEGSH)_4$-BAG_{10}, and is dependent on the amount of BAG nanoparticles added (Figure 4.24D). It is also worth mentioning that hydrogel nanocomposites adjusted at pH 7 exhibited a lower loss factor with a minimum at ~10 Hz, indicating the greater elasticity of the material.

4.2.2.3 Mechanical and deformation properties

The behavior of Au-$(PEGSH)_4$ dynamic hydrogel and Au-$(PEGSH)_4$-BAG hydrogel nanocomposites, all adjusted to pH 7, under compression stress is depicted in Figure 4.25. All nanocomposites showed high deformation under relatively low stress (< 0.1 MPa). For Au-$(PEGSH)_4$, less than 1 kPa was sufficient to induce more than 10 % deformation, whereas the presence of BAG nanoparticles clearly increased the stress required to achieve similar deformation. In more details, 10 % deformation was reached with applied stress at around 9, 12 and 25 kPa for Au-$(PEGSH)_4$-BAG_5, Au-$(PEGSH)_4$-BAG_{10} and Au-$(PEGSH)_4$-BAG_{20}, respectively.

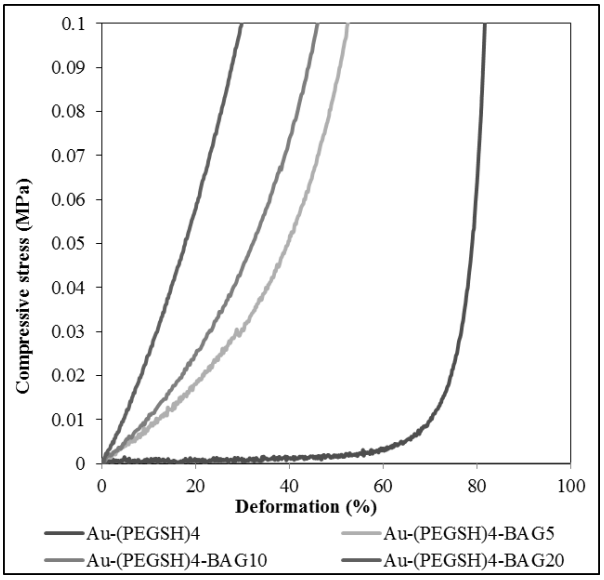


Figure 4.25: Compression stress vs. deformation curves of Au-$(PEGSH)_4$-BAG_5, Au-$(PEGSH)_4$-BAG_{10} and Au-$(PEGSH)_4$-BAG_{20} hydrogel nanocomposites and Au-$(PEGSH)_4$ for comparison.

4.2.2.4 Self-healing ability of nanocomposites and the effect of BAG presence on it

To verify the ability of hydrogel nanocomposites to self-heal, Au-$(PEGSH)_4$-BAG hydrogel nanocomposites adjusted at pH 7 were cut up into several pieces with a scalpel and placed back into the same mold to self-heal (Figure 4.26A-C). Visual inspection confirmed that Au-$(PEGSH)_4$-BAG_{10} was totally recovered. All hydrogel nanocomposites exhibited similar self-healing properties to the corresponding Au-$(PEGSH)_4$ hydrogel nanocomposite confirming that the presence of BAG nanoparticles does not hinder Au-S/disulfide exchange.

Figure 4.26D shows the dynamic rheology data obtained for all hydrogel nanocomposites, adjusted at pH 7, after self-healing. By comparing Figure 4.24B and Figure 4.26D, all nanocomposites exhibited a decrease of G' and G'' of approximately one order of magnitude, which indicates a weaker hydrogel network [65]. Complete recovery of the rheological properties was not achieved due to the breaking of the non-self-healing bond during the dissection of the hydrogel. However, around 90 % of the original mechanical properties were successfully recovered.

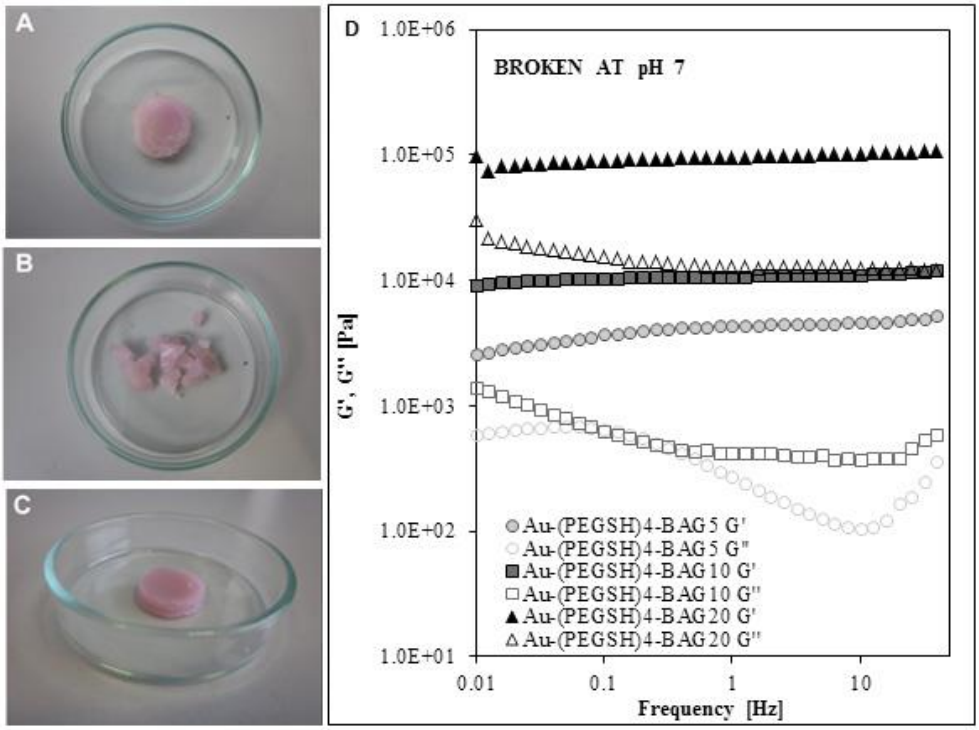


Figure 4.26: Digital pictures of Au-$(PEGSH)_4$-BAG_{10} hydrogel nanocomposite; as-prepared (A), cut into pieces with a scalpel (B) and self-healed overnight in a disc shaped mould (C); frequency sweep studies for Au-$(PEGSH)_4$-BAG hydrogel nanocomposites adjusted at pH 7 after being cut with a scalpel and self-healed in disc shape mould with light pressure overnight (D).

4.2.2.5 BAG degradation, pH change and *in vitro* formation of hydroxyapatite mineral

To estimate the relative dissolution rate of either the BAG nanoparticles alone or embedded in Au-$(PEGSH)_4$, samples were examined using a Franz cell with ultrapure water as the media and ambient T of 37 °C. The samples were placed at the top, while aliquots could be easily taken from the main chamber containing a high volume of water to avoid any salt saturation. The concentration of released ions was monitored by ICP-MS. Clearly from Figure 4.27A, ions were released much faster by BAG nanoparticles alone compared to Au-$(PEGSH)_4$-BAG_{10}. For both samples, BAG nanoparticles alone and Au-$(PEGSH)_4$-BAG hydrogel nanocomposites, Ca^{2+} ions were released more rapidly than Si^{4+} ions (Fig. 4.27A). As expected, the amount of ions released for similar time-scale was lower when BAG nanoparticles were embedded in the polymer matrix. In addition, it is worth mentioning that BAG nanoparticles sediment on the filter due to the large size of the aggregates. In contrast, within the polymeric matrix BAG nanoparticles were homogenously dispersed (Figure 4.22).

With the dilution of the material pH profile was also studied (Figure 4.27B). Under static conditions and low dilution, the pH of an aqueous solution of BAG nanoparticles increases rapidly to 10.7 within a minute. For Au-$(PEGSH)_4$-BAG_{10} the pH decreased from 7.8 to 7.2 after 6 hours, attributed to the calcium dissolution form BAG particles. The change of pH of Au-$(PEGSH)_4$-BAG_{10} hydrogel nanocomposite is similar to that of Au-$(PEGSH)_4$ hydrogel (8.2) with an initial decrease during the first hour. However, while the pH of Au-$(PEGSH)_4$ hydrogel is decreasing monotonically the pH of the hydrogel nanocomposite increases after 1 hour.

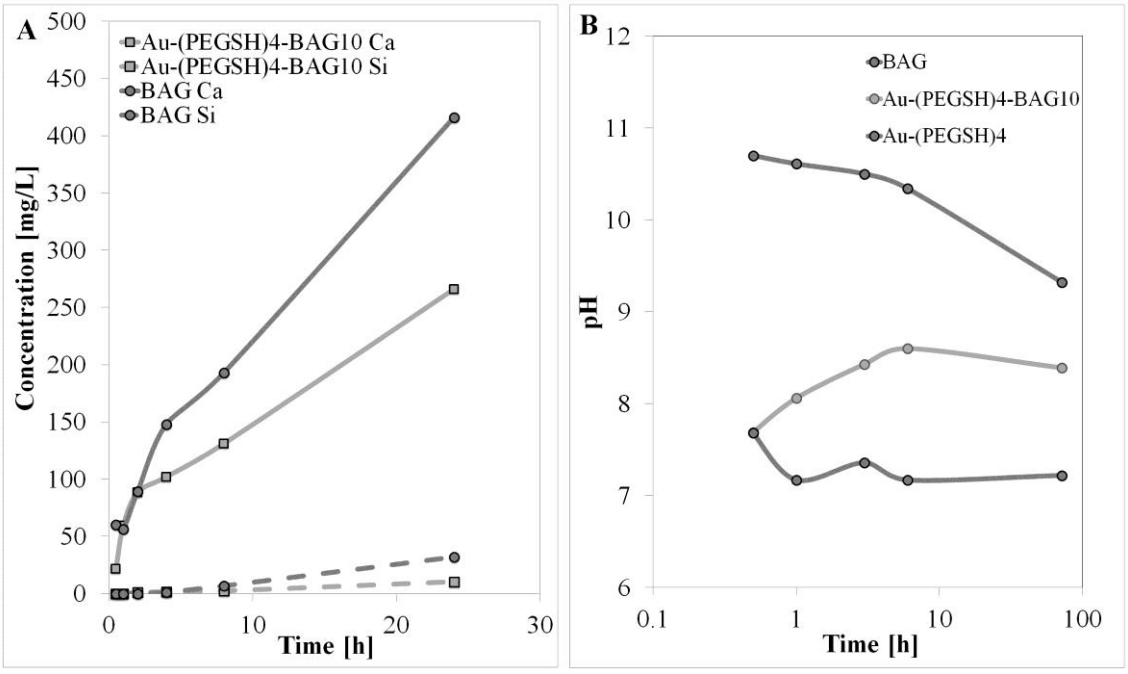


Figure 4.27: (A) Time-dependent concentration of silicon and calcium ions released during the degradation and detected by ICP-MS of BAG nanoparticles alone and Au-$(PEGSH)_4$-BAG_{10} hydrogel nanocomposite in ultrapure water using a Franz cell and (B) pH change.

To determine the bioactivity of Au-$(PEGSH)_4$-BAG_{10} hydrogel nanocomposite, the sample was immersed in the corresponding volume of SBF. As a control experiment, Au-$(PEGSH)_4$ dynamic hydrogel was as well immersed in SBF. The Au-$(PEGSH)_4$ could not form hydroxyapatite (HA), and the hydrogel was completely degraded within 30 days. In contrast, the presence of well-defined HA crystals (Ca:P=1.67), as judged by EDS analysis, was observed after 30 days with Au-$(PEGSH)_4$-BAG_{10}. It is noteworthy that after 30 days the polymer matrix was partly degraded, but appeared to remain structured with the presence of HA crystals (Figure 4.28).

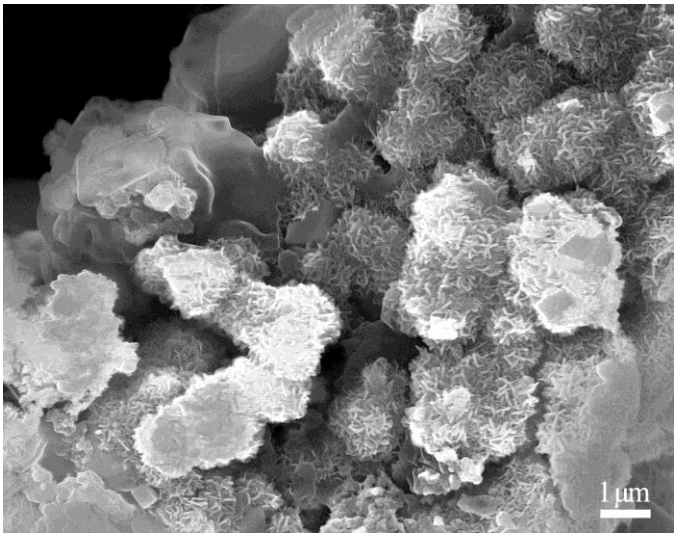


Figure 4.28: The FEG-SEM image of Au-$(PEGSH)_4$-BAG_{10} after 30 days immersion in SBF.

4.2.2.6 *In vitro* cell viability

Preliminary *in vitro* tests on HeLa cells were carried out to study the cytotoxicity of the released degradation products during the degradation of BAG nanoparticles, Au-$(PEGSH)_4$ dynamic hydrogel alone and Au-$(PEGSH)_4$-BAG_{10} hydrogel nanocomposite placed in an insert (Figure 4.29 and 4.30). Positive and negative control experiments consisting of only cells and cells in the presence of Triton X surfactant, respectively, were also carried out for comparison.

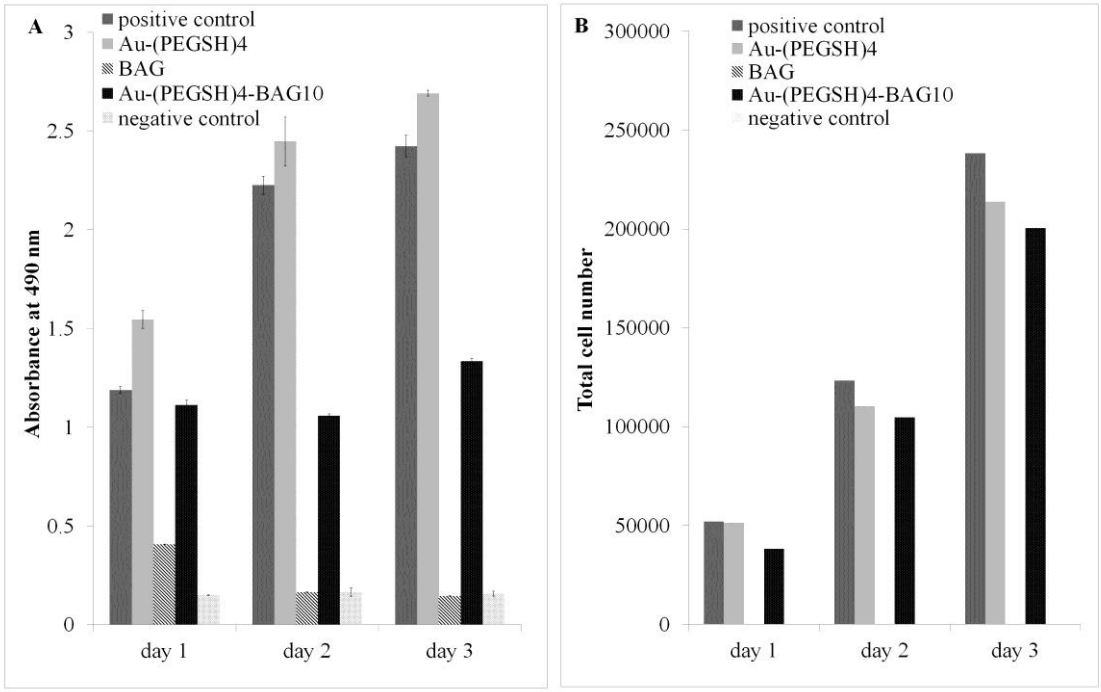


Figure 4.29: Cytotoxicity evaluation of BAG, Au-(PEGSH)4 hydrogel and Au-$(PEGSH)_4$-BAG_{10} hydrogel nanocomposite by MTS (A) and Tripan blue assay (B).

For Au-$(PEGSH)_4$ dynamic hydrogel, no cytotoxic effect was detected, confirming that the dynamic hydrogel does not release any cytotoxic substances. Unfortunately, high cytotoxicity was observed for BAG nanoparticles alone after only 24 h, estimated from the very low absorbance observed, similar to the negative control in Fig. 4.29A. Cells death occurred due to the inherent increase of pH. On the other hand, the viability of HeLa cells appeared to be constant over 3 days in the presence of Au-$(PEGSH)_4$-BAG_{10}, judged by MTS assay, despite containing the same amount of BAG nanoparticles as the BAG sample. In addition, LIVE/DEAD assay confirmed that only healthy cells (green in Fig 4.30) with characteristically spread morphology were observed.

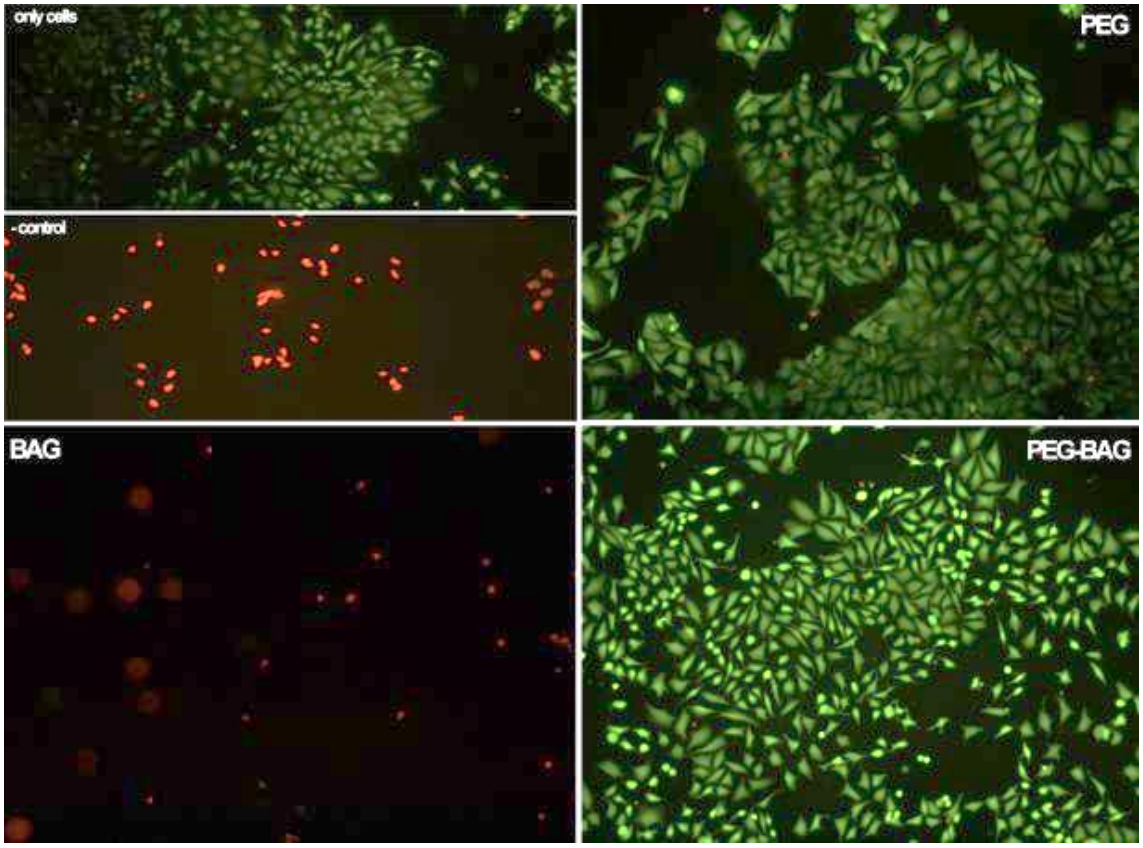


Figure 4.30: Representative fluorescence microscopy images of HeLa cells respond to degradation products of Au-$(PEGSH)_4$ (PEG), Au-$(PEGSH)_4$-BAG_{10} (PEG-10BAHG) and BAG after 72 hours.

Chapter 5

Discussion

Scaffolds for tissue engineering are supposed to provide a suitable 3-dimensional environment to stem cells, sufficiently firm support to the regenerating tissues and, preferably, chemically and biologically favorable degradation products to stimulate the regeneration. Sintered bioactive glasses with high porosity have been recognized in numerous studies as an attractive candidate group of materials; however, the brittleness limits the potential use of such scaffolds. Although attempts have been made to overcome this issue by impregnation of the weak struts by biopolymers [66], the resulting materials still did not meet the expectations. Conversely, in this work fine bioactive particles were incorporated as a reinforcing and bioactive phase into biopolymer matrix. To verify their potentially advantageous effect, two matrix materials were used: gellan gum, which enables the formation of porous structures that can be stored and used »off-the-shelf« [37] and thiolated polyethylene glycol, an injectable and self-healing material [60].

Several studies have previously reported on the incorporation of HA or TCP particles into polymeric matrices, such as collagen [67], chitosan [68, 69], gelatine/gellan [70] to overcome their limitations. Bioactive glass has also been used as a reinforcement phase in some biopolymers, such as polycaprolactone [66], polylactic acid [64, 65, 71] chitosan [72, 73], collagen [74] and collagen-hyaluronic acid-phosphatidylserine [75]. The lack of the appropriate mechanical properties is the main issue compromising the success of such scaffolds. However, recently some doubts if scaffolds need to withstand the whole load have been debated. For the stem cells to successfully proliferate and differentiate to osteogenic type faster stress relaxation, usually with more elastic matrices, is favorable [67]. Most of the polymers are too elastic and need some strengthening to stiffen the matrix to a certain extent. The reinforcement of gellan gum was recently achieved by the introduction of HA particles [76], while to the best of our knowledge the incorporation of BAG particles into GG to obtain a dry scaffold was not previously reported. PEG with BAG particles as a possible scaffolding material has been researched and previously reported; however, dynamically cross-linked Au-$(PEGSH)_4$ in combination with nano-sized BAG particles was not.

In the present study, two grades of sol-gel synthesized BAG [21] with a particle size of around 200 nm were used as reinforcement: a 2-component BAG (Siliceous, Calcium oxides, BAG-A) and a 4-component BAG (Siliceous, Calcium, Sodium and Phosphorus oxides, BAG-B). The powders, calcined after the modified sol-gel synthesis at 600 °C, were fully amorphous and partially agglomerated. As reported by Drnovšek et al. [68], the 4-component BAG has been confirmed in the previous study as highly degradable and osteoconductive: in 10-week *in vivo* test the 20 to 100 µm pores in titanium

structure, impregnated with BAG particles, were filled with the fully mineralized bone. In this study, also two-component BAG was used to verify potential effects of BAG composition on the properties of BAG-reinforced scaffolds for bone tissue engineering. Namely, there are many studies reported in literature presenting variations in the composition of bioactive glasses as highly important for tissue repair [69].

5.1 Bioactive Glass - Reinforced Gellan Gum Scaffolds

The BAG particles were introduced into gellan gum (GG) in different percentages, from 0 to 90 % (Table 3.1). The samples were prepared and analyzed in three forms: hydrogels, dry scaffolds (storing) and rehydrated scaffolds (ready to implant) (Figure 4.1-2).

Gellan gum, a biodegradable and bioinert natural biopolymer, was recently introduced as a novel material for tissue engineering. Despite its many advantageous features [37], like many other biodegradable polymers, also, GG lacks good mechanical properties and the ability to form a bone-like mineral phase. Unlike, for instance, polycaprolactone- and polylactic-acid-based synthetic polymers that have also been used in combination with bioactive glass particles [70-72], the GG is water soluble and hydrophilic by nature. Therefore, the processing of the material does not include any toxic substances and is relatively straightforward. In this study, the samples were prepared by casting of hot GG solution, containing Ca^{2+} for cross-linking, without or with admixed preheated BAG suspension in a broad range of concentrations. Upon cooling, hydrogels with different composition and properties were obtained.

The gelation of the GG-based solution occurs in two steps. The first step is a conformational change of GG from random coil to double helix and the second step is an aggregation of the double helixes via junction points resulting in gel [73]. The gelation mechanism of gellan gum solutions is governed by the decrease of temperature and the nature of cations. The divalent cations (e.g. Ca^{2+}) promote the gelation much more efficiently than the monovalent cations, which shield the electrostatic repulsion that benefits the aggregation of the double helixes. The divalent cations form ionic bonds directly with the carboxylic acid groups in gellan gum, causing the aggregation of the double helixes by the inter-chain bridging [74], resulting in more firmly packed double helixes and consequently in more firm hydrogel.

The rheological analyses of GG-based solutions revealed that the addition of BAG particles increases the viscosity of the GG solution and shifts the gelation temperature from ~37 °C for GG to higher temperatures. This implies that the BAG particles contribute to the network formation, most probably due to the fast increase in cation (Ca^{2+}) concentration dissolved from the fine BAG particles. Namely, the fully amorphous BAG, prepared by sol-gel precipitation [21] is comprised of loose silica network, modified with Ca^{2+} and other oxides, weakly bound in the network, causing rapid degradation. The storage modulus (G') increased with BAG addition, which suggests that the elastic modulus will further increase *in situ* due to the release of Ca^{2+} ions from the BAG. However, results from the compression test have demonstrated that with increased addition of $CaCl_2$ solution, the Young's modulus decreased. There are also some literature data showing similar trend in mechanical properties with various ion concentrations [75]. Higher Ca^{2+} concentration may disrupt the gellan gum network, so the observed improved mechanical properties may result from the formation of the double layer around bioactive glass particles [76].

Hydrogels hold a significant amount of water, in our samples from 83-98 %. Therefore, the processing of scaffolds is accompanied with drastic phenomena associated with water. By freezing, a part of water crystallizes, which can be exploited to form highly porous structures by sublimation. Freeze-drying is a well-established technique, used in pharmaceutics, food industry and for scaffold preparation and preservation of microorganisms [77]. Thus, the presence of freezable water and suitably controlled freezing conditions are highly necessary for the formation of a porous structure with the controlled porosity.

In general, water in hydrogels can be present in three states: non-freezable bound water, freezable bound water and free water. Non-freezable water, which does not contribute to the formation of pores during freeze-drying, present in the hydrogel, is closely associated with the polysaccharide and directly bound to its hydrophilic sites via hydrogen bonds. The bound freezing water in the hydrogels is usually associated with the free carboxylic groups. Based on the DSC analysis of the hydrogels during double cooling-heating cycles (Figures 4.4 and 4.5), it was concluded that some of the carboxylic groups in the GG hydrogel were associated with water despite of added cross-linker. The endothermic curves for GG and GG-33A observed exhibited two peaks, first typical for bound (the peak close to 0 °C) and the second for free freezing water (the peak above 9 °C). The intensity of the first endothermic peak decreased with increasing amount of BAG particles, suggesting less carboxylic groups were associated with water due to increased Ca^{2+} concentration. The peaks of freezable bound water were observed in GG and GG-33A, which intensity was low proposing low, unfortunately not quantifiable amount of bound freezable water. The freezing temperatures were quite below zero, ranging from -16 to -17.5 °C, suggesting super-cooling the hydrogels, where more energy was needed to induce the formation of ice crystals form the liquid phase inside the polymer network. The values of freezing temperatures in between the cooling cycles were comparable suggesting on more or less stable hydrogel, where water did not change its original state. Additionally, during the freezing the phase separation in hydrogels occurs, resulting in polymer-rich and polymer-poor phases. Part of the water in hydrogels was unable to determine by DSC as it is fully bound to the polymer.

In the gellan gum hydrogel preparation process water is essential to achieve a uniform polymer solution. When dissolution random coils are formed, which are negatively charged, they cause the coils to repel from each other [78]. These negatively charged groups attract water via hydrogen bonding, resulting in high hydrophilicity of gellan gum and the possibility to obtain a hydrogel. As mentioned above, with the temperature drop GG random coil chains form double helixes, entangling the water inside their network resulting in a free-standing hydrogel. When divalent ions are added during the gelation process, forming double helixes are fused together even more firmly, losing a negligible amount of the water.

In hydrogel form and other two presented scaffold states, water interacts differently with GG polymer. In hydrogels and rehydrated hydrogels free water molecules are attracted to the polymer via hydrogen bonds, resulting in an intense band in region between 2500 and 3600 cm^{-1}. The region is actually composed of two bands ascribed to -OH and the -CH stretching of the polymer glycoside ring. In spectrum of dry scaffolds this region is negligibly small, occurring possibly due to the air moisture, suggesting on highly hygroscopic properties. The water-polymer interactions influence the mechanical properties of the scaffolds. With free water present, the Young's modulus decreased in comparison to the dry scaffolds modulus, suggesting softening the dry scaffold by more interactions of scaffold with water. In dry scaffolds, the peak representing the COO-

stretching (at wavelength of 1618 cm^{-1}) is small, suggesting a high crosslinking degree of the composites. The peaks intensity decreases with an increasing percentage of BAG in the composite, suggesting that BAG further cross-linked the GG polymer. Gellan gum, in the composites, exhibits more or less the same peaks as in single material scaffold. However, for the BAG particles there are some peaks masked or not present in the composites, suggesting the formation of physical interactions between the components.

With the aim to prepare scaffolds for use when needed ("off-the-shelf"), the hydrogels were freeze-dried. The process was performed in a way to produce highly porous structures with interconnected pores suitable for facilitating cell seeding and migration. According to literature data [79] for osteoblasts, cells which produce the substance of bone pores larger than 100 µm are preferred for bone formation, and, therefore, this was set to the desired pore size. High porosity, more than 90 %, is chosen in many scaffold designs since it allows for adequate diffusion of nutrients during tissue culture and provides sufficient surface area for cell–biomaterial interactions.

The most critical step of freeze-drying is the freezing stage, when ice crystals are formed. By cooling, ice crystals start to form from nucleation points along the dispersed solvent, grow and gather up to until a solid-liquid system equilibrium is reached [80, 81]. To ensure sublimation (and not melting) it will take place during drying, the material must be cooled below its triple point and remain below the solid-liquid equilibrium throughout the duration of the drying process. The ice crystals formed during freezing leave holes in the structure when the sample is dried. In general, the size of the crystals depends on the cooling rate: slow freezing produces larger crystals while fast freezing produces small crystals [82].

According to the results of DSC analysis of the hydrogel samples with different compositions, freezing temperature for water in GG was cca. -16 °C (at atmospheric pressure, i.e. 1013 mbar) and did not change remarkably by the composition. As illustrated in Fig. 4.7, the pores in samples prepared by freezing at -20°C were larger than for those frozen at -80°C, and the reproducibility of the result was much lower. Similar result was obtained for both, GG and GG-BAG samples. We suppose that the difference in pore size results from different cooling rates. Another observation was that reproducibility of the results was much lower when freezing was performed at -20 °C pointing out the remarkable effect of the processing procedure. A relatively good reproducibility of the results (microstructure) was obtained only when the same experimental setup and procedure was used.

In the detailed study of the porosity, the presence and amount of BAG particles affected the scaffold porosity. Due to the increased concentration of cations (Ca^{2+} and Si^{4+}) dissolved from the BAG, a more uniform porosity was observed. Independently of the composition, the pore size in the dry scaffold was decreased by an increase in BAG content in a hydrogel that can be ascribed to the lower content of bound freezable water. As presented in Chapter 4.1.3.1, the pores in the GG scaffolds were more than 1 mm in size, while with the addition of 33 % BAG they were reduced to 500-600 µm and with 50 % BAG to 180-220 µm, irrespective of the BAG composition. For the latter, also, much narrower pore size distribution was observed. Both, porosity of over 90 % and pore size in the range between 150 and 500 µm classifies the scaffold as desired concerning the architecture. It has to be considered, however, that the dry scaffold will be rehydrated before implantation that will significantly alter its architectures as it will be discussed in continuation.

More detailed observation of the microstructure of dry scaffolds in cross-sections reveals that the BAG particles are agglomerated and relatively well embedded in the pore walls. These ~10-µm-large agglomerates were formed (or remained) during the addition to the GG from the originally globularly shaped BAG particles (~200 µm).

Although such a microstructure was not desired, the BAG agglomerates captured in the thin GG pore walls, the agglomerates increased the roughness of the pore walls, which can be assumed to be beneficial for the attachment of cells [83].

It is clear that a scaffold has to be sufficiently mechanically resistant for handling as well as for the loading after implantation. Literature data show that researchers use various techniques for evaluation, which makes the comparison difficult. Another vagueness appears due to the fact that some authors [84] present the mechanical properties (only) for the dry scaffolds, although the properties of rehydrated scaffolds are more relevant. In our work, we used a compression test to evaluate the Young's modulus of elasticity, compressive strength and deformation of the hydrogels/scaffolds in all three stages.

It is well known that, on the one hand, biopolymer hydrogels are typically too "soft", meaning that even at a low normal load a critically large deformation (or even failure) takes place, which corresponds to a low Young's modulus, typically around 100 kPa [85]. On the other hand, scaffolds produced from inorganic materials, such as HA, TCP and BAG, are too brittle and break at a certain load after negligible elastic, and without any plastic deformation. The difference between these two materials belonging to these two groups is illustrated in Figure 4.13A, although it is clear that due to the very different nature of both types of materials, such comparison is unreliable. In comparison with porous sintered BAG, the GG-based materials (hydrogel, dry scaffolds and rehydrated scaffolds) exhibit a much lower stiffness, a lower point of failure and in particular much larger deformation. As expected, the stress-strain curves for the GG-BAG composites appeared between the curves for the two individual materials (GG and BAG), implying a reasonable compromise in terms of properties. The obtained values of Young's modulus (estimated from stress-strain curves) were up to 2 MPa for the dry scaffolds, which is higher than those for the hydrogels and rehydrated scaffolds (up to ~1 MPa); however, they are mainly related to the durability during the manipulation and storage, while the behavior of the rehydrated scaffolds is the most relevant for describing the behavior of the scaffold.

The dry scaffolds, previously sterilized and stored, are supposed to be rehydrated before implantation with the cell media. Optionally, the scaffolds can be seeded with cells while its rehydration. During the rehydration step, large water uptake is observed due to high hydrophilicity of the polymer, causing swelling of the pore walls and filling the open pores with the solution. As expected, the amount of absorbed water decreases with increased BAG content. The observation of the samples at various stages of their preparation confirmed that from the apparently non-porous hydrogel, a highly porous network is formed by drying, and after rehydration, the porosity is partly retained.

While the composition of the BAG particles did not greatly affect the microstructure of the GG-BAG composites, it was found to have a significant effect on the mechanical properties of rehydrated hydrogels. The incorporation of the two-component BAG-A significantly increased the stiffness (Fig. 4.12C) and the strength of rehydrated hydrogels (Fig. 4.13D). The improvement was less pronounced for the four-component BAG-B, which might be attributed to the active role of the Ca^{2+}, which is known as an effective cross-linker for the GG [85], and is released from the BAG, thus contributing to the stiffness of the GG. In the four-component BAG-B, the CaO is partly replaced with Na_2O, which is a less efficient cross-linker [86]. The amount of BAG reinforcement plays a large role in mechanical properties, which can be partly ascribed to a decrease in the porosity with an increase of added BAG. For example, as a consequence of the porosity decrease from 85 to 75 %, the Young's modulus increased from 1.2 MPa for 33 % BAG to 1.9 MPa for 50 % BAG. Namely, in addition to the intrinsic properties of the material, the porosity of the material also has a significant effect on the Young's modulus [87].

Considering the similar microstructures of all four composites, the observed higher mechanical strength for the composites with BAG-A in comparison with those containing BAG-B, supports the above suggestion that in the case of the 2-component BAG-A, the released Ca^{2+} contributes to the cross-linking of the GG, while in the 4-component BAG-B the released monovalent Na^{+} detrimentally affects the cross-linking. Thus, the above findings suggest that with an optimal addition of BAG, preferably containing only two- and higher-valent ions, the behavior of the scaffold material with a certain degree of porosity can be tailored regarding the desired mechanical properties.

Although the mechanical properties of the GG were significantly improved by BAG addition (in particular BAG-A), the achieved Young's modulus and compression strength of the GG-BAG rehydrated hydrogel are still low, not only in comparison with reported values for sintered BAG scaffolds [88-90] but also when compared with some synthetic polymers and their composites [37, 70, 71, 91]. However, it should be pointed out that the reported relatively high strength is gained at the expense of a lower porosity of the scaffolds and a low bioresorption.

The mechanical properties of the artificial scaffolds are rarely compared to natural bones, which can be in part ascribed to high complexity of the bone structure and hardly defined characterization techniques suitable for both materials [92]. Lately, it has been doubted if scaffolds really have to mimic the exact mechanical characteristics of the bone. After all, it is expected that scaffolds will gradually degrade after implementation, but the newly formed tissue should compensate for the lost mechanical properties. This, however, has not been a subject of the present study.

After rehydration in aqueous media, degradation of the GG-based scaffolds soon starts to take place. Within the first 48 hours, approximately 10 % weight loss was observed, while within the following 30 days for the both, GG and BGG-BAG, a negligible weight change was recorded. At the same time, the hydroxyapatite was formed in GG-BAG, which suggests that the BAG was progressively replaced by another inorganic substance, HA. The process is accompanied by moderate pH increase due to the Ca^{2+} release. It is supposed that this increase occurs only under static conditions but it is not expected under physiological (dynamic, buffered) conditions.

While on one hand, the biodegradability of the scaffolds in body fluid is desired, on the other, their mechanical properties might be impaired during degradation. Ideally, the newly formed tissue compensates for the deterioration in the mechanical properties, like Marieke at el. [93] recently published. As proven in this study, the GG alone is unable, by its very nature, to produce a mineral phase, while the BAG is known for its relatively fast dissolution and strong ability to induce mineralization. Our results confirmed that, in addition to the above-discussed improvement of the microstructure and mechanical properties, the reinforcement of the GG with BAG particles also resulted in mineral phase formation in the presence of the simulated body fluid for all the BAG-containing samples. The appearance of the materials after the test suggests that the HA formation was faster than the dissolution of the polymer phase (see enlarged area in Figure 4.20). The appearance of HA in the central part of the GG-BAG hydrogels proves a high rate of ion diffusion through the hydrogel, which is sometimes mistakenly considered as a low-permeability structure. Thus, we assume that the GG-BAG composites have a potential to degrade without critical deterioration of mechanical properties during tissue repair.

The (rehydrated) scaffold material is expected to fully degrade within a certain time after the implantation, leaving behind no solid residues, except for the newly formed bone tissue. In this respect, BAG has advantages over HA or TCP, which were often observed to degrade only partially or too slowly. The BAG-B was confirmed in a previous study using *in vivo* tests to completely degrade within ten weeks, resulting in a fully

mineralized bone within a porous titanium structure [68]. In the present study, only short-term dissolution of the examined materials was examined and it was found that the rate is dependent on the BAG's composition. The addition of the 4-component BAG-B resulted in an increased rate of weight loss in comparison with the GG, while conversely, the 2-component BAG-A slightly hindered the dissolution. This can be understood as an additional confirmation of the effect of the released mono- and divalent ions on the GG cross-linking and, in addition, suggests the possibility to tailor the degradation rate using the composition of the BAG reinforcement.

It is known that the first cell-material contact is crucial for the scaffold's success and therefore the adhesion of the cells has to occur within a few hours to maintain good cell viability. Accordingly, the adhesion itself has great importance for various intercellular signaling pathways that direct the cell viability, proliferation and differentiation [94, 95]. In the present study, the cellular response to the GG-BAG rehydrated scaffolds in comparison with the GG was assessed using human-adipose stem cells (hASCs). After 72 hours of hASCs culture no clear differences in terms of cell viability and adhesion were observed between the GG and the GG-BAG rehydrated scaffolds. In addition, the hASCs exhibited favorable growth morphology, reflected in active cytoplasm extensions of the cell membrane and good cell viability, similar to the GG without the BAG. Moreover, no occlusion of the pores was observed during this short culturing period. In spite of the apparently unfavorable pore size in the rehydrated scaffolds, hASCs could also easily reach and adhere to the pore walls in the central part of the scaffold. Based on the known osteogenic properties of bioactive glasses resulting from the effect of the ionic dissolution products [96, 97], it is believed that the addition of BAG is beneficial for the GG material to promote cell adhesion and proliferation; however, this could not be expressed within a short-term test (72 h) and it should therefore be verified in a further, longer-term culture of hASCs within the GG-BAG materials.

5.2 Polyethylene Glycol – Bioactive Glass Nanocomposite Hydrogels

Injectable hydrogels, capable of absorbing a large amount of water, are particularly attractive as a vehicle and temporary scaffold for cells in TE to maintain the cells in the area to treat while offering a minimally invasive procedure for the patient [98]. The requirements for an ideal injectable hydrogel are fast gel formation with a gelation temperature close to body temperature for temperature-responsive hydrogels [99, 100] spontaneous recovery of the mechanical and rheological properties if damaged, biocompatible and preferably bioactive to enhance tissue formation.

While some hydrogels require super-physiological temperatures for gelation [101, 102], an advantage of Au-$(PEGSH)_4$ hydrogel is its instant gelation, induced by the spontaneous formation of Au-S species when aqueous solutions of $HAuCl_4$ and $(PEGSH)_4$ are mixed. In addition, gelation of Au-$(PEGSH)_4$ occurs at room temperature without generating the undesired heat. The same is also true for the Au-$(PEGSH)_4$-BAG composites, where the addition of BAG does not affect gelation. Au-$(PEGSH)_4$ hydrogel nanocomposite was produced using a double syringe system, where one syringe contains an aqueous solution/suspension of $(PEGSH)_4$ polymer and BAG nanoparticles while the second syringe contains an aqueous solution of $HAuCl_4$. Both aqueous solutions were mixed in a special mixing needle to instantaneously form the hydrogel nanocomposite offering a biocompatible injectable scaffold for minimally invasive applications. The dynamic bond allows the material to rearrange permanently resulting in self-healing properties and frequency-dependent stiffness. This latter property is also referred to as shock absorbing behavior for the material due to its increasing stiffness under high frequency stress. The resulting biocompatible hydrogel exhibited a self-healing property and frequency-dependent stiffness due to the permanent exchange between Au-S and disulphide groups readily occurring at physiological conditions. In addition, nucleophilic thiolate concentration, which promotes Au-S/SS exchange, could be varied by adjusting the pH of the hydrogel.

Preferably, an injectable hydrogel should behave as a low-viscosity liquid during application and as an elastic solid when filling the defect, with a fast transition between both states. In the case of Au-$(PEGSH)_4$-based hydrogels, the instantaneous gelation did not allow gelation point to be determined via rheology studies. Such rapid gelation ensures that any encapsulated species would be retained into the 3D network avoiding any diffusion into the surrounding tissues. With the prepared Au-$(PEGSH)_4$-based hydrogels it is important to note that G' is greater than G'' at all frequencies, which confirms that freestanding hydrogels were obtained independently of the amount of BAG nanoparticles incorporated and the pH. From Figure 4.24A and 4.24B, it can be seen that G' and G'' were proportionally increasing with BAG nanoparticles addition. Clearly, the hardening effect of BAG nanoparticles was more pronounced at neutral pH compared to alkaline pH. The pH-dependent rheological properties observed for Au-$(PEGSH)_4$-BAG hydrogel nanocomposites confirmed that there is no interaction, chemical or electrostatic, between BAG nanoparticles and the polymeric network. If such interactions had occurred, the inorganic additive would have acted as an additional cross-linker with no effect of the pH on the resulting rheological properties. In contrast, the stiffening effect observed at a higher amount of BAG nanoparticles is attributed to an increase of both, viscosity and polymer entanglements, due to the volume occupied by the 10 microns clusters, physically entrapped in the polymer network. As previously reported, Au-S/SS permanent exchange allows perpetual rearrangements of the network [60]. This exchange reaction confers frequency-dependent stiffness to the network depending on the frequency

of the deformation applied. For example, Figure 4.24C which represents the loss factor (tan δ = G''/G') illustrates this peculiar behavior. When the deformation is applied at increasing frequencies, but slower than the rate of Au-S/SS exchange, the network has enough time to reorganize. This rearrangement of the polymer chains results in an increase of the viscous character (G'') while the elastic behavior (G') slightly decreases, resulting in an increase of tan δ. On the other hand, when the deformation is applied at higher frequencies than the rate of the dynamic exchange G' increase while G'' decrease due to insufficient time for the network to rearrange, resulting in stiffening of the material and a decrease of tan δ. This phenomenon could be observed for Au-$(PEGSH)_4$ at both pH values and for Au-$(PEGSH)_4$-BAG hydrogel nanocomposites at pH 7, characteristic of dynamic hydrogel. Interestingly, for freestanding dynamic hydrogels, the frequency where tan δ is reaching its maximum, ω_c, has been used to estimate the relaxation time, λ_t, of the dynamic hydrogel via the relationship: $\lambda_t = 1/\omega_c$. λ_t can be considered as an approximation of the Au-S/SS exchange rate. For Au-based dynamic hydrogels, λ_t depends on the amount of nucleophilic thiolate present in the hydrogel. From Figure 4.24C, ω_c occurs at lower frequency when the amount of BAG nanoparticles is increased. Thus, the incorporation of BAG nanoparticles appears to slow down Au-S/SS exchange at pH 10 with longer λ_t from 0.18 s for Au-$(PEGSH)_4$ dynamic hydrogel to 0.5 s, 0.9 s and 1.25 s for Au-$(PEGSH)_4$-BAG_5, Au-$(PEGSH)_4$-BAG_{10} and Au-$(PEGSH)_4$-BAG_{20}, respectively. With increasing G' (Figure 4.24A) with higher amount of BAG nanoparticles, it is obvious that Au-S/SS exchange would be affected due to lower mobility of the polymer chains. At pH 7, this slowdown of Au-S/SS exchange was even more pronounced due to the effect of pH which dictates the amount of reactive thiolates. For instance, Au-based dynamic hydrogel at pH 10 contains more reactive thiolate than the same hydrogel at pH 7 due to the pKa of $(PEGSH)_4$ located at pH 8.3. Hence, as the pH is reduced from 10 to 7 the amount of nucleophilic thiolates decreases, resulting in more stable 3D structure as Au-S/SS exchange occurs at a slower rate. Therefore, the more rigid structure resulted in much lower mobility of $(PEGSH)_4$ polymer chains with increasing amount of BAG nanoparticles, as judged by rheology data (Figure 4.24B). This was observed with the disappearance of the maximum in tan δ for Au-$(PEGSH)_4$-BAG hydrogels nanocomposites (Figure 4.24D). It is noteworthy that a maximum of tan δ Au-$(PEGSH)_4$-BAG_5 is likely to occur at frequency lower than 0.01 Hz which confirms that the increasing stiffness is affecting the Au-S/SS exchange rate.

Interestingly, human bones exhibit shock-absorber properties and accordingly, over the frequency range associated with most daily activities exhibit tan δ comprised between 0.01 to 0.02, with a broad minimum [64]. In our case, the loss factor recorded for Au-$(PEGSH)_4$-BAG hydrogels nanocomposites are higher, but tan δ at around 0.04 was obtained for Au-$(PEGSH)_4$-BAG_{10} at pH 7 (Figure 4.23D). Despite a slight difference, Au-$(PEGSH)_4$-BAG_{10} could be considered as a fairly good approximation to mimic the mechanical environment of bone tissue.

Thanks to Au-S/SS exchange, Au-$(PEGSH)_4$ dynamic hydrogels exhibit self-healing properties, as previously reported [60]. Despite the slowdown effect of BAG nanoparticles on Au-S/SS exchange rate, self-healing abilities of Au-$(PEGSH)^4$-BAG hydrogel nanocomposites were studied. Figure 4.26D shows the dynamic rheology data obtained for all hydrogel nanocomposites, adjusted at pH 7, after self-healing. By comparing figure 4.24B and Figure 4.24D, Au-$(PEGSH)_4$-BAG hydrogels nanocomposites exhibited a decrease of G' and G'' of approximately one order of magnitude, which indicates a weaker hydrogel. Thus, full recovery of the rheological properties was not achieved due to the breaking of non-self-healing bond during the dissection of the hydrogel. However, around 90 % of the original mechanical properties were successfully recovered after this

dramatic shredding of the materials, which should (hopefully) not occur in relevant conditions for bone replacement. Thus, the recovery of the 3D network confirms that Au-S/SS was affected by the presence of BAG nanoparticles at pH 7 but not suppressed. In addition, the permanent exchange reaction allows the hydrogel nanocomposites to be shaped depending on the mold used with light pressure, as previously reported. Therefore, the instantaneous gelation of Au-$(PEGSH)_4$-BAG hydrogels nanocomposites might not be as inconvenient as light pressure would allow any defects and voids to be filled with this dynamic material.

With a pKa located at pH 8.3, less than 10 % of the total amount of Au-S species are on their thiolate form at pH 7 whereas more than 90 % of the reactive thiolate are present at pH 10. Lower amount of thiolate implies longer relaxation time required for the chain to rearrange. No λ_t could be estimated for hydrogel nanocomposites, which is completely different to the results previously obtained for Au-$(PEGSH)_4$ as λ_t was estimated at around 0.18 s. The different rheological behaviour observed in the presence of BAG nanoparticles strongly indicates that the inorganic agglomerated colloids interact with Au-$(PEGSH)_4$ network and slow down Au-S/disulfide exchange. Figure 4.24C and 4.24D, which represent the variation of tan δ at pH 10 and 7, respectively, confirmed that simple adjustment of the pH of the hydrogel nanocomposites resulted in different rheological behavior. For instance, tan δ exhibited a maximum attributed to Au-S/disulfide exchange at pH 10. In contrast, this maximum was not observed for the hydrogel nanocomposites at pH 7 confirming that Au-S/disulfide exchange is slower at neutral pH.

The hardening effect induced by the BAG nanoparticles previously observed by rheology was also confirmed by compression test. More than 90 % deformation was achieved for all hydrogels without any breaking. In contrast, to the GG scaffolds that despite reaching relatively high compressive stress (5 MPa) BAG nanoparticles alone could not be deformed (less than 5 %). GG based 3D constructs allowed the deformation to be improved. However, no more than 20 % deformation was reached before the rupture of the 3D network. With Au-$(PEGSH)_4$-BAG hydrogel nanocomposites, the high deformation obtained is attributed to Au-S/SS exchange responsible for the permanent rearrangement of the network. Similar maximum stress compared to BAG nanoparticles alone were obtained at high deformation for Au-$(PEGSH)_4$-BAG_5 and Au-$(PEGSH)_4$-BAG_{10}. More surprisingly, Au-$(PEGSH)_4$-BAG_{20} reached a maximum stress of around 25 MPa at 98 % deformation. In conclusion, major inconvenience from both individual materials, i.e. brittleness for BAG nanoparticles and relative soft consistency for the dynamic hydrogel, appears to be suppressed, resulting in a composite material with high deformation and high resistance to stress.

As previously mentioned, BAG nanoparticles are easily degraded by dissolution of Silicon and Calcium ions in aqueous media, which are known to enhance cell differentiation and stimulate osteogenesis [103]. The rapid dissolution of BAG nanoparticles is the consequence of fine particles and their fully amorphous structure, which allows the Ca-atoms within the silica tetrahedrons to be easily released, causing instant increase in pH values. During the dissolution, the ionic bonds between Ca and non-bridging oxygen in the silica network are also easily disrupted, allowing Ca to dissolve from the structure more easily than from co-bound silica tetrahedrons. As calcium is released, the silica network becomes looser, allowing it to dissolve at a much faster rate than for SiO_2. The drastic change of pH, observed with dissolution of highly concentrated BAG, was detrimental for cells survival and proliferation. However, the pH buffers present in the physiological fluids *in vivo* will surely be insufficient to maintain the local pH for high

concentrations of BAG nanoparticles. Further, there is no reason for the BAG particles to cause any damage in *in vivo* systems, if unintentionally released from the Au-$(PEGSH)_4$ matrix, as they are highly dissolvable.

As expected, the low diffusion inside the 3D network allowed the amount of ions released to be considerably reduced for Au-$(PEGSH)_4$-BAG_{10} hydrogel nanocomposite at similar time-scale. In addition, it is worth mentioning that BAG nanoparticles were sedimented on the filter due to the large size of the aggregated inorganic colloids. In contrast, BAG nanoparticles were homogenously dispersed within the polymeric matrix. One can assume that if BAG nanoparticles clusters could have been dispersed homogeneously, much faster ions release would have been observed. Therefore, despite higher surface contact area of homogenously dispersed inorganic clusters, lower diffusion inside Au-$(PEGSH)_4$-BAG_{10} can effectively delay the degradation/dissolution of BAG nanoparticles. The ability of the hydrogel to prevent the fast dissolution of BAG nanoparticles might promote mineralization and formation of hydroxyapatite. Although our results cannot be used to estimate the ionic concentration or the change in *pH in vivo*, this experiment shows a good indication of the materials behavior under static conditions. In the preliminary cytotoxicity evaluation, HeLa cells exhibited low proliferation, however dead cells were not observed in the presence of the Au-$(PEGSH)_4$-BAG_{10} hydrogel nanocomposite. The slow release of the degradation by-product in the polymeric matrix, resulting in the maintenance of the overall pH, proved to be sufficient to lower the cytotoxicity of BAG nanoparticles.

When a Ca-releasing material is immersed into a simulated body fluid [61], mineralization may take place as a result of calcium and phosphorous super-saturation. This is typically not observed for polymeric materials but does occur during the degradation of Ca-phosphates and BAG nanoparticles. The use of apatite formation in simulated body fluid as a predictor of bioactivity has been criticized [104], but it remains one of the characteristics usually used as an indicator of the enhanced ability of a material to mineralize in supersaturated solutions. With Au-$(PEGSH)_4$-BAG_{10} hydrogel nanocomposite the polymer matrix was partially degraded after 30 days SBF immersion, but appeared to remain structured with the presence of HA crystals. Thus, in addition to induce hydroxyapatite formation the presence of BAG nanoparticles also allowed the degradation of the dynamic hydrogel to be delayed. The maintenance of the 3D scaffold during a relatively long period of time is crucial in TE as regeneration of large bone defects might require several weeks.

5.3 Potential Applications of the GG-BAG and Au-$(PEGSH)_4$-BAG Scaffolds

As bone defects can be very specific and very diverse, still multiple options have great potential in bone TE application. Despite the high number of available 3D constructs in the market, there are still opportunities for improved solutions. The GG-BAG with various BAG percentage, as a fully biodegradable "off-the-shelf" scaffold, has a great potential to be implanted with or without cells, to low- and non-bearing defect sites, or to be used as a 3D construct to grow tissue in vitro. The dynamically cross-linked nanocomposite of Au-$(PEGSH)_4$-BAG, has the advantage over freestanding scaffolds in minimally invasive application via injection. The Au-$(PEGSH)_4$-BAG hydrogel nanocomposite is a great solution for filling bone where esthetics is important. This hydrogel could be also used as a vehicle for administering the cell directly into the site of the defect.
Both types of the 3D composite constructs are bioactive, in biological environment are able to induce bone mineral formation, which is due to the modification of the polymeric matrix with bioactive glass. With bone tissue regeneration, not only the formation of bone mineral is desirable but also stimulation of cells to differ to osteogenic type is a great benefit. Bioactive glass has been previously proven to stimulate osteogenesis and vascularization with its degradation products (usually Calcium and Siliceous ions) [105, 106]. However, bioactive glass single material 3D porous scaffolds are brittle in nature and degrade quite fast, due to the amorphous nature of the BAG. For these characteristics, they are not the perfect fit for most bone regenerating applications. With embedding BAG particles into the GG or Au-$(PEGSH)_4$ matrix, a viscoelastic 3D construct was obtained, which also solved a problem of BAG alkalinity when dissolving.

The GG-BAG composite scaffolds are proposed to be prepared in the form of highly porous "off-the-shelf" products, which are stored dry and sterilized. Before use, they can be either rehydrated in aqueous media and seeded with cells or rehydrated with cell media containing the cells.

To demonstrate the applicability of the Au-$(PEGSH)_4$-BAG system as an injectable hydrogel nanocomposite, a double barrel syringe was used to prepare the hydrogel nanocomposites. The first barrel of the syringe was filled with suspension of $(PEGSH)_4$-BAG_{10} mixture and the second one was filled with corresponding cross-linker solution. When the content of the both barrels as simultaneously pressed down into the mixing needle, the component combined. At the end of the syringe, the nanocomposite hydrogel formed nicely demonstrating that the material could be injected for the minimally invasive procedure. The system was used at the room temperature and without any hazardous chemicals.

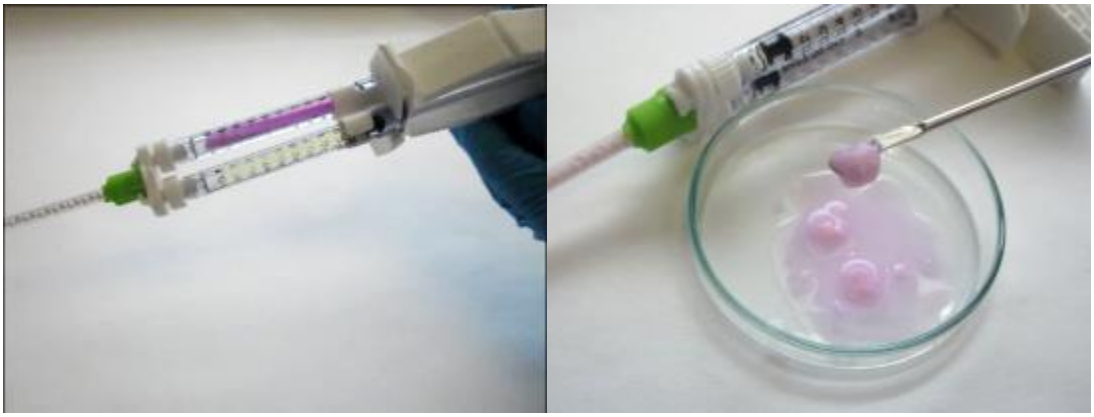


Figure 5.1: Double syringe experiment demonstrating a possible application.

Chapter 6

Conclusions

In the presented work, biodegradable and osteoconductive three-dimensional composite scaffolds for potential applications in bone tissue regeneration were developed. Nano-sized bioactive glass particles were incorporated into a polymer matrix to enhance the mineral bone formation. Two directions were followed in the study: the composites were either prepared as "off-the-shelf" scaffolds or as injectable self-healing hydrogels. In the first case, the matrix polymer was gellan gum (GG) and in the other, it was 4-arm thiolated polyehilene glycol (Au-$(PEGSH)_4$).

To prepare GG-BAG composites, two chemically different bioactive glass powders (2- or 4-component), synthesized via modified sol-gel method, were added in different percentage (up to 90 w/w %) to the gellan gum. The addition of BAG particles reflected in significant improvement of the freeze-dried scaffold characteristics in comparison with the GG. The impact of the BAG composition was moderate, while its increasing amount resulted in porosity decrease, narrower pore size distribution and improvement in mechanical properties. A significant difference appeared in the Young's modulus of the rehydrated scaffolds: lower values were observed for the 4-component BAG that was ascribed to weaker hydrogel network due to the presence of monovalent ions. Namely, differently from the Ca-ions, the contribution of the Na-ions released from BAG, to the cross-linking of the GG, is minor. The agglomerates of BAG particles were homogeneously incorporated into the GG pore walls. During degradation in simulated body fluid, they release ions to form hydroxyapatite.

Dry scaffolds with 50 w/w % of the 2-component BAG addition exhibited the most favorable architecture among the samples, i.e. porosity of 75 %, mean pore size of ~180 µm and narrow pore size distribution, as well as favorable mechanical properties (Young's modulus ~1.8 MPa). Although this is significantly higher than that for the GG alone (0.7 MPa), the mechanical properties of the GG-50BAG composite were still not in the range of the properties of bone. The large amount (>50 %) of BAG particles unfortunately resulted in too low porosity and the attempts to increase the porosity by foaming with hydrogen peroxide were unsuccessful (the resulting porous scaffolds were highly brittle).

As the "off-the-shelf" dry scaffolds are supposed to be rehydrated before use, the properties of the rehydrated scaffolds are highly relevant. The study revealed that by

rehydration, the GG-BAG composites swell mostly on account of the pore size. The dissolution of BAG and hence release of Ca-ions induce only minor increase in pH (up to pH 7.7). During a 30-day degradation test, the structures of the GG-BAG scaffolds were preserved, despite the GG degradation, which is due to the hydroxyapatite formation. This phenomenon was not observed with GG scaffolds. Due to the stepwise transformation of the BAG to hydroxyapatite, the integrity of the scaffold is preserved. Primary biocompatibility was confirmed by short-term cytotoxicity test.

Further, the advantageous effects of the bioactive glass were verified also as an osteoconductive additive for injectable hydrogels based on thiolated polyethylene glycol cross-linked by dynamic mechanism, which enable minimally invasive application - direct injection into the defect site.

The Au-$(PEGSH)_4$ hydrogel prepared with or without BAG particles exhibited self-healing behavior. Increasing amount of the BAG particles resulted in increased stiffness of the hydrogel and decreased deformation at a certain load, indicating that the composite hydrogel can sustain higher loads. In comparison with the GG-BAG composites, during degradation test of Au-$(PEGSH)_4$-BAG in water, more pronounced pH increase was observed. While the pH of the Au-$(PEGSH)_4$ alone decreased from the initial 7.8 to 7.2 after 80 hours, it increased to 8.3 for the Au-$(PEGSH)_4$-BAG composite. Despite, no cytotoxic effect was observed for the composite hydrogels within three days. In simulated body fluid, hydroxyapatite-rich structure was formed, while the Au-$(PEGSH)_4$ alone degraded completely.

The present study confirms that the bioactive glass particles embedded into a polymeric matrix, gellan gum or 4-arm thiolated polyehilene glycol, improve the behavior of the tissue engineering scaffold. While the BAG itself is usually too alkaline, resulting in cytotoxicity, the composites with BAG particles are biocompatible as the pH change is only moderate. In addition, the embedded particles contribute to enhanced mechanical properties. During the scaffold degradation in aqueous-based media, the hydroxyapatite is formed that prevents rapid disintegration of the scaffold due to degradation of the polymer. Thus, the BAG-containing polymers represent a good compromise between the brittle cytotoxic but osteoconductive (sintered) BAG scaffolds and flexible biocompatible but not osteoconductive biopolymers.

References

[1] R. Langer and J. P. Vacanti, "Tissue engineering," *Science,* vol. 260, pp. 920-6, May 14 1993.

[2] D. W. Hutmacher, T. Schantz, I. Zein, K. W. Ng, S. H. Teoh, and K. C. Tan, "Mechanical properties and cell cultural response of polycaprolactone scaffolds designed and fabricated via fused deposition modeling," *Journal of biomedical materials research,* vol. 55, pp. 203-16, May 2001.

[3] A. R. Boccaccini and P. X. Ma, *Tissue engineering using ceramics and polymers*: Elsevier, 2014.

[4] H.-Y. Mi, X. Jing, and L.-S. Turng, "Fabrication of porous synthetic polymer scaffolds for tissue engineering," *Journal of Cellular Plastics,* April 14, 2014 2014.

[5] B. D. Ratner, A. S. Hoffman, F. J. Schoen, and J. E. Lemons, *Biomaterials science: an introduction to materials in medicine*: Academic press, 2004.

[6] V. Migonney, "History of Biomaterials," in *Biomaterials*, ed: John Wiley & Sons, Inc., 2014, pp. 1-10.

[7] L. L. Hench, "Bioceramics - from Concept to Clinic," *American Ceramic Society Bulletin,* vol. 72, pp. 93-98, Apr 1993.

[8] V. A. Dubok, "Bioceramics - Yesterday, today, tomorrow," *Powder Metallurgy and Metal Ceramics,* vol. 39, pp. 381-394, Jul-Aug 2000.

[9] J. O. Hollinger, T. A. Einhorn, B. Doll, and C. Sfeir, *Bone Tissue Engineering*: Taylor & Francis, 2004.

[10] A. D. P. Bankoff, "Biomechanical Characteristics of the Bone," in *Human Musculoskeletal Biomechanics*, D. T. Goswami, Ed., ed, 2012.

[11] B. M. Holzapfel, J. C. Reichert, J. T. Schantz, U. Gbureck, L. Rackwitz, U. Noth, F. Jakob, M. Rudert, J. Groll, and D. W. Hutmacher, "How smart do biomaterials need to be? A translational science and clinical point of view," *Advanced Drug Delivery Reviews,* vol. 65, pp. 581-603, Apr 2013.

[12] M. Borden, M. Attawia, Y. Khan, and C. T. Laurencin, "Tissue engineered microsphere-based matrices for bone repair: design and evaluation," *Biomaterials,* vol. 23, pp. 551-9, Jan 2002.

[13] M. S. Chapekar, "Tissue engineering: Challenges and opportunities," *Journal of Biomedical Materials Research,* vol. 53, pp. 617-620, Dec 5 2000.

[14] E. S. Place, J. H. George, C. K. Williams, and M. M. Stevens, "Synthetic polymer scaffolds for tissue engineering," *Chemical Society Reviews,* vol. 38, pp. 1139-1151, 2009.

[15] K. J. L. Burg, S. Porter, and J. F. Kellam, "Biomaterial developments for bone tissue engineering," *Biomaterials,* vol. 21, pp. 2347-2359, Dec 2000.

[16] L. Ambrosio, *Biomedical Composites*: Elsevier Science, 2009.

[17] J. E. Lemons, "Handbook of bioactive ceramics. vol. 1, bioactive glasses and glass-ceramics and vol. 2, calcium phosphate and hydroxylapatite ceramics. T. Yamamuro L. Hench J. Wilson CRC Press, Boca Raton, FL, 1990," *Journal of biomedical materials research,* vol. 25, pp. 903-904, 1991.

[18] J. C. Knowles, "Phosphate based glasses for biomedical applications," *Journal of Materials Chemistry,* vol. 13, pp. 2395-2401, 2003.

[19] L. L. Hench, R. J. Splinter, W. C. Allen, and T. K. Greenlee, "Bonding mechanisms at the interface of ceramic prosthetic materials," *Journal of biomedical materials research,* vol. 5, pp. 117-141, 1971.

[20] L. L. Hench, "Bioceramics: From Concept to Clinic," *Journal of the American Ceramic Society,* vol. 74, pp. 1487-1510, 1991.

[21] N. Drnovšek, *Development of coatings on Ti6Al4V alloy for new generation implants bone with improved osseointegration*, 2012.

[22] D. J. S. Hulmes, "The collagen superfamily - diverse structures and assemblies," *Essays in Biochemistry, Vol 27,* vol. 27, pp. 49-67, 1992.

[23] V. Ottani, M. Raspanti, and A. Ruggeri, "Collagen structure and functional implications," *Micron,* vol. 32, pp. 251-260, Apr 2001.

[24] G. Vaissiere, B. Chevallay, D. Herbage, and O. Damour, "Comparative analysis of different collagen-based biomaterials as scaffolds for long-term culture of human fibroblasts," *Medical and Biological Engineering and Computing,* vol. 38, pp. 205-210, 2000/03/01 2000.

[25] S. V. Madihally and H. W. T. Matthew, "Porous chitosan scaffolds for tissue engineering," *Biomaterials,* vol. 20, pp. 1133-1142, 1999.

[26] C. Saitow, D. L. Kaplan, and J. J. Castellot, "Heparin stimulates elastogenesis: Application to silk-based vascular grafts," *Matrix Biology,* vol. 30, pp. 346-355, Jun 2011.

[27] S. Bhumiratana, W. L. Grayson, A. Castaneda, D. N. Rockwood, E. S. Gil, D. L. Kaplan, and G. Vunjak-Novakovic, "Nucleation and growth of mineralized bone matrix on silk-hydroxyapatite composite scaffolds," *Biomaterials,* vol. 32, pp. 2812-20, Apr 2011.

[28] P. H. G. Chao, S. Yodmuang, X. Q. Wang, L. Sun, D. L. Kaplan, and G. Vunjak-Novakovic, "Silk hydrogel for cartilage tissue engineering," *Journal of Biomedical Materials Research Part B-Applied Biomaterials,* vol. 95B, pp. 84-90, Oct 2010.

[29] J. Sun and H. Tan, "Alginate-Based Biomaterials for Regenerative Medicine Applications," *Materials,* vol. 6, p. 1285, 2013.

[30] R. Barbucci, R. Rappuoli, A. Borzacchiello, and L. Ambrosio, "Synthesis, chemical and rheological characterization of new hyaluronic acid-based hydrogels," *Journal of Biomaterials Science-Polymer Edition,* vol. 11, pp. 383-399, 2000.

[31] N. J. Lowe, C. A. Maxwell, P. Lowe, M. G. Duick, and K. Shah, "Hyaluronic acid skin fillers: Adverse reactions and skin testing," *Journal of the American Academy of Dermatology,* vol. 45, pp. 930-933, Dec 2001.

[32] M. N. Collins and C. Birkinshaw, "Hyaluronic acid based scaffolds for tissue engineering—A review," *Carbohydrate Polymers,* vol. 92, pp. 1262-1279, 2013.

[33] D. D. Allison and K. J. Grande-Allen, "Review. Hyaluronan: A powerful tissue engineering tool," *Tissue engineering,* vol. 12, pp. 2131-2140, Aug 2006.

[34] M. R, C. G. T, S. P. A, B. J. K, and K. K. S, "PS-60: A New Gel-Forming Polysaccharide," in *Solution Properties of Polysaccharides.* vol. 150, ed: AMERICAN CHEMICAL SOCIETY, 1981, pp. 111-124.

[35] K. S. Kang, G. T. Veeder, P. J. Mirrasoul, T. Kaneko, and I. W. Cottrell, "Agar-Like Polysaccharide Produced by a Pseudomonas Species - Production and Basic Properties," *Applied and Environmental Microbiology,* vol. 43, pp. 1086-1091, 1982.

[36] E. Ogawa, "Temperature dependence of the conformational properties of sodium-type gellan gum in aqueous solutions," in *Physical Chemistry and Industrial Application of Gellan Gum.* vol. 114, K. Nishinari, Ed., ed: Springer Berlin Heidelberg, 1999, pp. 8-14.

[37] L. P. da Silva, M. T. Cerqueira, R. A. Sousa, R. L. Reis, V. M. Correlo, and A. P. Marques, "Engineering cell-adhesive gellan gum spongy-like hydrogels for regenerative medicine purposes," *Acta biomaterialia,* vol. 10, pp. 4787-97, Nov 2014.

[38] J. T. Oliveira, A. Crawford, J. Mundy, A. Moreira, M. E. Gomes, P. V. Hatton, and R. Reis, "A cartilage tissue engineering approach combining starch-polycaprolactone fibre mesh scaffolds with bovine articular chondrocytes," *Journal of Materials Science: Materials in Medicine,* vol. 18, pp. 295-302, 2007.

[39] L. G. Griffith, "Polymeric biomaterials," *Acta Materialia,* vol. 48, pp. 263-277, Jan 1 2000.

[40] T. Hayashi, "Biodegradable Polymers for Biomedical Uses," *Progress in Polymer Science,* vol. 19, pp. 663-702, 1994.

[41] A.-C. Albertsson and I. K. Varma, "Recent Developments in Ring Opening Polymerization of Lactones for Biomedical Applications," *Biomacromolecules,* vol. 4, pp. 1466-1486, 2003/11/01 2003.

[42] J. Yang, G. Shi, J. Bei, S. Wang, Y. Cao, Q. Shang, G. Yang, and W. Wang, "Fabrication and surface modification of macroporous poly(L-lactic acid) and poly(L-lactic-co-glycolic acid) (70/30) cell scaffolds for human skin fibroblast cell culture," *Journal of biomedical materials research,* vol. 62, pp. 438-446, 2002.

[43] M. R. Huglin, "Hydrogels in medicine and pharmacy Edited by N. A. Peppas, CRC Press Inc., Boca Raton, Florida, 1986 (Vol. l), 1987 (Vols 2 and 3). Vol. 1 Fundamentals, pp. vii + 180, £72.00, ISBN 0-8493-5546-X; Vol. 2 Polymers, pp. vii + 171, £72.00, ISBN 0-8493-5547-8; Vol. 3 Properties and Applications, pp. vii + 195, £8000, ISBN 0-8493-5548-6," *British Polymer Journal,* vol. 21, pp. 184-184, 1989.

[44] J. M. Rosiak and F. Yoshii, "Hydrogels and their medical applications," *Nuclear Instruments & Methods in Physics Research Section B-Beam Interactions with Materials and Atoms,* vol. 151, pp. 56-64, May 1999.

[45] W. E. Hennink and C. F. van Nostrum, "Novel crosslinking methods to design hydrogels," *Advanced Drug Delivery Reviews,* vol. 64, pp. 223-236, Dec 2012.

[46] H. Park, K. Park, and W. S. Shalaby, *Biodegradable hydrogels for drug delivery*: CRC Press, 2011.

[47] S. A. Robb, B. H. Lee, R. McLemore, and B. L. Vernon, "Simultaneously Physically and Chemically Gelling Polymer System Utilizing a Poly(NIPAAm-co-cysteamine)-Based Copolymer," *Biomacromolecules,* vol. 8, pp. 2294-2300, 2007/07/01 2007.

[48] L. Yu and J. D. Ding, "Injectable hydrogels as unique biomedical materials," *Chemical Society Reviews,* vol. 37, pp. 1473-1481, 2008.

[49] D. W. Hutmacher, "Scaffolds in tissue engineering bone and cartilage," *Biomaterials,* vol. 21, pp. 2529-2543, Dec 2000.

[50] S. F. Yang, K. F. Leong, Z. H. Du, and C. K. Chua, "The design of scaffolds for use in tissue engineering. Part 1. Traditional factors," *Tissue Engineering,* vol. 7, pp. 679-689, Dec 2001.

[51] Y. S. Nam and T. G. Park, "Porous biodegradable polymeric scaffolds prepared by thermally induced phase separation," *Journal of Biomedical Materials Research,* vol. 47, pp. 8-17, Oct 1999.

[52] M. S. Widmer, P. K. Gupta, L. C. Lu, R. K. Meszlenyi, G. R. D. Evans, K. Brandt, T. Savel, A. Gurlek, C. W. Patrick, and A. G. Mikos, "Manufacture of porous biodegradable polymer conduits by an extrusion process for guided tissue regeneration," *Biomaterials,* vol. 19, pp. 1945-1955, Nov 1998.

[53] A. Atala, *Methods of tissue engineering*: Gulf Professional Publishing, 2002.

[54] W. J. Li, C. T. Laurencin, E. J. Caterson, R. S. Tuan, and F. K. Ko, "Electrospun nanofibrous structure: A novel scaffold for tissue engineering," *Journal of Biomedical Materials Research,* vol. 60, pp. 613-621, Jun 15 2002.

[55] S. K. L. Levengood and M. Q. Zhang, "Chitosan-based scaffolds for bone tissue engineering," *Journal of Materials Chemistry B,* vol. 2, pp. 3161-3184, 2014.

[56] S. J. Hollister, "Porous scaffold design for tissue engineering," *Nature materials,* vol. 4, pp. 518-24, Jul 2005.

[57] N. Barbani, G. D. Guerra, C. Cristallini, P. Urciuoli, R. Avvisati, A. Sala, and E. Rosellini, "Hydroxyapatite/gelatin/gellan sponges as nanocomposite scaffolds for bone reconstruction," *Journal of Materials Science: Materials in Medicine,* vol. 23, pp. 51-61, 2012.

[58] J. T. Oliveira, L. Martins, R. Picciochi, I. B. Malafaya, R. A. Sousa, N. M. Neves, J. F. Mano, and R. L. Reis, "Gellan gum: A new biomaterial for cartilage tissue engineering applications," *Journal of Biomedical Materials Research Part A,* vol. 93A, pp. 852-863, Jun 1 2010.

[59] M. T. Cerqueira, L. P. da Silva, T. C. Santos, R. P. Pirraco, V. M. Correlo, R. L. Reis, and A. P. Marques, "Gellan Gum-Hyaluronic Acid Spongy-like Hydrogels

and Cells from Adipose Tissue Synergize Promoting Neoskin Vascularization," *ACS Applied Materials & Interfaces,* vol. 6, pp. 19668-19679, 2014/11/26 2014.

[60] P. Casuso, A. P.-S. Vicente, H. Iribar, A. Gutierrez-Rivera, A. Izeta, I. Loinaz, G. Cabanero, H.-J. Grande, I. Odriozola, and D. Dupin, "Aurophilically cross-linked "dynamic'' hydrogels mimicking healthy synovial fluid properties," *Chemical Communications,* vol. 50, pp. 15199-15201, 2014 2014.

[61] T. Kokubo and H. Takadama, "How useful is SBF in predicting in vivo bone bioactivity?," *Biomaterials,* vol. 27, pp. 2907-2915, May 2006.

[62] M. T. Cerqueira, R. P. Pirraco, T. C. Santos, D. B. Rodrigues, A. M. Frias, A. R. Martins, R. L. Reis, and A. P. Marques, "Human Adipose Stem Cells Cell Sheet Constructs Impact Epidermal Morphogenesis in Full-Thickness Excisional Wounds," *Biomacromolecules,* vol. 14, pp. 3997-4008, 2013/11/11 2013.

[63] J. Stepišnik, S. Lasič, A. Mohorič, I. Serša, and A. Sepe, "Spectral characterization of diffusion in porous media by the modulated gradient spin echo with CPMG sequence," *Journal of Magnetic Resonance,* vol. 182, pp. 195-199, 2006.

[64] E. Garner, R. Lakes, T. Lee, C. Swan, and R. Brand, "Viscoelastic dissipation in compact bone: Implications for stress-induced fluid flow in bone," *Journal of Biomechanical Engineering-Transactions of the Asme,* vol. 122, pp. 166-172, Apr 2000.

[65] B. Yang, Y. L. Zhang, X. Y. Zhang, L. Tao, S. X. Li, and Y. Wei, "Facilely prepared inexpensive and biocompatible self-healing hydrogel: a new injectable cell therapy carrier," *Polymer Chemistry,* vol. 3, pp. 3235-3238, Dec 2012.

[66] Q. Z. Chen and A. R. Boccaccini, "Poly(D,L-lactic acid) coated 45S5 Bioglass (R)-based scaffolds: Processing and characterization," *Journal of Biomedical Materials Research Part A,* vol. 77A, pp. 445-457, Jun 1 2006.

[67] O. Chaudhuri, L. Gu, D. Klumpers, M. Darnell, S. A. Bencherif, J. C. Weaver, N. Huebsch, H.-p. Lee, E. Lippens, G. N. Duda, and D. J. Mooney, "Hydrogels with tunable stress relaxation regulate stem cell fate and activity," *Nature materials,* vol. advance online publication, 2015.

[68] N. Drnovšek, S. Novak, U. Dragin, M. Čeh, M. Gorenšek, and M. Gradišar, "Bioactive glass enhances bone ingrowth into the porous titanium coating on orthopaedic implants," *International orthopaedics,* vol. 36, pp. 1739-1745, 2012/08/01 2012.

[69] J. R. Jones, "Reprint of: Review of bioactive glass: From Hench to hybrids," *Acta biomaterialia,* vol. 23, Supplement, pp. S53-S82, 2015.

[70] N. Barroca, A. L. Daniel-da-Silva, P. M. Vilarinho, and M. H. V. Fernandes, "Tailoring the morphology of high molecular weight PLLA scaffolds through bioglass addition," *Acta biomaterialia,* vol. 6, pp. 3611-3620, Sep 2010.

[71] Z. Hong, R. L. Reis, and J. F. Mano, "Preparation and in vitro characterization of novel bioactive glass ceramic nanoparticles," *Journal of Biomedical Materials Research Part A,* vol. 88A, pp. 304-313, Feb 2009.

[72] P. Fabbri, V. Cannillo, A. Sola, A. Dorigato, and F. Chiellini, "Highly porous polycaprolactone-45S5 Bioglass® scaffolds for bone tissue engineering," *Composites Science and Technology,* vol. 70, pp. 1869-1878, 2010.

[73] E. Ogawa, R. Takahashi, H. Yajima, and K. Nishinari, "Thermally induced coil-to-helix transition of sodium gellan gum with different molar masses in aqueous salt solutions," *Biopolymers,* vol. 79, pp. 207-217, Nov 2005.

[74] S. Kanesaka, T. Watanabe, and S. Matsukawa, "Binding effect of Cu2+ as a trigger on the sol-to-gel and the coil-to-helix transition processes of polysaccharide, gellan gum," *Biomacromolecules,* vol. 5, pp. 863-868, May-Jun 2004.

[75] R. Mao, J. Tang, and B. G. Swanson, "Texture properties of high and low acyl mixed gellan gels," *Carbohydrate Polymers,* vol. 41, pp. 331-338, 2000.

[76] D. J. Shaw, "1 - The colloidal state," in *Introduction to Colloid and Surface Chemistry (Fourth Edition)*, D. J. Shaw, Ed., ed Oxford: Butterworth-Heinemann, 1992, pp. 1-20.

[77] G. Nireesha, L. Divya, C. Sowmya, N. Venkateshan, M. N. Babu, and V. Lavakumar, "Lyophilization/Freeze Drying-An Review ‘," *Inter J Novel Trends in Pharm Sci,* vol. 3, pp. 87-98, 2013.

[78] G. Sworn, "9 - Gellan gum," in *Handbook of Hydrocolloids (Second edition)*, G. O. Phillips and P. A. Williams, Eds., ed: Woodhead Publishing, 2009, pp. 204-227.

[79] S. F. Hulbert, F. A. Young, R. S. Mathews, J. J. Klawitter, C. D. Talbert, and F. H. Stelling, "Potential of ceramic materials as permanently implantable skeletal prostheses," *Journal of biomedical materials research,* vol. 4, pp. 433-456, 1970.

[80] A. Holden and P. Morrison, *Crystals and crystal growing*: MIT press, 1982.

[81] K. E. Zachariassen and E. Kristiansen, "Ice nucleation and antinucleation in nature," *Cryobiology,* vol. 41, pp. 257-279, Dec 2000.

[82] K. Scoffin. (2011). *Scaling the Scaffolds: Control of Pore Size in Tissue Engineering Scaffolds.* Available: http://www.americanlaboratory.com/913-Technical-Articles/36280-Scaling-the-Scaffolds-Control-of-Pore-Size-in-Tissue-Engineering-Scaffolds/

[83] H.-I. Chang and Y. Wang, *Cell Responses to Surface and Architecture of Tissue Engineering Scaffolds*, 2011.

[84] P. X. Ma and J. W. Choi, "Biodegradable polymer scaffolds with well-defined interconnected spherical pore network," *Tissue engineering,* vol. 7, pp. 23-33, Feb 2001.

[85] H. Yamaoka, H. Asato, T. Ogasawara, S. Nishizawa, T. Takahashi, T. Nakatsuka, I. Koshima, K. Nakamura, H. Kawaguchi, U.-i. Chung, T. Takato, and K. Hoshi, "Cartilage tissue engineering using human auricular chondrocytes embedded in different hydrogel materials," *Journal of Biomedical Materials Research Part A,* vol. 78A, pp. 1-11, 2006.

[86] E. Miyoshi, T. Takaya, and K. Nishinari, "Rheological and thermal studies of gel-sol transition in gellan gum aqueous solutions," *Carbohydrate Polymers,* vol. 30, pp. 109-119, 1996.

[87] L. M. Mathieu, T. L. Mueller, P.-E. Bourban, D. P. Pioletti, R. Müller, and J.-A. E. Månson, "Architecture and properties of anisotropic polymer composite scaffolds for bone tissue engineering," *Biomaterials,* vol. 27, pp. 905-916, 2006.

[88] N. Doiphode, T. Huang, M. Leu, M. Rahaman, and D. Day, "Freeze extrusion fabrication of 13–93 bioactive glass scaffolds for bone repair," *Journal of Materials Science: Materials in Medicine,* vol. 22, pp. 515-523, 2011/03/01 2011.

[89] X. Liu, M. N. Rahaman, and Q. Fu, "Oriented bioactive glass (13-93) scaffolds with controllable pore size by unidirectional freezing of camphene-based suspensions: Microstructure and mechanical response," *Acta biomaterialia,* vol. 7, pp. 406-416, 2011.

[90] X. Liu, W. Huang, H. Fu, A. Yao, D. Wang, H. Pan, and W. Lu, "Bioactive borosilicate glass scaffolds: improvement on the strength of glass-based scaffolds for tissue engineering," *Journal of Materials Science: Materials in Medicine,* vol. 20, pp. 365-372, 2009/01/01 2009.

[91] B. Cao, D. Zhou, M. Xue, G. Li, W. Yang, Q. Long, and L. Ji, "Study on surface modification of porous apatite-wollastonite bioactive glass ceramic scaffold," *Applied Surface Science,* vol. 255, pp. 505-508, 2008.

[92] X. E. Guo, "Mechanical Properties of Cortical Bone and Cancellous Bone Tissue," in *Bone Mechanics Handbook, Second Edition*, ed: CRC Press, 2001, pp. 10-1-10-23.

[93] S. A. H. de Vries, M. v. Doeselaar, B. P. Meij, M. A. Tryfonidou, and K. Ito, "The Stimulatory Effect of Notochordal Cell-Conditioned Medium in a Nucleus Pulposus Explant Culture," *Tissue Engineering Part A,* 2015.

[94] R. O. Hynes, "Integrins: Bidirectional, Allosteric Signaling Machines," *Cell,* vol. 110, pp. 673-687, 2002.

[95] B. G. Keselowsky, D. M. Collard, and A. J. García, "Surface chemistry modulates focal adhesion composition and signaling through changes in integrin binding," *Biomaterials,* vol. 25, pp. 5947-5954, 2004.

[96] P. Valerio, M. M. Pereira, A. M. Goes, and M. F. Leite, "The effect of ionic products from bioactive glass dissolution on osteoblast proliferation and collagen production," *Biomaterials,* vol. 25, pp. 2941-2948, 2004.

[97] V. G. Varanasi, J. B. Owyoung, E. Saiz, S. J. Marshall, G. W. Marshall, and P. M. Loomer, "The ionic products of bioactive glass particle dissolution enhance periodontal ligament fibroblast osteocalcin expression and enhance early mineralized tissue development," *Journal of Biomedical Materials Research Part A,* vol. 98A, pp. 177-184, 2011.

[98] H. Tan and K. G. Marra, "Injectable, Biodegradable Hydrogels for Tissue Engineering Applications," *Materials,* vol. 3, pp. 1746-1767, Mar 2010.

[99] K. H. Bae, L.-S. Wang, and M. Kurisawa, "Injectable biodegradable hydrogels: progress and challenges," *Journal of Materials Chemistry B,* vol. 1, pp. 5371-5388, 2013.

[100] X. Chen, Y. Zhao, S. Geng, R. J. Miron, Q. Zhang, C. Wu, and Y. Zhang, "In vivo experimental study on bone regeneration in critical bone defects using PIB

nanogels/boron-containing mesoporous bioactive glass composite scaffold," *International Journal of Nanomedicine,* vol. 10, pp. 839-846, 2015.

[101] T. E. L. Douglas, W. Piwowarczyk, E. Pamula, J. Liskova, D. Schaubroeck, S. C. G. Leeuwenburgh, G. Brackman, L. Balcaen, R. Detsch, H. Declercq, K. Cholewa-Kowalska, A. Dokupil, V. M. J. I. Cuijpers, F. Vanhaecke, R. Cornelissen, T. Coenye, A. R. Boccaccini, and P. Dubruel, "Injectable self-gelling composites for bone tissue engineering based on gellan gum hydrogel enriched with different bioglasses," *Biomedical Materials,* vol. 9, Aug 2014.

[102] B. Jeong, Y. H. Bae, D. S. Lee, and S. W. Kim, "Biodegradable block copolymers as injectable drug-delivery systems," *Nature,* vol. 388, pp. 860-862, Aug 28 1997.

[103] A. Hoppe, N. S. Güldal, and A. R. Boccaccini, "A review of the biological response to ionic dissolution products from bioactive glasses and glass-ceramics," *Biomaterials,* vol. 32, pp. 2757-2774, 2011.

[104] H. Pan, X. Zhao, B. W. Darvell, and W. W. Lu, "Apatite-formation ability – Predictor of "bioactivity"?," *Acta biomaterialia,* vol. 6, pp. 4181-4188, 2010.

[105] A. Arkudas, A. Balzer, G. Buehrer, I. Arnold, A. Hoppe, R. Detsch, P. Newby, T. Fey, P. Greil, R. E. Horch, A. R. Boccaccini, and U. Kneser, "Evaluation of Angiogenesis of Bioactive Glass in the Arteriovenous Loop Model," *Tissue Engineering. Part C, Methods,* vol. 19, pp. 479-486, 2013.

[106] L. L. Hench, "Genetic design of bioactive glass," *Journal of the European Ceramic Society,* vol. 29, pp. 1257-1265, 2009.

Bibliography

Publications Related to the Thesis

Original Scientific Articles

A. Gantar, L. P. da Silva, J. M. Oliveira, A. P. Marques, V. M. Correlo, S. Novak, R. L. Reis, "Nanoparticulate bioactive-glass-reinforced gellan-gum hydrogels for bone-tissue engineering," *Materials science & engineering. C, Biomimetic materials, sensors and systems*, vol. 43, pp. 27-36, 2014.

D. Kytýř, T. Doktor, M. Adorna, M. Neuhauserova, J. Šleichrt, N. Fenclová, A. Gantar, S. Novak, "Deformation behaviour of gellan gum based scaffold subjected to compression loading," *Applied mechanics and materials,* vol. 821, pp. 665-670, 2016.

I. Kumpová, D. Vavřík, T. Fíla, P. Koudelka, I. Jandejsek, J. Jakůbek, D. Kytýř, P. Zlámal, M. Vopálenský, A. Gantar, "High resolution micro-CT of low attenuating organic materials using large area photon-counting detector," *Journal of Instrumentation*, vol. 11, pp. 1-7, 2016.

Conference Paper

A. Gantar, L. P. da Silva, J. M. Oliveira, A. P. Marques, N. Drnovšek, V. M. Correlo, R. L. Reis, S. Novak, "Bioactive glass reinforcement of 3D gellan gum scaffolding material," *In: MiMe - materails in medicine: conference guide, final program and abstract book,* Feanza, Italy, 2013.

A. Gantar, N. Drnovšek, R. Podlipec, J. Štrancar, S. Novak, 2Bioactive-glass/collagen composite scaffollds for bone regeneration," *In: 2nd Joint Meeting of the COST action MP1005 NAMABIO, Programme & book of abstracts*, University of Technology, Vienna, Austria, 2012.

Published scientific conference contribution abstract

A. Gantar, P. Casuso, A. Perez, D. Dupin, S. Novak, I. Loinaz, "Composite bioactive glass and PEG metallophilic hydrogel as potential cellular scaffold," *In: N. Kavčič (ed.), et al. 9th Young researchers' day, Ljubljana : program and abstract book*, Institut Jožef Stefan, Ljubljana, Slovenia, 2015.

R. Kocen, A. Gantar, S. Novak, C. Hellmich, M. Gasik, „Mechanical properties of hydrogel-"ceramic" composites," *In: N. Kavčič (ed.), et al. 9th Young researchers' day, Ljubljana : program and abstract book*, Institut Jožef Stefan, Ljubljana, Slovenia, 2015.

R. Kocen, A. Gantar, S. Novak, C. Hellmich, M. Gasik, „Viscoelastic properties of hydrogel - "ceramic" composites for tissue-engineering scaffolds," *In: N. Antonova (ed.), I. Velcheva (ed.), E. Zvetkova (ed.). Scientific program and abstracts of the 5th Eurosummer School on Biorheology and Symposium on Micro and Nanomechanics and Mechanobiology of Cells Tissues and Systems*, Varna, Bolgaria, 2015.

A. Gantar, P. Casuso, A. Perez, D. Dupin, S. Novak, I. Loinaz, "Bioactive glass nanoparticles in PEG metallophilic hydrogel as cellular scaffold," *In: Unified scientific approaches towards REgenerative ORthopaedic and DEntistry, International [COST action MP1005 NAMABIO] Conference REDEOR, conference book*, San Servolo Island, Venice, Italy, 2015.

R. Kocen, A. Gantar, M. Pastrama, C. Hellmich, M. Gasik, S. Novak, "Characterization of mechanical properties of hydrogel-"ceramic" used for tissue engineering scallolds," *In: Unified scientific approaches towards REgenerative ORthopaedic and DEntistry, International [COST action MP1005 NAMABIO] Conference REDEOR, conference book,* San Servolo Island, Venice, Italy, 2015.

A. Gantar, R. Kocen, S. Novak, "Highly reinforced bioactive glass - gellan gum composite hydrogels for biomedical applications," *In: 26th Annual Conference [of] European Society for Biomaterials, Final program,* Liverpool, United Kingdom, 2014.

R. Kocen, A. Gantar, S. Novak, „Viscoelastic properties of gellan gum scaffolds with bioactive glass particles," *In: Journal of tissue engineering and regenerative medicine*, TERMIS EU 2014 Meeting, Genova, Italy, 2014.

R. Kocen, A. Gantar, S. Novak, „Viscoelastic properties of scaffolds for tissue engineering," *In: 8th Young Researchers' Day, 2014, Ljubljana. V. Žunič (ed.), et al. Program and abstract book*, Jožef Stefan Institute, Ljubljana, Slovenia, 2014.

L. Girandon, B. Dovgan, M. Fröhlich, A. Gantar, N. Drnovšek, S. Novak, N. Kregar-Velikonja, „The effect of sintering on active bioglass cytotoxicity evaluated by human primary," *In: 25th European Conference on Biomaterials, ESB 2013, XXV Symposium of the European Society for Biomaterials. From the design to the application of biomaterials: book of abstracts,* Madrid, Spain, 2013.

A. Gantar, N. Drnovšek, B. Horvat, S. Novak, L. Girandon, B. Dovgan, N. Kregar-Velikonja, "Study of bioactive glass glass particulate reinforcement for ostoechondral scaffolds," *In: 25th European Conference on Biomaterials, ESB 2013, XXV Symposium of the European Society for Biomaterials. From the design to the application of biomaterials: book of abstracts,* Madrid, Spain, 2013.

A. Gantar, L. P. da Silva, J. M. Oliveira, A. P. Marques, S. Novak, V. M. Correlo, R. L. Reis, "Preparation and characterization of gellan gum - bioactive glass composite hydrogels," *In: 7th Young Researchers' Day. D. Lisjak (ed.), P. Dušak (ed.), S. Kralj (ed.). Program and abstract book*, Jožef Stefan Institute, Ljubljana, Slovenia, 2013.

A. Gantar, L. P. da Silva, J. M. Oliveira, A. P. Marques, N. Drnovšek, V. M. Correlo, R. L. Reis, S. Novak, "Bioactive glass reinforcement of 3D gellan gum scaffolding material,"

In: 21st International Conference on Materials and Technology. M. Godec, et al. Program and book of abstracts Portorož, Slovenia, 2013.

S. Novak, N. Drnovšek, A. Gantar, L. Girandon, A. Barlič, B. Dovgan, N. Kregar-Velikonja, "Preliminary study of nanoparticulate bioactive glass as a substrate for cartiage tissue engineering," *In: 3rd TERMIS Word Congress 2012. Journal of tissue engineering and regenerative medicine*, Vienna, Austria, 2012.

A. Gantar, N. Drnovšek, S. Novak, "Bioative glass scaffolds for bone repair," *In: 20. Jubilee Conference on Materials and Technology. M. Godec (ed.), et al. Program and book of abstracts,* Portorož, Slovenia, 2012.

A. Gantar, N. Drnovšek, S. Novak, "Bioactive glass scaffolds for bone repair," *In: First International Conference Processing, Characterization and Applications of Nanostructured Materials and Nanotechnology, NanoBelgrade 2012. B. Obradović (ed.). Programme & Book of Abstracts,* Faculty of Technology and Merallurgy, Belgrade, Serbia, 2012.

Final research reports

A. Gantar, "Bioactive glass-gellan gum scaffolds for bone tissue engineering applications," *Short term scientific report,* 2013.

A. Gantar, "Injectable composite hydrogel with nano-sized bioactive glass particles," *Short term scientific mission report*, 2014.